Strategies For Limiting Interference and Interception of Free Space Optical Communications

by

Manishika P. Agaskar

S.B. Electrical Science and Engineering
Massachusetts Institute of Technology (2012)

Submitted to the Department of Electrical Engineering and Computer Science
in Partial Fulfillment of the Requirements for the Degree of

Master of Engineering in Electrical Engineering and Computer Science
at the
Massachusetts Institute of Technology

February 2013

Signature of Author:_____
Department of Electrical Engineering and Computer Science
January 18, 2013

Certified by:_____
Vincent W. S. Chan
Joan and Irwin Jacobs Professor of Electrical Engineering and Computer Science
Thesis Supervisor

Accepted by:_____
Dennis M. Freeman
Chairman, Masters of Engineering Thesis Committee

Strategies For Limiting Interference and Interception of Free Space Optical Communications

by

Manishika P. Agaskar

Submitted to the Department of Electrical Engineering and Computer Science
on January 10, 2013 in Partial Fulfillment of the Requirements for the
Degree of Master of Engineering in Electrical Engineering and Computer Science

Abstract

Free space optical systems provide an attractive solution to communication needs that require inexpensive, easily deployable links capable of high data rate transmissions. A major challenge of free space optical communication is ensuring the integrity and confidentiality of the transmitted information. In an optical wireless network with close-in users, communication between two users could interfere with another link in the network. Such systems are also susceptible to eavesdropping, especially inside the main lobe of the transmitted beam.

In this thesis, we propose a method of controlling the direction of energy propagation from an optical transmitter to maximize the power received by the remote terminal of a link while limiting the power received in a broadly defined region within the main lobe of the transmission. We consider specifically an optical transmitter comprised of an array of apertures with controllable amplitudes and phases, and we approximate the intended suppression region with a finite number of points. We assume the total transmitted power is held fixed. Via iterative numerical methods, we solve a nonlinear optimization problem for the weight vector that maximizes the intensity at the receiver while limiting the intensity at the specified suppression points to below some fraction of the intensity at the receiver.

For a linear aperture array, we show that without overly limiting the power to the intended receiver, it is possible to suppress the signal intensity in a 1 beamwidth region located 0.2 beamwidths from the intended user down to one tenth of the intensity at the intended receiver. For a two dimensional array, we show that we can similarly suppress a 1×1 beamwidth region as close as 0.2333 beamwidths to the intended receiver. We further show that by increasing the number of suppression points used to approximate the suppression region, we can suppress a region much closer to the receiver, but at the cost of significantly lowering the intensity at the receiver. We also observe a tradeoff between the size of the suppression region and our ability to limit the signal intensity throughout the entire region. We show that our ability to successfully suppress power to the required region is limited by both our available transmit power and our uncertainty of the position of the eavesdropper or network user.

Thesis Supervisor: Vincent W. S. Chan
Title: Joan and Irwin Jacobs Professor of Electrical Engineering and Computer Science

Acknowledgments

I would first and foremost like to thank my thesis supervisor Professor Vincent W. S. Chan for the time and attention he devoted not only to this project, but also to my academic and professional development. His expertise and guidance were invaluable, and his patient encouragement made my first research experience a true pleasure.

I would also like to thank Donna Beaudry and my fellow students in the Claude E. Shannon Communication and Network Group for their support, conversation, and friendly advice.

I am hugely grateful to my MIT family at 2-282 Random Hall, who kept me company on countless late nights, and who were a constant source of encouragement.

Finally, I want to express my incredible gratitude for my family. My brother and sister-in-law, Ameya and Cheri Agaskar, have been sources of both sound technical advice and delicious food. My mother, Rohini Agaskar, has never stopped believing in my ability to overcome any challenge that comes my way – and has never stopped reminding me of that. This thesis is dedicated to her.

Table of Contents

List of Figures

List of Tables

Chapter 1

Introduction

Free-space optical communication systems offer several advantages over other communication systems. Without the bandwidth constraints of licensed microwave channels and without the need to deploy fiber, free-space optical systems can transmit at high data rates and can provide cheap, easily deployable solutions for both short-term and long-term communication needs [1]. These systems have several potential applications in future space-terrestrial networks (Figure 1.1) that include communication between buildings, ships, aircrafts, and satellites [7].

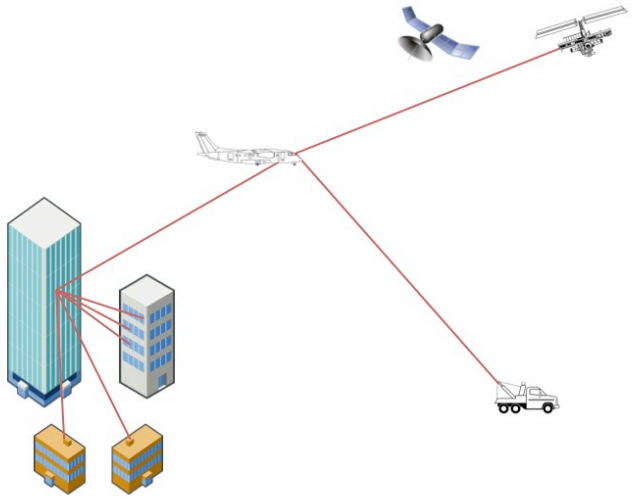

Figure 1.1 Potential future space-terrestrial free space optical communication network.

For ground-to-ground or ground-to-air applications, the first major challenge of free-space optical communication is maintaining a high data rate over a turbulent atmospheric channel. Atmospheric temperature fluctuations lead to changes in the index of refraction of the channel and can cause fading and corruption of the signal at the receiver [4]. Diversity is one technique that can reduce this effect. Spatial diversity can be achieved through a sparse aperture

system, comprised of multiple transmit and receive apertures. Using feedback from the receiver to determine the turbulence state of the channel, the amplitude and phase at each transmit sub-aperture can be controlled to send power through the spatial modes with minimum loss [1]. If the turbulence state is not known, the sparse aperture system with identical amplitude and phase at each transmitter still reduces the effect of turbulence-induced fading [6], though with less performance gain.

In this thesis, we address a second major challenge of free-space optical communication: ensuring the integrity and confidentiality of the transmitted information. We propose to limit both interference and unintended reception by controlling the direction of energy propagation from the optical transmitter. Despite the high directionality of free space optical communication in comparison to systems with longer wavelengths (e.g. RF communication), there is still significant spreading of the signal energy in the vicinity of the receiver, particularly if the receiver is in the far-field of the transmission. The divergence of the beam is in some cases necessary to allow the receiver some flexibility in position and to prevent the need for an expensive beam-tracking system.

However, in an optical wireless network such as that of Figure 1.2, a transmission with a diverging beam along one link can interfere with the receiver of another link. Each transmitter therefore must prevent excess energy from corrupting another user's transmission. In doing so, the transmitter would also be able to simultaneously send different transmissions to different users. Additionally, free space optical systems are susceptible to eavesdropping, especially inside the main lobe of the transmitted beam, as in Figure 1.3, or in high intensity grating lobes. In an urban environment, this susceptibility can be particularly pronounced, and limiting energy propagation in a certain direction would increase the confidentiality of the transmission.

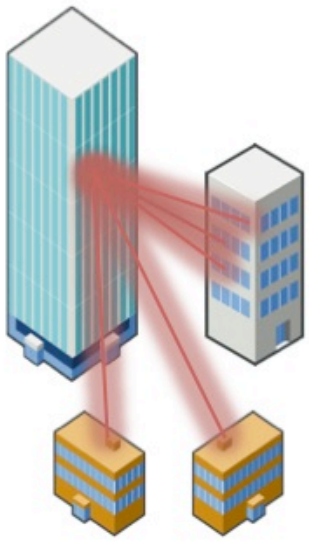

Figure 1.2 If users in a free space optical network are too close to one another, transmissions intended for one user can interfere with transmission to another user.

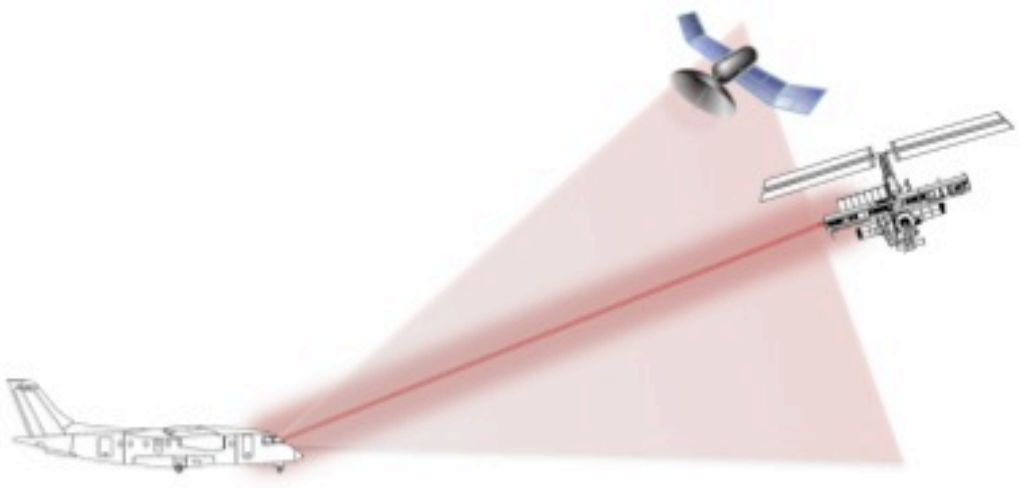

Figure 1.3 If a free space optical transmission to an intended user is overly divergent, an eavesdropper could potentially access the signal.

To prevent interference and interception, the user should be able to maximize the signal power transmitted to the intended receiver and simultaneously limit the power transmitted in the direction of the other user or eavesdropper. This is particularly difficult if the users in an optical network are close to one another, or if a potential eavesdropper can access the signal from inside the main lobe of the transmitted beam. Additionally, if users are mobile and/or their exact positions are unknown, it may be necessary to limit power to an entire region where another user or eavesdropper may be. (See Figure 1.4.) Further complicating matters, the sparse aperture system described above that reduces the effects of atmospheric turbulence is more difficult to secure than a filled aperture transmitter because the far-field radiation pattern created by the multiple sub-apertures has grating lobes with higher power than the side lobes of a filled aperture radiation pattern. These grating lobes extend through the area of the main lobe of an individual sub-aperture – which is substantially wider than the main lobe of the encompassing transmitter array.

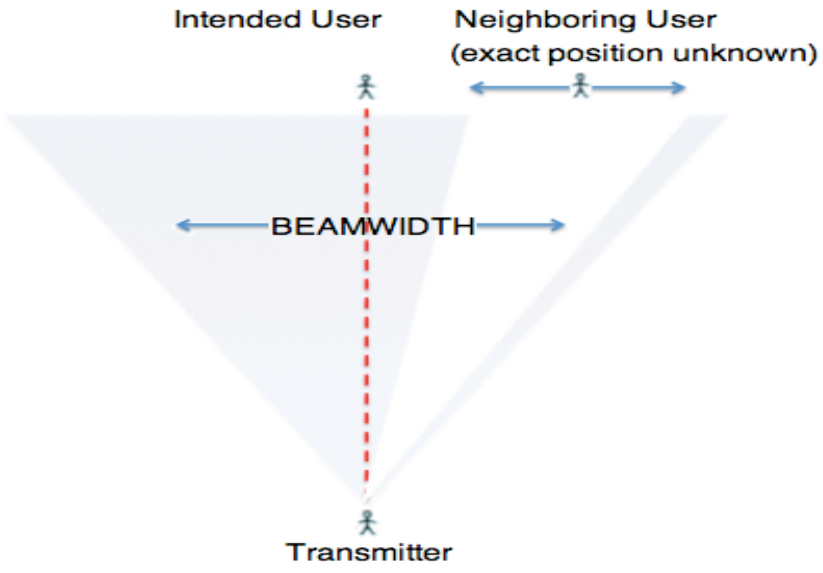

Figure 1.4 Position of neighboring user or eavesdropper is unknown. Power must be suppressed to defined suppression region (white).

1.1 Problem Statement

In this thesis, we propose a method of controlling the direction of energy propagation from an optical transmitter to maximize the power received by the remote terminal of a link while limiting the power received in a broadly defined region within the main lobe of the transmission. The goal of this scheme is threefold:

a) As in Figure 1.5, if the link is part of a multiple-user network in which a neighboring user's position is variable within a defined area, the transmitted signal to that area should be suppressed. The extent of the suppression should be such that the transmitted signal will minimally interfere with signals intended for the neighboring user.

b) If the communication link is susceptible to an eavesdropper whose position within a defined area is unknown, the transmitted signal to that area should again be optimally suppressed. Here, the extent of the suppression should be such that the ability of an eavesdropper to obtain the signal is significantly reduced.[1]

c) In both cases, the optimal scheme requires that the intended receiver be maximally able to successfully receive the transmitted information while the constraint on the suppression region is met.

In order to take advantage of previous work in mitigating the effects of atmospheric turbulence on free-space optical communications, we focus on performing the necessary beam-forming on the sparse aperture system. However, we also devote some attention to different transmit architectures, particularly filled aperture systems.

[1] For example, we can decide to suppress the desired region to -10 dB of the power received by the user. If the user's receiver is near the quantum optimum, the eavesdropper will be denied.

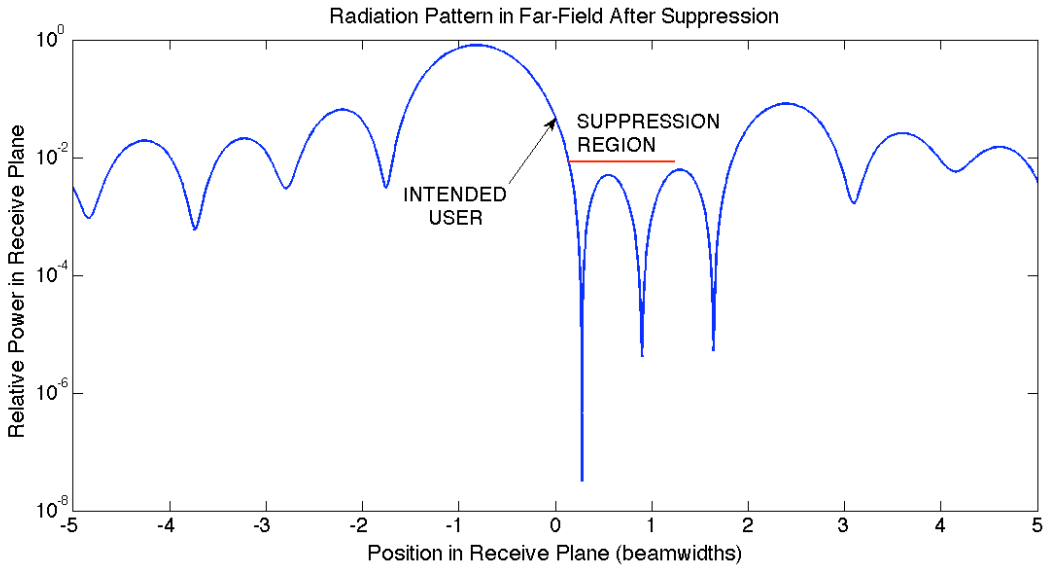

Figure 1.5 Radiation pattern in far-field after suppression, for linear array. The suppression region is marked in red.

1.2 Previous Work

Steering the output beam of a sparse aperture array is similar to the well-studied problem of steering an RF phased array. The physics of the two systems are different due to their vastly different operational wavelengths, but the mathematical formulation is similar. An interference nulling algorithm for an RF array antenna that completely cancels the signal received from a particular direction is treated in [5]. This formulation can be reversed to maximize the transmitted signal power to the intended receiver while cancelling the signal transmitted to another point. The placement of multiple nulls to cancel the signal received from a wideband jammer is studied in [8]. This is shown to result in the non-complete suppression of the signal from an angular sector. The optimum antenna gain pattern to place a single null at a particular user in a multiple-user satellite network is formulated in [2]. Putting a complete null at a given point (i.e. transmitting zero power to that location) is shown in [2] to significantly attenuate the power sent to the intended user and is not the optimum strategy. The power at the receiver can

be optimized by limiting the signal power at the nulling location to some acceptable nonzero threshold. The optimum nulling strategy for a single known eavesdropper of a sparse aperture system in atmospheric turbulence is developed in [1].

In this thesis, we use some of the same techniques used for RF phased arrays as in [5], but extend them to suppress power to a continuous region within a defined region. Using insight from [2], we do not place complete nulls at points in this region, but rather suppress the power in the region to either some specified power threshold or some specified fraction of the power at the intended receiver. We also neglect the effects of turbulence: the effect of turbulence will not significantly compromise the signal suppression in the denied area, but the user may require slightly more link margin, especially if the transmit array consists of a small number of apertures.

1.3 Thesis Organization

In Chapters 2 through 4, we develop the theoretical basis of this thesis. In Chapter 2, we develop an idealized model of a full aperture transmitter, and discuss methods of optimizing the transmittance function of this aperture. We discuss in depth the sparse aperture model that is analyzed throughout the rest of this thesis, and we present the nonlinear optimization problem that is the basis of our proposed suppression scheme. In Chapter 3, we solve a toy example to analytically predict the significance of various system parameters. In Chapter 4, we discuss the numerical methods used to solve the optimization problem and specify the system parameters used in our analysis.

In Chapter 5, we present results for a linear aperture array. We observe the effect of changing various system parameters on both the achievable signal-to-suppression-region power

ratio and on the decrease in power at the receiver after suppression. In Chapter 6, we present results for a two-dimensional aperture array. We consider a fixed transmit power and again observe the effects of variation in system parameters on the signal-to-suppression-region power ratio and the intensity at the receiver.

In Chapter 7, we summarize the functional relationship between system parameters and the signal-to-suppression-region power ratio and receive power for the two-dimensional array case. We consider the effect of these relationships on the design of secure free space optical systems. We summarize our findings and suggest potential modifications to our suppression scheme in Chapter 8.

Chapter 2

Characteristics of System Model

The communication system we consider in this thesis consists of an optical transmitter comprised of one or more apertures transmitting to a remote terminal at least 100 meters away. For receivers within a closer range, a more elaborate propagation model with a near field description of significant fidelity is required. Nonetheless, the process to be followed to solve the problem will largely be the same, albeit with more mathematical (as in numerical) complexity. In this chapter, we provide the theoretical background necessary to analyze this system, and we state the assumptions that we make in our analysis.

2.1 Theoretical Background

Figure 2.1 diagrams our generalized system setup. We label the coordinates of the transmit plane (ξ, η) and the coordinates of the receive plane (x, y). k and λ are the wavenumber and wavelength respectively of the transmitted light, where $k = \frac{2\pi}{\lambda}$. Throughout this thesis, we take λ to be 10^{-6} meters and thus consider specifically near-infrared communication. The receive plane is a distance L (in meters) away from the transmitter. We consider an aperture in the transmit plane with an input transmittance function $U_i(\xi, \eta)$ defined in the aperture region A_T.

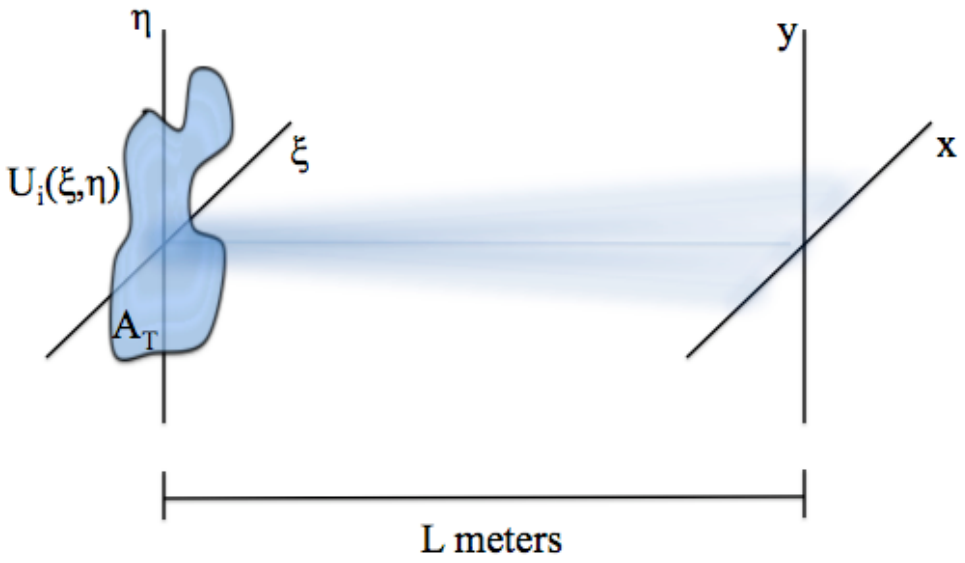

Figure 2.1 Diagram of near-infrared communication link analyzed in this thesis.

A detailed survey of scalar diffraction theory can be found in, e.g., Goodman [3]. We now briefly summarize the significant results. The propagation of a wave beyond an aperture with transmittance function $U_i(\xi,\eta)$ is described by the Fresnel-Kirchhoff diffraction formula and through a separate formulation by the Rayleigh-Sommerfeld diffraction formula. These formulas both justify the Huygens-Fresnel principle, which represents the output radiation pattern $U_o(x,y)$ in the receive plane as the superposition of spherical wavefronts derived from point sources at each point in the aperture.

Via appropriate approximations, these complicated formulas can be reduced to the much simpler Fresnel and Fraunhofer diffraction formulas. The Fresnel formula approximates the spherical wavefronts derived from the Huygens-Fresnel principle as parabolic wavefronts. The output radiation pattern under this approximation is given by

$$U_o(x,y) = \frac{e^{jkL}e^{j\frac{k}{2L}(x^2+y^2)}}{j\lambda L}\iint_{A_T}\left\{U_i(\xi,\eta)e^{j\frac{k}{2L}(\xi^2+\eta^2)}\right\}e^{-j\frac{2\pi}{\lambda L}(x\xi+y\eta)}d\xi d\eta$$

The Fresnel diffraction formula is sufficiently accurate when

$$L^3 \gg \frac{\pi}{4\lambda}\max((x-\xi)^2+(y-\eta)^2)^2$$

$$\forall\ (\xi,\eta) \text{ in the transmit aperture and } \forall \text{ observed } (x,y).$$

The Fraunhofer diffraction formula further simplifies the expression for the output radiation pattern, but requires a more stringent accuracy condition:

$$L \gg \max\left(\frac{k(\xi^2+\ \eta^2)}{2}\right)$$

$$\forall\ (\xi,\eta) \text{ in the transmit aperture.}$$

In the Fraunhofer limit, corresponding output radiation pattern $U_o(x,y)$ in the far-field receive plane is then defined by

$$U_o(x,y) = \frac{e^{jkL}e^{j\frac{k}{2L}(x^2+y^2)}}{j\lambda L}\iint\limits_{A_T} U_i(\xi,\eta)e^{-j\frac{2\pi}{\lambda L}(x\xi+y\eta)}d\xi d\eta$$

The intensity in the receive plane is then defined by

$$I_o(x,y) = \frac{\left|\iint_{A_T} U_i(\xi,\eta)e^{-j\frac{2\pi}{\lambda L}(x\xi+y\eta)}d\xi d\eta\right|^2}{\lambda^2 L^2}$$

If the receiver is located at $(x,y) = (0,0)$, the intensity at the receiver is

$$I_o(0,0) = \frac{\left|\iint_{A_T} U_i(\xi,\eta)d\xi d\eta\right|^2}{\lambda^2 L^2}$$

Given an optical aperture with a 1-centimeter diameter transmitting at a wavelength of 1 micron, the Fraunhofer diffraction pattern is valid for distances $L \gg 300$ meters. The "antenna designer's formula" loosens this constraint and requires instead that

$$L > \frac{2d^2}{\lambda},$$

where d is the diameter of the aperture [3]. Using this formula, we can use the Fraunhofer diffraction formula for any $L > 200$ meters. The largest diameter aperture we consider in this thesis is 6 centimeters. For this aperture, we can use the Fraunhofer diffraction formula for $L > 7200$ meters.

2.2 Idealized Filled Aperture Model

We now assume that we can control the transmittance function of an optical aperture with area A_T. Our goal is to find the optimum filled aperture transmittance function $U_i(\xi, \eta)$ that delivers maximum power to the intended receiver while suppressing the power delivered to a defined region in the receive plane. We therefore formulate the optimization problem that maximizes the intensity at the receiver $I_o(0,0)$ subject to $I_o(x, y) \leq \mathrm{I_T}$ for all (x, y) in the suppression region A_R^{supp}. $\mathrm{I_T}$ is the threshold to which the power in the suppression region must be limited. The input transmittance function is subject to a power constraint such that $\iint |U_i(\xi, \eta)|^2 \, d\xi d\eta = 1$.

The optimization problem can be constructed in two ways:

Maximize $\left|\iint_{A_T} U_i(\xi,\eta)d\xi d\eta\right|^2$

Subject to

(1) $\left|\iint_{A_T} U_i(\xi,\eta)e^{-j\frac{2\pi}{\lambda L}(x\xi+y\eta)}d\xi d\eta\right|^2 \leq \mathrm{I_T}\lambda^2L^2,\ \forall\ (x,y)\text{ in } A_R^{supp}$

or $\max_{(x,y)\text{ in }A_R^{supp}}\left(\iint_{A_T} U_i(\xi,\eta)e^{-j\frac{2\pi}{\lambda L}(x\xi+y\eta)}d\xi d\eta\right) \leq \mathrm{I_T}\lambda^2L^2$

(2) $\iint_{A_T}|U_i(\xi,\eta)|^2\,d\xi d\eta = 1$

Finding the optimum filled aperture transmittance function $U_{i\_opt}(\xi,\eta)$ that maximizes the power at the receiver while constraining the power to the entire suppression region to under some threshold is difficult: the problem either contains an infinite number of nonlinear inequality constraints (one for each point in A_R^{supp}) or a single inequality constraint of the form of a nontrivial maximum function (i.e. constraining the maximum intensity of the set of points in A_R^{supp}).

To simplify this problem, we only suppress power to a finite number of points (P) in the suppression region. If the set of P points in the desired suppression region is dense enough , we should be able to effectively limit the power to the entire region without actively constraining the power at each point. We show in Chapters 5 and 6 that the required density is dependent on the distance of the suppression region from the intended user. Let I_0 represent the receiver intensity we want to maximize:

$$I_0 = \iint_{A_T} U_i(\xi,\eta)d\xi d\eta \iint_{A_T} U_i{}^*(\xi,\eta)d\xi d\eta$$

Let J_i represent the intensity at a desired suppression point (x_i, y_i) for $1 \le i \le P$:

$$J_i = \iint_{A_T} U_i(\xi,\eta) e^{-j\frac{2\pi}{\lambda L}(x_i\xi + y_i\eta)} d\xi d\eta \iint_{A_T} U_i^*(\xi,\eta) e^{j\frac{2\pi}{\lambda L}(x_i\xi + y_i\eta)} d\xi d\eta \le \mathrm{I}_{\mathrm{T}} \lambda^2 L^2$$

Let H be the input power, normalized to 1.

$$H = \iint_{A_T} U_i(\xi,\eta) U_i^*(\xi,\eta)\, d\xi d\eta = 1$$

If the operator δ denotes the variation of a functional, and φ_i and μ are multipliers, then the necessary Karush-Kuhn-Tucker conditions for the optimization problem require that

$$\begin{cases} \delta I + \sum_{i=1}^{T} \varphi_i \delta J_i + \mu \delta H = 0 \\ \varphi_i (J_i - \mathrm{I}_{\mathrm{T}} \lambda^2 L^2) = 0, \qquad \forall\, 1 \le i \le P \\ \varphi_i \ge 0, \qquad \forall\, 1 \le i \le P \\ J_i \le \mathrm{I}_{\mathrm{T}} \lambda^2 L^2, \qquad \forall\, 1 \le i \le P \\ H = 1 \end{cases}$$

These conditions are shown in Appendix A to be equivalent to the following set of equations:

$$\begin{cases} 0 = \iint_{A_T} U_i(\xi,\eta)d\xi d\eta + \sum_{i=1}^{T} \varphi_i e^{j\frac{2\pi}{\lambda L}(x_i\xi + y_i\eta)} \iint_{A_T} U_i(\xi,\eta) e^{-j\frac{2\pi}{\lambda L}(x_i\xi + y_i\eta)} d\xi d\eta + \mu U_i(\xi,\eta) \\ \varphi_i \left(\iint_{A_T} U_i(\xi,\eta) e^{-j\frac{2\pi}{\lambda L}(x_i\xi + y_i\eta)} d\xi d\eta \iint_{A_T} U_i^*(\xi,\eta) e^{j\frac{2\pi}{\lambda L}(x_i\xi + y_i\eta)} d\xi d\eta - \mathrm{I}_{\mathrm{T}} \lambda^2 L^2 \right) = 0, \quad \forall\, 1 \le i \le P \\ \varphi_i \ge 0, \quad \forall\, 1 \le i \le P \\ \iint_{A_T} U_i(\xi,\eta) e^{-j\frac{2\pi}{\lambda L}(x_i\xi + y_i\eta)} d\xi d\eta \iint_{A_T} U_i^*(\xi,\eta) e^{j\frac{2\pi}{\lambda L}(x_i\xi + y_i\eta)} d\xi d\eta \le \mathrm{I}_{\mathrm{T}} \lambda^2 L^2, \quad \forall\, 1 \le i \le P \\ \iint_{A_T} U_i(\xi,\eta) U_i^*(\xi,\eta)\, d\xi d\eta = 1 \end{cases}$$

Even with only a finite number of constrained points in the suppression region, this large set of equations would be computationally very expensive to solve. Instead, a more practical solution may be to pre-determine a satisfactory output radiation pattern in the receive plane that satisfies the output constraints, and then find a corresponding input transmittance function that satisfies the input constraints and most closely approximates the desired output.

This reverse formulation of the problem could be approached in two ways. One, the suppression region of the output radiation pattern could be specified to some desired threshold I_T, or two, some amount of power could be subtracted from the maximum output radiation pattern in the suppression region. In both cases, the fact that the output radiation pattern is being changed means that the intensity at the receiver must decrease; whatever input function most closely results in such a pattern will not be the globally best function for maximizing the power

at the receiver. However, an input transmittance function that best approximates these output patterns given the input constraints could provide a reasonably high power at the receiver and acceptably low power in the suppression region.

Suppose $U_{i\_max}(\xi,\eta)$ is the transmittance function that leads to the maximum power at the receiver, located at $(x,y) = (0,0)$. If the input aperture area is A_T, then $U_{i\_max}(\xi,\eta) = \frac{1}{\sqrt{A_T}}$ for (ξ,η) in A_T^{aper}. The Cauchy-Schwarz Theorem implies that this is the optimal solution for maximizing power to the receiver under the input power constraint, $\iint |U_i(\xi,\eta)|^2 \, d\xi d\eta = 1$.

We assume the transmit aperture has shape $g(\xi,\eta)$, where

$$g(\xi,\eta) = \begin{cases} 1, & \text{in aperture (area } A_T) \\ 0, & \text{elsewhere} \end{cases}$$

The suppression region has shape $h(x,y)$ where

$$h(x,y) = \begin{cases} 1, & \text{in suppression region } A_R^{supp} \\ 0, & \text{elsewhere} \end{cases}$$

The output radiation pattern which maximizes power at the receiver while satisfying input power constraints is

$$U_{o\_max}(x,y) = \frac{e^{jkz} e^{\frac{jk}{2z}(x^2+y^2)}}{j\lambda z} \frac{1}{\sqrt{A_T}} \Im\{g(\xi,\eta)\}\big|_{f_x=\frac{x}{\lambda z}, f_y=\frac{y}{\lambda z}}$$

$U_{o\_supp}(x,y)$ describes an output pattern that is has a uniform intensity of $\mathrm{I_T}$ in the null region and zero elsewhere. Let $U_{o\_supp}(x,y)$ be defined by:

$$U_{o\_supp}(x,y) = \frac{e^{jkz} e^{\frac{jk}{2z}(x^2+y^2)}}{j\lambda z} \lambda z \sqrt{\mathrm{I_T}}\, h(x,y)$$

Ideally, the output radiation pattern $U_{o\_opt}(x,y)$ will be $U_{o\_supp}(x,y)$ inside the null region and $U_{o\_max}(x,y)$ every where else, including at the receiver.

$$U_{o\_opt}(x,y) = \begin{cases} U_{o\_max}(x,y), & \text{for } (x,y) \notin A_R^{supp} \\ U_{o\_supp}(x,y), & \text{for } (x,y) \exists A_R^{supp} \end{cases}$$

$$= U_{o\_supp}(x,y) + \big(1 - h(x,y)\big)U_{o\_max}(x,y)$$

Taking the inverse Fourier Transform to find the corresponding input transmittance function, we obtain

$$U_{i\_opt}(\xi,\eta) = \lambda z\sqrt{\mathrm{I_T}}\Im^{-1}\{h(x,y)\} + \frac{1}{\sqrt{A_T}}\, g(\xi,\eta) - \frac{1}{\sqrt{A_T}} g(\xi,\eta) * \Im^{-1}\{h(x,y)\}$$

This function is of infinite extent in the transmit plane, so it cannot be perfectly represented in the transmit aperture. However, before addressing this issue, we first show that the overall power used to generate the new output function is no more than the maximum power available, that is, $\iint \left|U_{i\_opt}(\xi,\eta)\right|^2 d\xi d\eta \leq 1$.

$$\iint \left|U_{i\_max}(\xi,\eta)\right|^2 d\xi d\eta = 1$$

$$\Longrightarrow \iint \left|U_{i\_opt}(\xi,\eta)\right|^2 d\xi d\eta \leq \iint \left|U_{i\_max}(\xi,\eta)\right|^2 d\xi d\eta$$

$$\Longrightarrow \iint \left|U_{o\_opt}(x,y)\right|^2 dxdy \leq \iint \left|U_{o\_max}(x,y)\right|^2 dxdy$$

We expand the left term of the inequality and note that the cross terms in the square product cancel.

$$\iint \left|U_{o\_opt}(x,y)\right|^2 dxdy = \iint \left|U_{o\_supp}(x,y) + \big(1-h(x,y)\big)U_{o\_max}(x,y)\right|^2 dxdy$$

$$= \iint \left|U_{o\_supp}(x,y)\right|^2 + \big(1-h(x,y)\big)\left|U_{o\_max}(x,y)\right|^2 dxdy$$

We know from the power constraint that

$$\iint \left|U_{o\_supp}(x,y)\right|^2 + \big(1-h(x,y)\big)\left|U_{o\_max}(x,y)\right|^2 dxdy \leq \iint \left|U_{o\_max}(\xi,\eta)\right|^2 d\xi d\eta$$

This power constraint reduces to

$$\iint \left|U_{o\_supp}(x,y)\right|^2 dxdy \leq \iint h(x,y)\left|U_{o\_max}(x,y)\right|^2 dxdy$$

A physical justification of this constraint follows. The output pattern that maximizes the power at the receiver uses all the available input power; in order for the new pattern to be physically viable, the power in the suppression region must have decreased. This constraint is therefore easy to satisfy because most desired output functions will have on average less power in the suppression region. Possible exceptions might occur if $U_{o\_max}(x,y)$ is very oscillatory in the suppression region, and the spatially averaged power in the region before suppression is less than the desired intensity threshold.

To minimize the squared error of the input transmittance function, the desired input function will be truncated such that

$$U_i(\xi,\eta) = g(\xi,\eta)U_{i_{opt}}(\xi,\eta)$$

$$U_i(\xi,\eta) = g(\xi,\eta)\left[\lambda z\sqrt{\mathrm{I_T}}\Im^{-1}\{h(x,y)\} + \frac{1}{\sqrt{A_T}}\, g(\xi,\eta) - \frac{1}{\sqrt{A_T}} g(\xi,\eta) * \Im^{-1}\{h(x,y)\}\right]$$

We want the power in both the first and third terms to be concentrated inside $g(\xi,\eta)$ to preserve as much information as possible before transmission. This is dependent on $h(x,y)$. If $h(x,y)$ has a gradual roll-off as opposed to sharp cutoff from 1 to 0 at the boundary of the suppression region, $\Im^{-1}\{h(x,y)\}$ will have more power inside $g(\xi,\eta)$. This would result in, e.g., an upward sloping acceptable threshold at the edges of the suppression region. After the truncation, the output radiation power will have changed slightly, and the power at the receiver will decrease, since the new input transmittance function is sub-optimum. The output radiation pattern will be

$$U_o(x,y) = G(x,y) * U_{o\_opt}(x,y)$$

where $G(x,y) = \Im\{\, g(\xi,\eta)\}$. This expression makes clear that increasing the size of the input aperture significantly improves the optimality of the suppression.

Practically, we cannot arbitrarily increase the size of the transmit aperture, nor can we exactly specify its transmittance function. We therefore need to discretize the aperture into sub-apertures of controllable amplitude and phase. In doing so, we can decrease the system cost by lowering the fill factor to form a sparse aperture array. This has the additional benefit of increasing the spatial diversity of the system and thus mitigating the effects of turbulence,

although it also creates grating lobes that may need to be suppressed. We devote the rest of this chapter to developing the sparse aperture transmitter model.

2.3 Sparse Aperture Model

The sparse aperture system as described in [1] is comprised of an array of n_{tx} rectangular apertures in the transmit plane transmitting a signal to an array of n_{rx} detectors in the receive plane. The power from a single laser source is divided via an optical power splitter among the n_{tx} transmitters. This optical power splitter controls the amplitude of the optical wave emitted by each transmitter. The phase of each wave is adjusted by a phase modulator connected to each aperture. The amplitude and phase are assumed constant over each aperture. The sparse aperture transmitter is diagrammed in Figure 2.2.

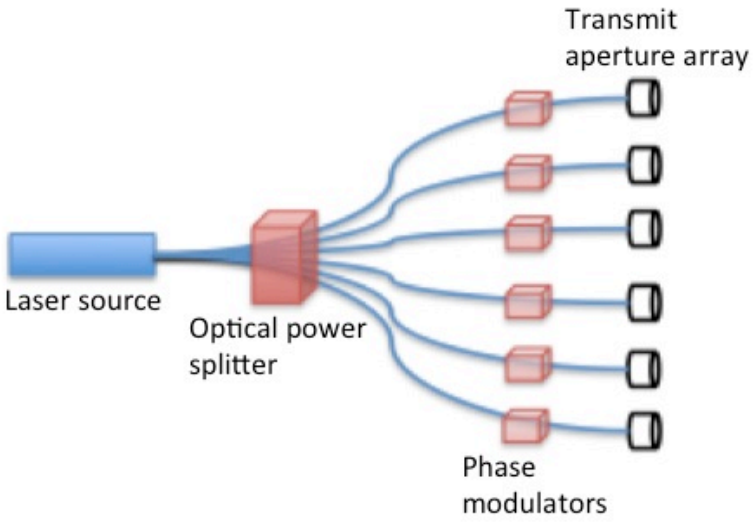

Figure 2.2 Light from a single laser source is divided by a variable optical power splitter and coupled into an array of apertures, each modulated by an independent phase modulator.

The scalar field of the optical wave emitted from each transmitter can be described in the far-field by the Fraunhofer diffraction pattern of a rectangular aperture. The radiation pattern from the entire sparse aperture transmitter is the sum of the scalar fields resulting from each of the n_{tx} apertures. The intensity at each point in the receive plane is proportional to the squared value of this sum.

Assuming we can control the amplitude and phase of each transmit aperture in the sparse aperture array, we can adjust these values to cause constructive or destructive interference at specific points in the receive plane. Specifically, we desire destructive interference in our desired suppression region and constructive interference at our intended receiver. Atmospheric turbulence randomizes this far-field radiation pattern. Statistical models describing the effects of atmospheric turbulence on laser beam propagation are presented in [4]. The optical beam emitted from the transmit apertures travels through an atmospheric channel with a time-varying index of refraction that affects the constructive and destructive interference in the receive plane. In this thesis, we neglect the effects of turbulence on the output. The effects of turbulence on the user's signal will be mostly mitigated by transmitter and receiver diversity; the signal in the suppression region may see some energy spikes, but they will not be of long enough duration to increase detectability significantly. We thus assume that adjusting the amplitudes and phases at each transmit aperture can to a considerable extent deterministically control the time-average of the far-field radiation pattern.

Adjusting the amplitudes and phases of each aperture in the transmit array can be treated similarly to the antenna gain patterning problem for RF phased arrays. The amplitude and relative phase of each aperture form the components of an n_{tx}-dimensional input vector $\vec{\boldsymbol{w}}$. A corresponding n_{tx}-dimensional vector $\vec{\boldsymbol{h}}$ can be formed where each component is the scalar field

in the receive plane resulting from a unit-amplitude signal from the corresponding aperture. The inner product of these two vectors is the scalar field resulting from the superposition of all n_{tx} apertures. In the RF case, each component of the second vector is a phase shift that is a function of position in the receive plane. For the optical apertures, each component is the Fraunhofer diffraction pattern for rectangular apertures shifted according to the corresponding aperture position.

Table 2.1 summarizes some parameters and functions we use in our analysis of the sparse aperture system model. We use this definitions for the remainder of the chapter.

h_{ik}	Scalar. The scalar field at location i in the receive plane that is derived from a unit-amplitude, zero-phase input from aperture k in the transmit plane.
N	Scalar. The number of apertures in the transmit array.
P	Scalar. The number of points used to define the suppression region. The number of points to which power is constrained.
$\vec{\boldsymbol{w}}$	N-dimensional column vector. $w_k = A_k e^{j\phi_k}$ is the amplitude and phase of aperture k. $\boldsymbol{w} = \begin{bmatrix} w_1 \\ w_2 \\ \vdots \\ w_N \end{bmatrix}$
$\overrightarrow{\boldsymbol{h_i}}$	N-dimensional row vector. The nth component h_{in} is the unit-amplitude, zero-phase contribution of the nth aperture to the field at point i. $\overrightarrow{\boldsymbol{h_i}} = [h_{i1} \quad h_{i2} \quad \ldots \quad h_{iN}]$
$\overrightarrow{\boldsymbol{h_i}} \cdot \vec{\boldsymbol{w}}$	Scalar. The total field at point i in receive plane. $\overrightarrow{\boldsymbol{h_i}} \cdot \vec{\boldsymbol{w}} = \sum_{j=1}^{N} h_{ij} w_j$
$\left\lvert \overrightarrow{\boldsymbol{h_i}} \cdot \vec{\boldsymbol{w}} \right\rvert^2$	Scalar. The intensity at point i.

Table 2.1: Summary of Relevant Functions and Parameters

2.3.1 Effects of Sparse Aperture Transmitter In Receive Plane

Assuming we can control the amplitude and phase of each transmit aperture in the sparse aperture array, we can adjust these values to constructively interfere at the receiver to direct maximum power to that location. For maximum power at the receiver, the input vector $\vec{\boldsymbol{w}}$ must be parallel to the scalar field vector evaluated at the intended receiver. Figure 2.3 shows an example radiation pattern from a linear aperture array when $\vec{\boldsymbol{w}}$ is chosen to maximize the intensity at $x = 0$. In order to create a complete null at a given point, $\vec{\boldsymbol{w}}$ must instead be orthogonal to the scalar field vector evaluated at the desired null. In [5], it is shown that the optimum input vector for complete cancellation at one or more nulls is found by projecting the scalar field vector evaluated at the intended receiver onto the nullspace of the subspace spanned by the scalar field vectors evaluated at the desired nulls. Figure 2.4 shows the output radiation pattern when $\vec{\boldsymbol{w}}$ is chosen to maximize power at $x = 0$ while completely nulling the signal at $x = 0.5$ beamwidths.

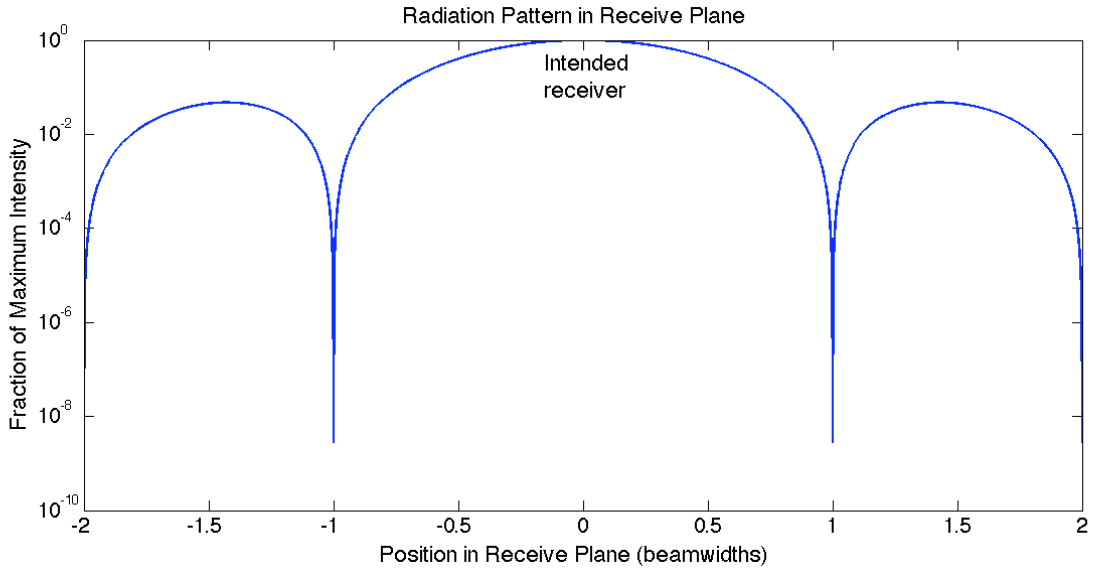

Figure 2.3 Example radiation pattern in receive plane with maximum power at the receiver.

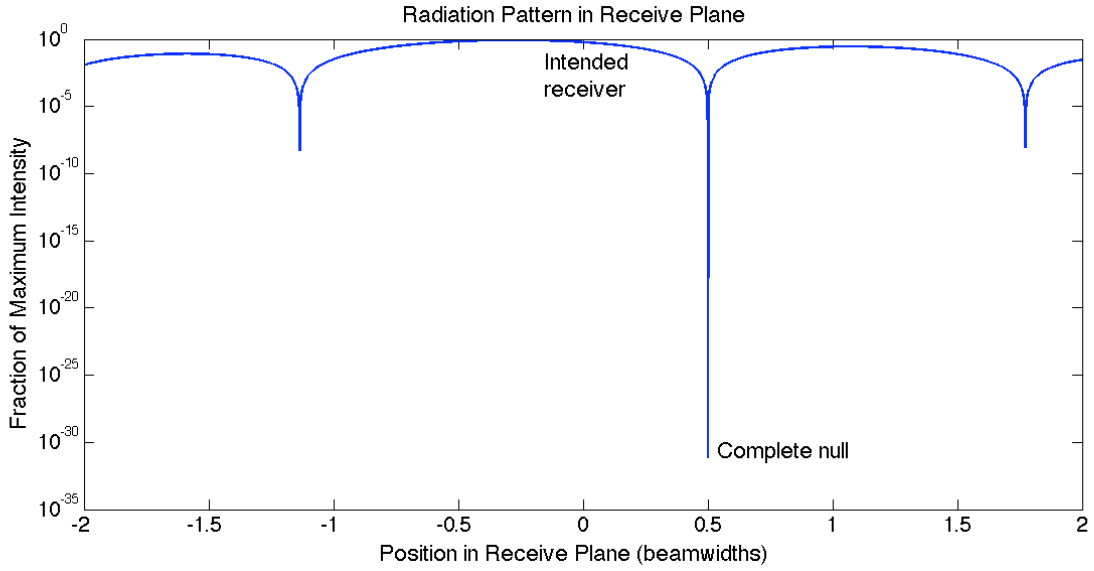

Figure 2.4 Example radiation pattern in receive plane with complete null at $x = 0.5$ beamwidths.

We now derive the optimum weight vector to maximize power to a single receiver and completely null multiple specified suppression points. Let U_{rx} be the scalar field at the receiver.

The power at the receiver is proportional to the square of U_{rx}. We constrain the value of the scalar field U_{supp_k} at each suppression point to zero.

Each component of $\vec{\boldsymbol{w}}$ is the amplitude and phase at a particular transmit aperture. $\vec{\boldsymbol{w}}$ is normalized such that $\sum_k \left| w_k e^{j\phi_k} \right|^2 = 1$.

$$\vec{\boldsymbol{w}} = \begin{bmatrix} w_1 e^{j\phi_1} \\ w_2 e^{j\phi_2} \\ \vdots \end{bmatrix}$$

We define a matrix

$$\boldsymbol{H} = \begin{bmatrix} h_{11} & h_{12} & h_{13} & \cdots \\ h_{21} & h_{22} & h_{23} & \ldots \\ \vdots & \ddots & & \end{bmatrix}$$

of which each component h_{ik} is the scalar field from aperture k at location i in the receive plane. Each h_{ik} is scaled by $w_k e^{j\phi_k}$, the amplitude and phase at aperture k. The sum of h_{ik} over all apertures k is the scalar field at location i. The first row of $\boldsymbol{H}$ contains the scalar field from each aperture at the receiver in location $i = 1$; the subsequent rows contain the scalar fields at the desired suppression points. Thus we need to find $\vec{\boldsymbol{w}}$ that satisfies the following equation and maximizes U_{rx}.

$$\begin{bmatrix} U_{rx} \\ 0 \\ 0 \\ \vdots \end{bmatrix} = \begin{bmatrix} h_{11} & h_{12} & h_{13} & \cdots \\ h_{21} & h_{22} & h_{23} & \ldots \\ \vdots & \ddots & & \end{bmatrix} \begin{bmatrix} w_1 e^{j\phi_1} \\ w_2 e^{j\phi_2} \\ \vdots \end{bmatrix}$$

To solve this, we define a matrix

$$\boldsymbol{H'} = \begin{bmatrix} h_{21} & h_{22} & h_{23} & \cdots \\ h_{31} & h_{32} & h_{33} & \ldots \\ \vdots & \ddots & & \end{bmatrix}$$

Then $\boldsymbol{H'}\ \vec{\boldsymbol{w}} = 0$.

The optimum value of $\vec{\boldsymbol{w}}$ maximizes

$$\overrightarrow{\boldsymbol{h_1}} \cdot \vec{\boldsymbol{w}} = U_{rx}$$

under the suppression constraint

$$\boldsymbol{H'}\ \vec{\boldsymbol{w}} = 0$$

and the normalization condition

$$\sum_k \left| w_k e^{j\phi_k} \right|^2 = 1$$

If there is only a single desired null to constrain, the above reduces to:

$$\begin{bmatrix} U_{rx} \\ 0 \end{bmatrix} = \begin{bmatrix} h_{11} & h_{12} & h_{13} & \cdots \\ h_{21} & h_{22} & h_{23} & \ldots \end{bmatrix} \begin{bmatrix} A_1 e^{j\phi_1} \\ A_2 e^{j\phi_2} \\ A_3 e^{j\phi_3} \\ \vdots \end{bmatrix}$$

If $\overrightarrow{\boldsymbol{h_2}} \cdot \vec{\boldsymbol{w}} = 0$ and $\sum_k \left| w_k e^{j\phi_k} \right|^2 = 1$, then $\overrightarrow{\boldsymbol{h_1}} \cdot \vec{\boldsymbol{w}}$ is maximized by finding the normalized projection of $\overrightarrow{\boldsymbol{h_1}}$ onto the nullspace of $\overrightarrow{\boldsymbol{h_2}}$ (or $\boldsymbol{H'}$ in multiple null case).

$$\boldsymbol{S} = \text{Nullspace}\left(\overrightarrow{\boldsymbol{h_2}}\right) = \begin{bmatrix} \frac{-h_{22}}{h_{21}} & \frac{-h_{24}}{h_{21}} & \frac{-h_{23}}{h_{21}} & \dots \\ 1 & 0 & 0 & \dots \\ 0 & 1 & 0 & \dots \\ 0 & 0 & 1 & 0 \\ \vdots & \vdots & 0 & \ddots \end{bmatrix}$$

The projection matrix $\boldsymbol{P} = \boldsymbol{S}(\boldsymbol{S^T S})^{-1}\boldsymbol{S^T}$ is given by

$$\frac{1}{\sum_{i=1}^{N} h_{2i}} \begin{bmatrix} \sum_{i=1}^{n}(h_{2i})^2 - {h_{21}}^2 & -h_{22}h_{21} & -h_{23}h_{21} & -h_{24}h_{21} & \dots & -h_{2N}h_{21} \\ -h_{21}h_{22} & \sum_{i=1}^{n}(h_{2i})^2 - {h_{22}}^2 & -h_{23}h_{22} & -h_{24}h_{22} & \dots & -h_{2N}h_{22} \\ -h_{21}h_{23} & -h_{22}h_{23} & \sum_{i=1}^{n}(h_{2i})^2 - {h_{23}}^2 & -h_{24}h_{23} & \dots & -h_{2N}h_{23} \\ -h_{21}h_{24} & -h_{22}h_{24} & -h_{23}h_{24} & \ddots & & -h_{2N}h_{24} \\ \vdots & \vdots & \vdots & & \ddots & \vdots \\ -h_{21}h_{2N} & -h_{22}h_{2N} & -h_{23}h_{2N} & \dots & \dots & \sum_{i=1}^{N}(h_{2i})^2 - {h_{2N}}^2 \end{bmatrix}$$

The projection $\vec{\boldsymbol{p}}$ of $\overrightarrow{\boldsymbol{h_1}}$ onto $\boldsymbol{S}$ is given by

$$\boldsymbol{P} \cdot \overrightarrow{\boldsymbol{h_1}} = \frac{1}{\sum_{i=1}^{N} h_{2i}} \begin{bmatrix} h_{11}\left(\sum_{i=1}^{N}(h_{2i})^2 - {h_{21}}^2\right) - h_{21}\left(\sum_{i=1}^{N}(h_{1i}h_{2i}) - h_{1j}h_{2j}\right) \\ h_{12}\left(\sum_{i=1}^{N}(h_{2i})^2 - {h_{22}}^2\right) - h_{22}\left(\sum_{i=1}^{N}(h_{1i}h_{2i}) - h_{1j}h_{2j}\right) \\ \vdots \\ h_{1N}\left(\sum_{i=1}^{N}(h_{2i})^2 - {h_{2n}}^2\right) - h_{2N}\left(\sum_{i=1}^{N}(h_{1i}h_{2i}) - h_{1j}h_{2j}\right) \end{bmatrix}$$

We normalize $\vec{\boldsymbol{p}}$ to find $\vec{\boldsymbol{w}}$.

$$\vec{\boldsymbol{w}}_{null} = \frac{\vec{p}}{|\vec{p}|}$$

Recalling that

$$\vec{\boldsymbol{w}}_{max} = \frac{\overrightarrow{h_1}}{|\overrightarrow{h_1}|}$$

we can calculate the fraction of power remaining at the receiver after completely nulling a single suppression point.

$$\frac{(\overrightarrow{h_1} \cdot \vec{w}_{null})^2}{(\overrightarrow{h_1} \cdot \vec{w}_{max})^2} = \frac{(\overrightarrow{h_1} \cdot \vec{w}_{null})^2}{\sum_{i=1}^{n}(h_{1i}^* h_{1i})}$$

$$= \frac{1}{\sum_{i=1}^{N}(h_{1i}^* h_{1i})}\left(\frac{\sum_{j=1}^{N}\left[h_{1j}^* h_{1j}\left(\sum_{i=1}^{N}(h_{2i}^* h_{2i}) - {h_{2j}}^2\right) - h_{2j} h_{1j}\left(\sum_{i=1}^{N}(h_{1i}^* h_{2i}) - h_{1j}^* h_{2j}\right)\right]}{\sum_{j=1}^{N}\left[h_{1j}^* h_{1j}\left(\sum_{i=1}^{N}(h_{2i}^* h_{2i}) - {h_{2j}}^2\right) - h_{2j} h_{1j}\left(\sum_{i=1}^{N}(h_{1i}^* h_{2i}) - h_{1j}^* h_{2j}\right)\right]^2}\right)^2$$

In Figure 2.4 we see that the power at the receiver has somewhat decreased after the signal has been suppressed at the desired null. The decrease in power at the receiver should be a function of the distance of the null from the receiver and also the number of such nulls. If the desired null is very close to the receiver, in order to suppress power to that point, the power directed to the receiver will be correspondingly small. If the desired null is very far away from the receiver, the receiver should receive the same amount of power as if there were no

constrained suppress point. The more points that are deliberately nulled, the lower we expect the power at the receiver to be.

In practice, it is unnecessary to place complete nulls at points within the suppression region. Instead, we can limit the power at these points to some fraction of the power at the receiver and then scale the transmit power such that the intended receiver can detect the signal. This could successfully prevent interference in an optical wireless network where all the users had similar receivers. If another user were in the suppression region, a signal intended for it would be significantly greater and could be distinguished from the interfering signal.

It is harder to prevent interception than friendly interference, since an eavesdropper could increase his receive aperture size to counter the effects of the signal suppression. However, suppressing the power to a potential eavesdropper to some fraction of the power at the receiver would make it much more difficult for the eavesdropper to intercept the signal. The more the signal is suppressed, the more expensive interception will be for the eavesdropper, and the more secure the transmission will be. In general, ensuring confidential transmission would require multiple anti-eavesdropping strategies, such as, e.g., transmitting a high-amplitude noise signal in the direction of the eavesdropper in addition to suppressing the signal in that direction (this is briefly treated in Chapter 8).

2.3.2 Optimization Problem Setup

We now formulate the nonlinear optimization problem whose solution is the optimum input vector $\vec{\boldsymbol{w}}$. The optimum $\vec{\boldsymbol{w}}$ will maximize the power at the receiver while maintaining an upper limit on the power ratio between each suppression point and the receiver. We label the

receiver's position v, and the P suppression points are labeled $u_1, u_2, \ldots, u_P$. The desired signal-to-suppression power ratio is $1/R$. The optimization problem is then constructed as follows.

Maximize $|\boldsymbol{h}_v \cdot \boldsymbol{w}|^2$

subject to

(1) $\dfrac{|\boldsymbol{h}_{u_k}\boldsymbol{w}|^2}{|\boldsymbol{h}_v\boldsymbol{w}|^2} \leq \mathrm{R}, \qquad \forall\ 1 \leq k \leq P$

(2) $|\boldsymbol{w}|^2 = 1$

The following is an expansion of the objective function.

$$f_0(\vec{\boldsymbol{w}}) = |\boldsymbol{h}_v\boldsymbol{w}|^2 = \boldsymbol{w}^\dagger \boldsymbol{h}_v{}^\dagger \boldsymbol{h}_v\boldsymbol{w}$$

We user Wirtinger derivatives to calculate the gradient of the objective function with respect to $\vec{\boldsymbol{w}}$, so we can construct the Karush-Kuhn-Tucker conditions using standard differential calculus. (See [10] for a treatment of Wirtinger calculus; a similar analysis is presented in [5] as the method of complex gradients). The gradient of the objective function is then defined as below.

$$\frac{\partial f_0}{\partial \boldsymbol{w}^*} = \boldsymbol{h}_v{}^\dagger \boldsymbol{h}_v\boldsymbol{w}$$

There are P inequality constraints, one for each suppression point, defined as follows.

$$f_k(\vec{\boldsymbol{w}}) = \frac{|\boldsymbol{h}_{u_k}\boldsymbol{w}|^2}{|\boldsymbol{h}_v\boldsymbol{w}|^2} - R = \frac{\boldsymbol{w}^\dagger \boldsymbol{h}_{u_k}{}^\dagger \boldsymbol{h}_{u_k}\boldsymbol{w}}{\boldsymbol{w}^\dagger \boldsymbol{h}_v{}^\dagger \boldsymbol{h}_v\boldsymbol{w}} - \mathrm{R} \leq 0$$

Again using Wirtinger derivatives, we calculate the gradient of the inequality constraints.

$$\frac{\partial f_k}{\partial \boldsymbol{w}^*} = \frac{\left(\boldsymbol{w}^\dagger {\boldsymbol{h}_v}^\dagger \boldsymbol{h}_v \boldsymbol{w}\right)\left({\boldsymbol{h}_{u_k}}^\dagger \boldsymbol{h}_{u_k} \boldsymbol{w}\right) - \left(\boldsymbol{w}^\dagger {\boldsymbol{h}_{u_k}}^\dagger \boldsymbol{h}_{u_k} \boldsymbol{w}\right)\left({\boldsymbol{h}_v}^\dagger \boldsymbol{h}_v \boldsymbol{w}\right)}{\left(\boldsymbol{w}^\dagger {\boldsymbol{h}_v}^\dagger \boldsymbol{h}_v \boldsymbol{w}\right)^2}$$

Lastly, we require that the input vector the be normalized such that its 2-norm is equal to 1.

$$h(\vec{\boldsymbol{w}}) = |\boldsymbol{w}|^2 - 1 = \boldsymbol{w}^\dagger \boldsymbol{w} - 1 = 0$$

The gradient of this equality constraint is as follows.

$$\frac{\partial h}{\partial \boldsymbol{w}^*} = \boldsymbol{w}$$

Although this normalization seems on the surface equivalent to the power constraint required in the filled aperture problem formulation, that equivalence only holds if the area of each aperture is kept constant. Since we may be varying the total number of apertures and the size of apertures as we consider different fill factors, the weight constraint we employ will not result in equal transmit power from every system even if the total array area stays the same. In order to compare the intensity in the receive plane between different aperture configurations, we will need to divide the intensity by the area of a single aperture within the array. This will effectively normalize each output radiation pattern to the same transmit power.

It can also be of interest to instead normalize each output radiation pattern by the maximum achievable intensity at the intended receiver. If we do this, we can compare the relative decrease in power at the intended receiver for different aperture configurations with varying suppression constraints. This will allow us to note which aperture configurations are most sensitive to various parameters.

The Karush-Kuhn-Tucker necessary conditions for the optimization problem follow.

$$\begin{cases} \dfrac{\boldsymbol{w}^{\dagger}\boldsymbol{h_{u_k}}^{\dagger}\boldsymbol{h_{u_k}}\boldsymbol{w}}{\boldsymbol{w}^{\dagger}\boldsymbol{h_v}^{\dagger}\boldsymbol{h_v}\boldsymbol{w}} - \mathrm{R} \;\; \leq 0, & \forall\, 1 \leq k \leq T \text{ null points} \\ \lambda_k \;\geq 0, & \forall\, 1 \leq k \leq T \text{ null points} \\ \lambda_k \left(\dfrac{\boldsymbol{w}^{\dagger}\boldsymbol{h_{u_k}}^{\dagger}\boldsymbol{h_{u_k}}\boldsymbol{w}}{\boldsymbol{w}^{\dagger}\boldsymbol{h_v}^{\dagger}\boldsymbol{h_v}\boldsymbol{w}} - \mathrm{R} \right) \;= 0, & \forall\, 1 \leq k \leq T \text{ null points} \\ \boldsymbol{w}^{\dagger}\boldsymbol{w} - 1 = 0 & \\ \boldsymbol{h_v}^{\dagger}\boldsymbol{h_v}\boldsymbol{w} + \displaystyle\sum_{k=1}^{T} \lambda_k \frac{\left(\boldsymbol{w}^{\dagger}\boldsymbol{h_v}^{\dagger}\boldsymbol{h_v}\boldsymbol{w}\right)\left(\boldsymbol{h_{u_k}}^{\dagger}\boldsymbol{h_{u_k}}\boldsymbol{w}\right) - \left(\boldsymbol{w}^{\dagger}\boldsymbol{h_{u_k}}^{\dagger}\boldsymbol{h_{u_k}}\boldsymbol{w}\right)\left(\boldsymbol{h_v}^{\dagger}\boldsymbol{h_v}\boldsymbol{w}\right)}{\left(\boldsymbol{w}^{\dagger}\boldsymbol{h_v}^{\dagger}\boldsymbol{h_v}\boldsymbol{w}\right)^{2}} + \mu\boldsymbol{w} = 0 & \end{cases}$$

The optimization problem is formulated such that we seek to maximize instead of minimize a convex function. The objective function is monotonically non-decreasing from $\vec{\boldsymbol{w}} = \vec{\boldsymbol{0}}$. Further, it is monotonically increasing along the direction of $\overrightarrow{\boldsymbol{h_v}}$. Since the normalization constraint on the weight vector is a hollow N-dimensional sphere, the optimum input vector in the absence of a designated suppression region lies at the intersection of this sphere and $\alpha\overrightarrow{\boldsymbol{h_v}}$ for some α. (α must be $\frac{1}{|\overrightarrow{\boldsymbol{h_v}}|}$ if the 2-norm of $\vec{\boldsymbol{w}} = 1$.) As the normalized $\vec{\boldsymbol{w}}$ approaches $\overrightarrow{\boldsymbol{h_v}}$, the value of the objective function increases. Thus the optimum input vector is the vector $\vec{\boldsymbol{w}}$ that is closest to $\overrightarrow{\boldsymbol{h_v}}$ while still satisfying all inequality constraints. Determining the input vectors that satisfy the inequality constraints is less straightforward. The inequality constraints are rational functions, the ratio of two quadratic expressions. The closer (in the Euclidean metric space) that $\overrightarrow{\boldsymbol{h_v}}$ is to the space spanned by suppression vectors $\overrightarrow{\boldsymbol{h_{u_k}}}$ ($\forall\, 1 \leq k \leq P$), the smaller the set of input vectors that satisfy all the inequality constraints.

Although the objective function is a simple quadratic expression, the inequality and equality constraints are not affine functions, and therefore we cannot obtain an analytical solution using quadratic programming techniques. Further complicating matters, the vectors $\boldsymbol{h_v}$ and $\boldsymbol{h_{u_k}}$ do not have a simple relationship with many of the system parameters of interest. Thus there is no simple method of converging to a global optimum nor an easily obtained analytical formula that can exactly describe the effect of various system parameters on the achievability of different suppression constraints.

Therefore, the optimum weight vector for any particular system must be obtained numerically. In the next chapter, we analyze a toy example to predict the effect of various system parameters on the intensity at the receiver after suppression and the achievable signal-to-suppression-region power ratio. We later compare these predictions with our numerical results. In Chapters 5-6, we solve several numerical examples with varying system parameters to shed light on the issues involved in using this method to suppress a desired area. In Chapter 7, we generalize the trends we observe and discuss the design considerations they reveal.

Chapter 3

Analysis of Toy Example

We consider a transmitter with two square apertures and one suppression point. We constrain the input vector such that $\overrightarrow{\boldsymbol{w}} \in \mathbb{R}^2$ and similarly constrain the receiver and suppression vectors to the real domain. We now define the major parameters for this example.

$$\overrightarrow{\boldsymbol{h_v}} = \begin{bmatrix} b\cos\gamma \\ b\sin\gamma \end{bmatrix}$$

$$\overrightarrow{\boldsymbol{h_u}} = \begin{bmatrix} a\cos\theta \\ a\sin\theta \end{bmatrix}$$

$$\overrightarrow{\boldsymbol{w}} = \begin{bmatrix} x \\ y \end{bmatrix}$$

for $a < b$ and $R < 1$

As we discussed in Chapter 2, the objective function we want to maximize is $|\boldsymbol{h_v} \cdot \boldsymbol{w}|^2$. Figure 3.1 depicts an example objective function.

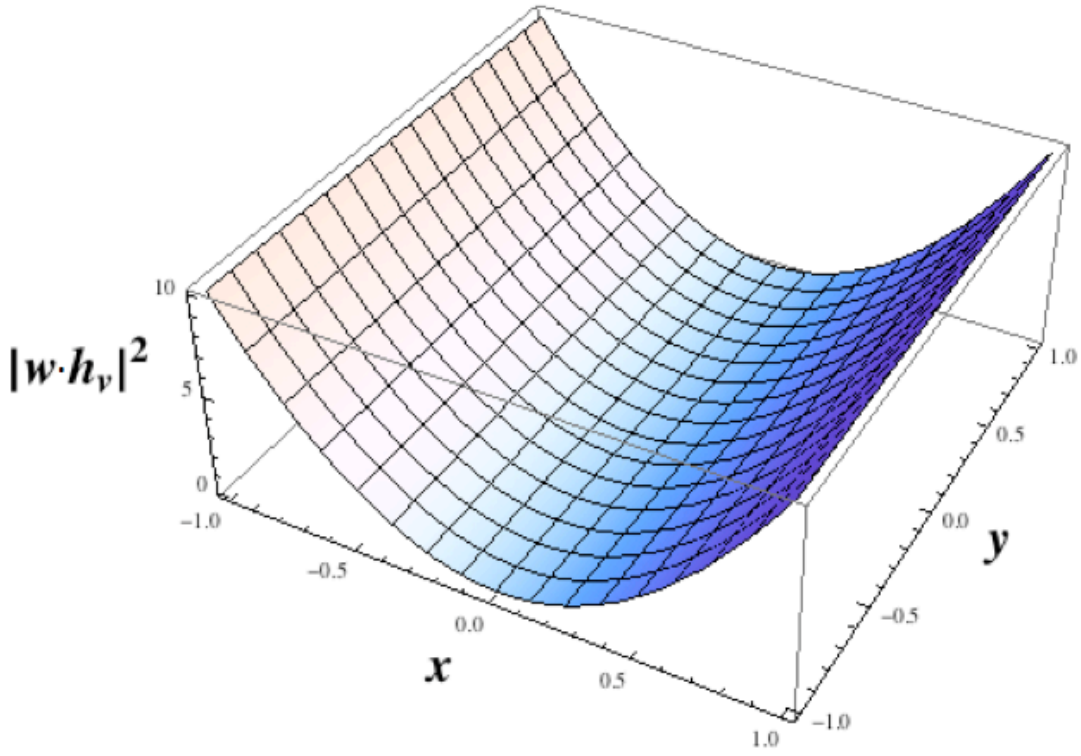

Figure 3.1 An example objective function where $\overrightarrow{\boldsymbol{h_v}} = \begin{bmatrix} 10 \\ 0 \end{bmatrix}$.

The inequality constraint restricts the power sent in the direction of $\overrightarrow{\boldsymbol{h_u}}$, and can be expanded as follows:

$$\frac{|\boldsymbol{h_u} \cdot \boldsymbol{w}|^2}{|\boldsymbol{h_v} \cdot \boldsymbol{w}|^2} \leq R$$

$$\frac{(ax\cos\theta + ay\sin\theta)^2}{(bx\cos\gamma + by\sin\gamma)^2} \leq R$$

$$(ax\cos\theta + ay\sin\theta)^2 \leq R(bx\cos\gamma + by\sin\gamma)^2$$

Figure 3.2 shows a rational function of the intensity at the suppression point divided by the intensity at the receiver for varying $\vec{\boldsymbol{w}}$. The figure also shows four dotted lines representing possible weight vectors. The purple line shows weight vectors that would be parallel to h_v, i.e.

weight vectors that maximize power towards the receiver. The red line shows weight vectors that are perpendicular to h_v and thus completely cancel power to the receiver. The yellow line marks weight vectors that would be parallel to h_u and would therefore maximize power to the desired suppression point; the green line marks weight vectors that are orthogonal to h_u and cancel power to the desired suppression point.

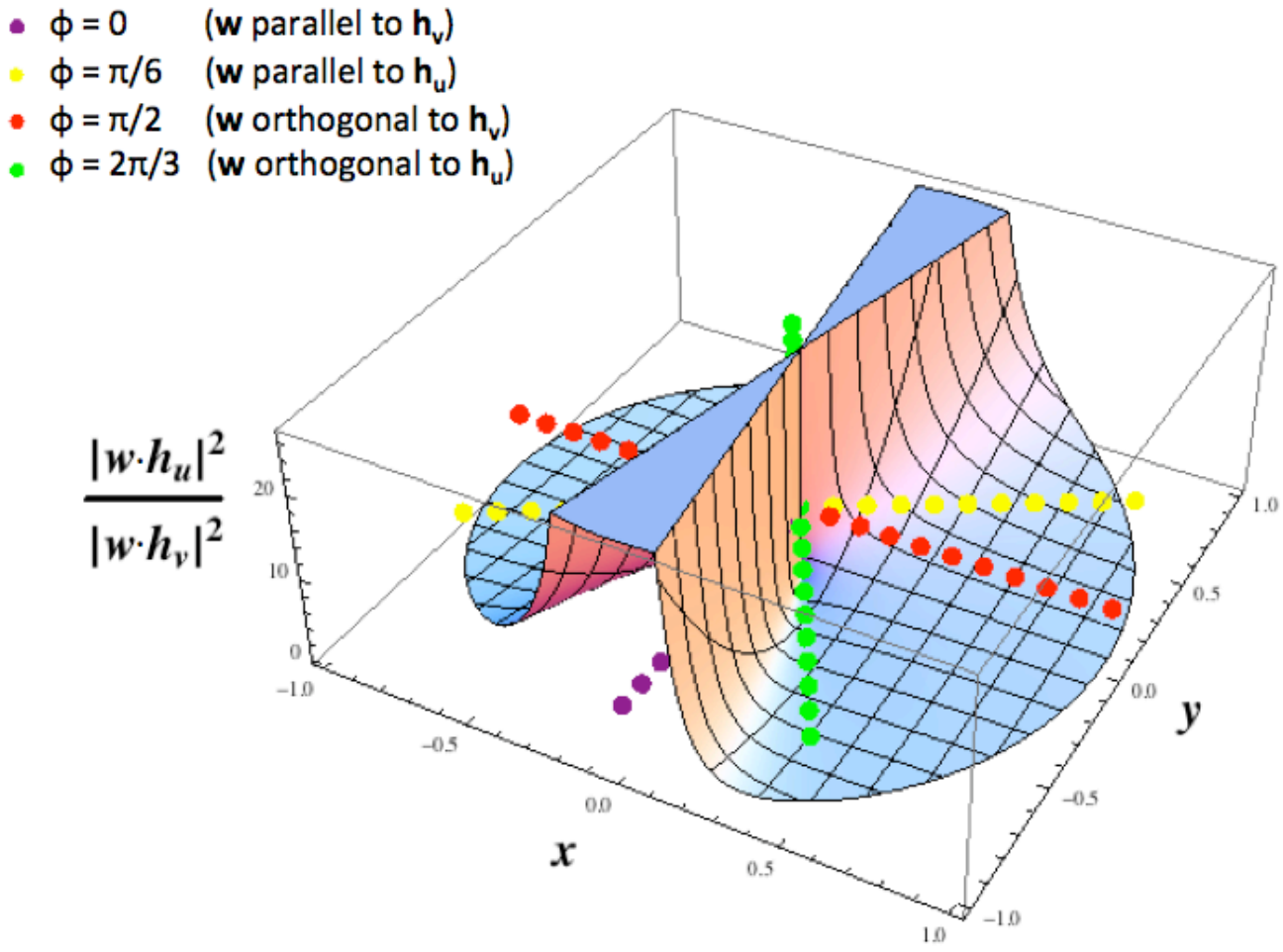

Figure 3.2 The ratio of the intensity at the suppression point to the intensity at the receiver. The inequality constraint is satisfied when this function is less than some $R < 1$. In this example, $\overrightarrow{\boldsymbol{h_v}} = \begin{bmatrix} 10 \\ 0 \end{bmatrix}$ and $\overrightarrow{\boldsymbol{h_u}} = \begin{bmatrix} 5\cos\left(\frac{\pi}{6}\right) \\ 5\sin\left(\frac{\pi}{6}\right) \end{bmatrix}$.

Without loss of generality, we let $\gamma = 0$ such that $\theta = \measuredangle(\overrightarrow{\boldsymbol{h_u}}, \overrightarrow{\boldsymbol{h_v}})$. As before, we normalize $\overrightarrow{\boldsymbol{w}}$ so $x^2 + y^2 = 1$. We can then write $x = \cos\phi$ and $y = \sin\phi$. The feasible region becomes all values of ϕ that satisfy the following equations.

$$(ax\cos\theta + ay\sin\theta)^2 \leq R(bx)^2$$

$$(a\cos\phi\cos\theta + a\sin\phi\sin\theta)^2 \leq R(b\cos\phi)^2$$

$$\boxed{\frac{\boldsymbol{a^2\cos^2(\phi-\theta)}}{\boldsymbol{Rb^2}} \leq \boldsymbol{\cos^2\phi}}$$

Figure 3.3 plots the feasible region of the optimization problem for three different values of $\theta = \measuredangle(\overrightarrow{\boldsymbol{h_u}}, \overrightarrow{\boldsymbol{h_v}})$. We slightly modify the weight constraint to $x^2 + y^2 \leq 1$. As θ approaches $\frac{\pi}{2}$, the range of possible feasible values of ϕ increases and ϕ approaches 0 (recall $\gamma = 0$.) In each of the plots in Figure 3.3, the yellow line marks the weight vectors that are parallel to h_v, and the red line marks the weight vectors that are parallel to h_u. It is clear that as the angle θ between these two lines increases, the angle ϕ between the feasible weight vectors and h_v decreases. This indicates that the power at the receiver after suppression increases as θ increases.

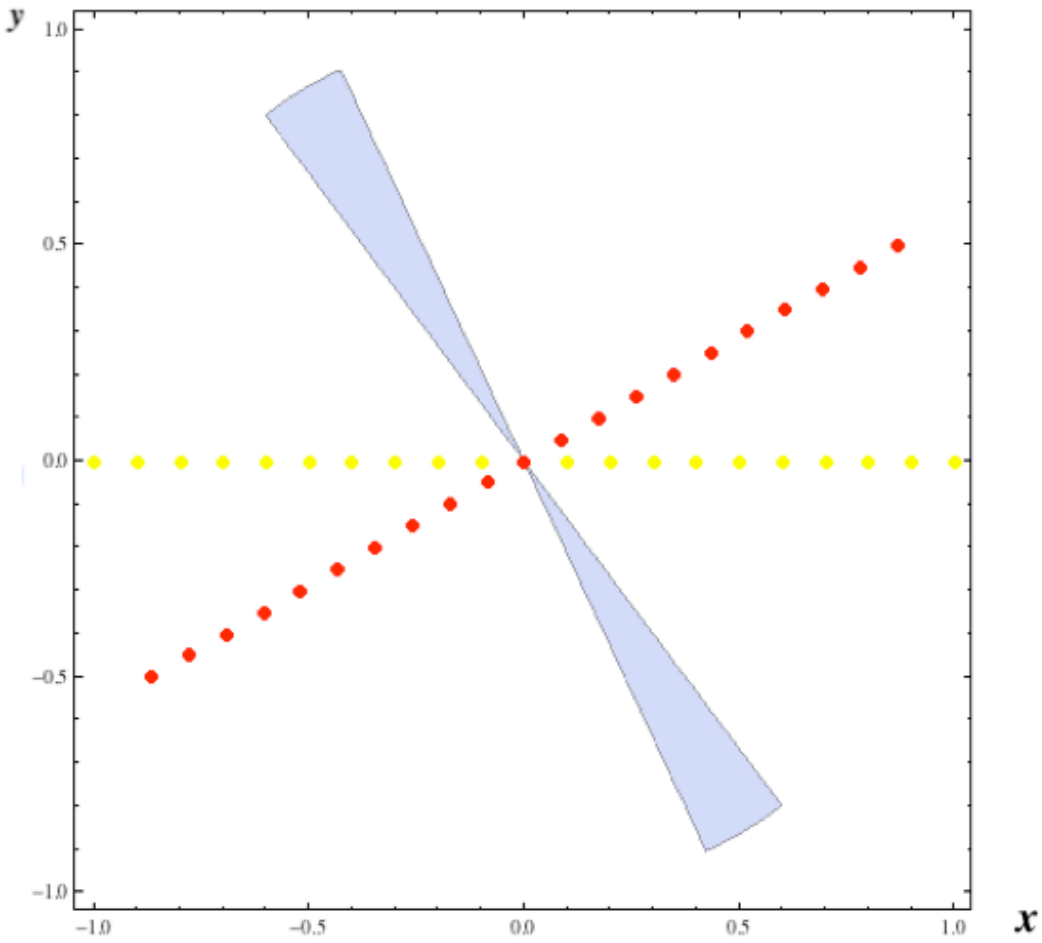

Figure 3.3a Feasible region for $a = 5, b = 10, \theta = \frac{\pi}{6}$.

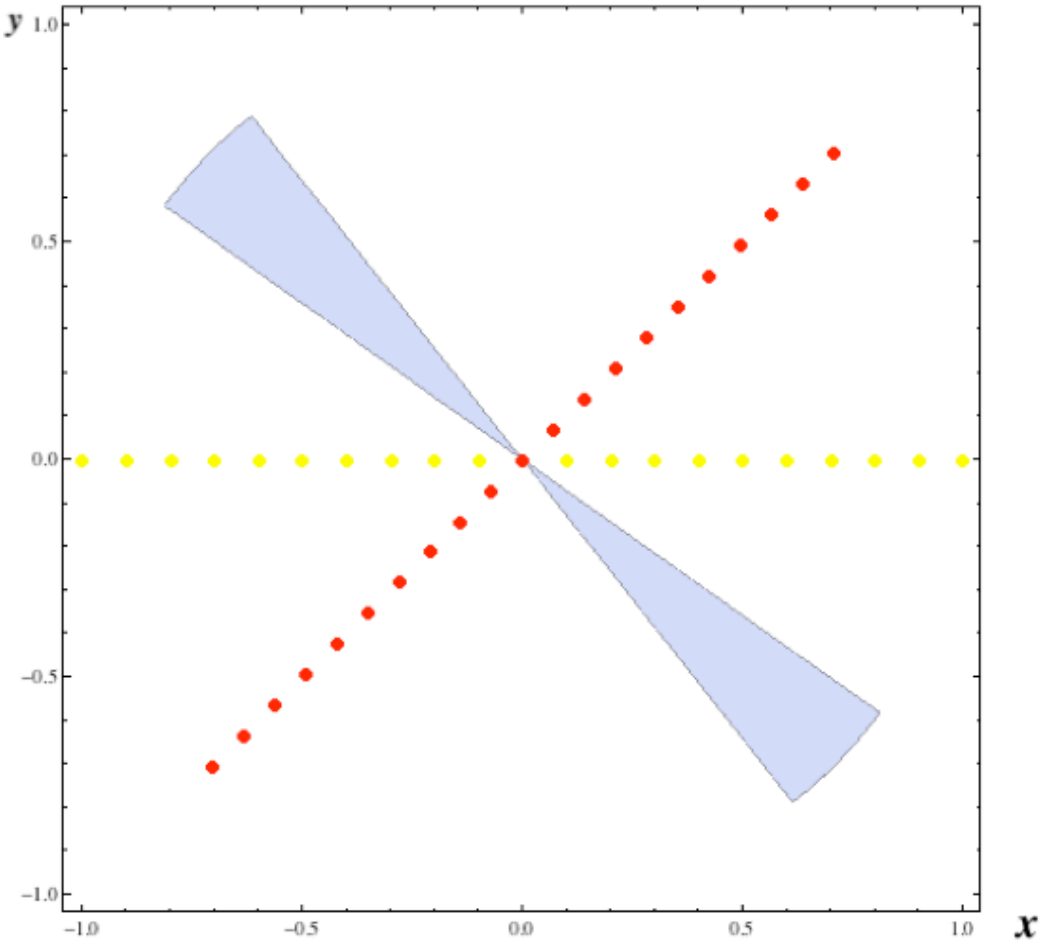

Figure 3.3b Feasible region for $a = 5, b = 10, \theta = \frac{\pi}{4}$.

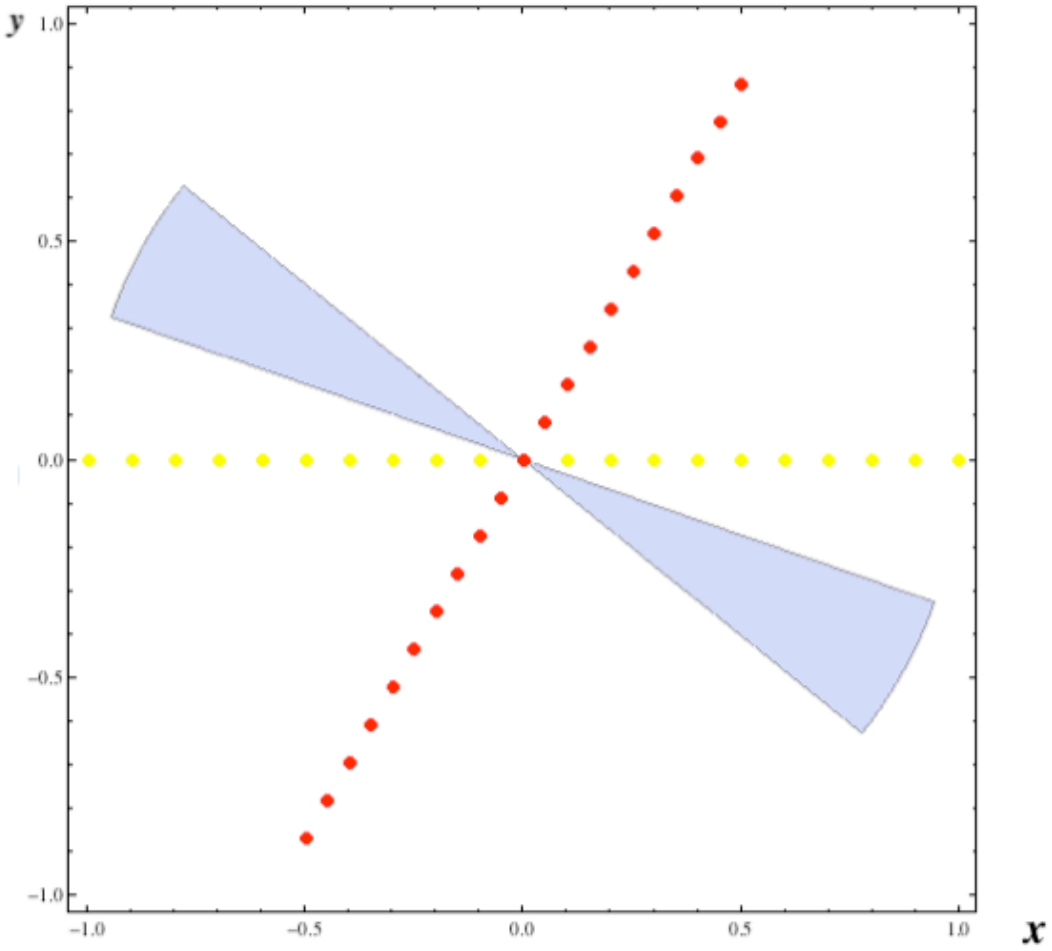

Figure 3.3c Feasible region for $a = 5, b = 10, \theta = \frac{\pi}{3}$.

In order to determine which point in the feasible region maximizes the objective function, we turn to the complementary slackness condition of the KKT conditions. This condition requires that one of the following conditions be satisfied.

1.) In Case 1, the inequality constraint is satisfied when maximum power is directed at receiver, so no suppression is necessary. Since the objective function $|\boldsymbol{h_v} \cdot \boldsymbol{w}|^2 = bx^2$ is monotonically increasing along exactly one dimension, we find the solution to the optimization problem by following the objective function along this increasing dimension until it intersects the weight constraint $x^2 + y^2 = 1$.

2.) In Case 2, the inequality constraint is not satisfied when maximum power directed at receiver. Suppression is necessary. The solution lies at the boundary of the inequality constraint and the weight constraint, along the increasing dimension of the objective function.

CASE 1:

If the equality constraint satisfied, $x^2 + y^2 = 1$. To maximize bx^2,

$$x = \pm 1, y = 0$$

$$\boldsymbol{w} = \begin{bmatrix} \pm 1 \\ 0 \end{bmatrix} \Longrightarrow \phi = 0$$

The inequality constraint is satisfied in this case if

$$\frac{a^2 \cos(\theta)}{b^2 R} \leq 1$$

Given $\overrightarrow{\boldsymbol{h_v}} = \begin{bmatrix} b \\ 0 \end{bmatrix}$, we want to know for what $\overrightarrow{\boldsymbol{h_u}}$ is the solution in case 1.

$$a^2 \cos^2(\theta) \leq b^2 R$$

$$|\boldsymbol{h_u}|^2 \cos^2(\theta) \leq |\boldsymbol{h_v}|^2 R$$

$$\cos^2(\theta) \leq \frac{|\boldsymbol{h_v}|^2}{|\boldsymbol{h_u}|^2} R$$

This is always true if

$$\frac{|\boldsymbol{h_v}|^2}{|\boldsymbol{h_u}|^2} \geq \frac{1}{R} = SSR_{desired}$$

which occurs if the ratio of the receiver intensity to the suppression point intensity before suppression is greater than the desired signal-to-suppression-region power ratio, independent of the angle between the two vectors. In other words, Case 1 holds if the suppression point is sufficiently far away from the intended receiver.

Case 1 is also true if

$$c \leq \theta \leq c'$$

$$c = \cos^{-1}\left(\frac{|h_v|}{|h_u|}\sqrt{R}\right)$$

$$c' = 2\pi - c$$

This expression bounds the angle θ between $\overrightarrow{\boldsymbol{h_v}}$ and $\overrightarrow{\boldsymbol{h_u}}$ to a region around $\frac{\pi}{2}$, whose size is dependent on the desired signal-to-suppression region power ratio and the pre-suppression ratio between the receiver and the suppression point. In reality, of course, we cannot separate θ and the amplitudes of $\overrightarrow{\boldsymbol{h_u}}$. However, in this example, we consider them separately under the assumption that b represents the envelope of $|\boldsymbol{h_u}|$ that generally decreases as the suppression point moves further away from the receiver, while θ represents the oscillations – maxima and nulls – within that envelope.

CASE 2:

Again, the equality constraint satisfied, and $x^2 + y^2 = 1$. This time the inequality constraint is satisfied with equality, such that

$$\frac{a^2 \cos^2(\phi - \theta)}{Rb^2} = \cos^2 \phi$$

Let $f(\phi) = \cos^2 \phi$.

$$\frac{a^2}{b^2 R} f(\phi - \theta) = f(\phi)$$

$$0 \leq f(\phi) \leq 1$$

$$\Longrightarrow 0 \leq \frac{a^2}{b^2 R} f(\phi - \theta) \leq \frac{a^2}{b^2 R}$$

$$\Longrightarrow 0 \leq f(\phi) \leq \frac{a^2}{b^2 R}$$

$$\frac{a^2}{b^2 R} = \frac{|h_u|^2}{|h_v|^2} \cdot \frac{1}{R}$$

$$\frac{b^2}{a^2} = SSR_{pre-suppression} \Longrightarrow \frac{a^2}{b^2} \cdot \frac{1}{R} = \frac{SSR_{desired}}{SSR_{pre-suppression}}$$

If $\frac{a^2}{Rb^2} \leq 1$, the condition in Case 1 would be satisfied, no suppression would be necessary. The solution to the maximum $|h_v w|^2$ would be as in Case 1. Therefore, for the solution in Case 2 to be valid, $\frac{a^2}{b^2 R} > 1$, and therefore:

$$SSR_{desired} > SSR_{pre-suppression}$$

However, since the inequality constraint is satisfied with equality and $f(\phi) \leq 1$,

$$\frac{a^2}{b^2 R} f(\phi - \theta) \leq 1$$

$$f(\phi - \theta) \leq \frac{b^2}{a^2 R} = \frac{SSR_{pre-suppression}}{SSR_{desired}}$$

The solution to $\frac{a^2 \cos^2(\phi-\theta)}{Rb^2} = \cos^2 \phi$ in Case 2 therefore occurs when $f(\phi - \theta) \leq \frac{b^2}{a^2 R}$.

Figure 3.4 shows an example region in which this condition is true. This region is symmetric about $\theta = \frac{\pi}{2}$ and shrinks in size as $\frac{SSR_{pre-suppression}}{SSR_{desired}}$ decreases, which happens as the suppression point moves closer to the receiver, and/or when the desired signal-to-suppression region power ratio increases. This suggests that $\overrightarrow{\boldsymbol{w}}$ must be "more orthogonal" to $\overrightarrow{\boldsymbol{h_u}}$ as the pre-suppression ratio decreases or as the desired post-suppression ratio increases.

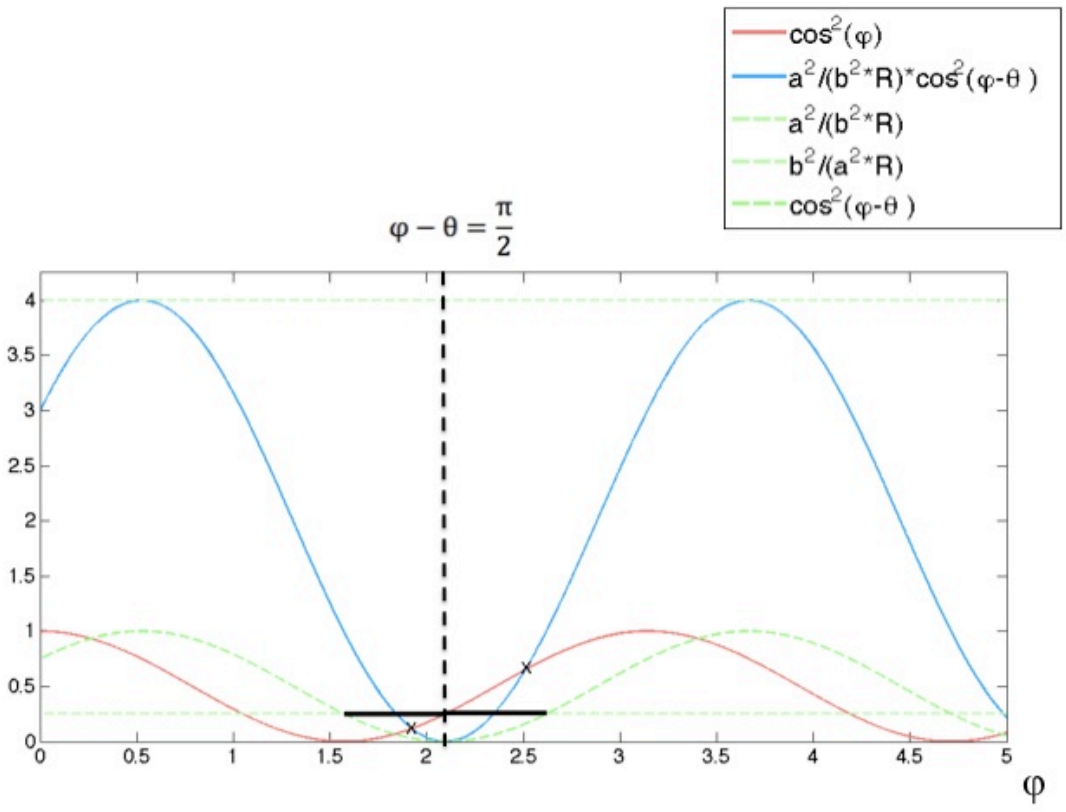

Figure 3.4 The region where $f(\phi-\theta) \leq \frac{b^2}{a^2R}$ is marked in black. This region is symmetric about $\phi-\theta$. The solutions to $\frac{a^2\cos^2(\phi-\theta)}{Rb^2} = \cos^2\phi$ are marked with X's. As $\frac{a^2}{Rb^2}$ increases, these solutions move closer to $\phi-\theta$.

To simplify the numerical calculations, we want to relax the weight constraint to an inequality constraint $x^2+y^2 \leq 1$. If we do so, we have to consider a third case in which the signal-to-suppression region power ratio constraint is satisfied with equality but the weight constraint were slack. We now show that there is no solution that could lie in this region without satisfying the weight constraint with equality. In other words, the solution to Case 3 is the same solution as for Case 2.

CASE 3:

We now relax the weight constraint to an inequality and review the implication of such a change. For many practical numerical algorithms, inequality and equality constraints must be handled separately, so relaxing the equality constraint could improve numerical performance.

Let $x = k\cos\phi$ and $y = k\sin\phi$, for $k \leq 1$. The inequality constraint with a relaxed weight constraint is

$$\frac{a^2\, k^2 \cos^2(\phi - \theta)}{Rb^2} = k^2 \cos^2\phi$$

The value of ϕ here is the same as in Case 2, so the objective function $bx^2 = bk^2\cos^2\phi$ is maximized at $k = 1$, which is when the equality constraint is exactly satisfied. Figure 3.5 shows both a contour plot and a 3D plot of an example feasible region that confirms our conclusions in Case 2 and Case 3.

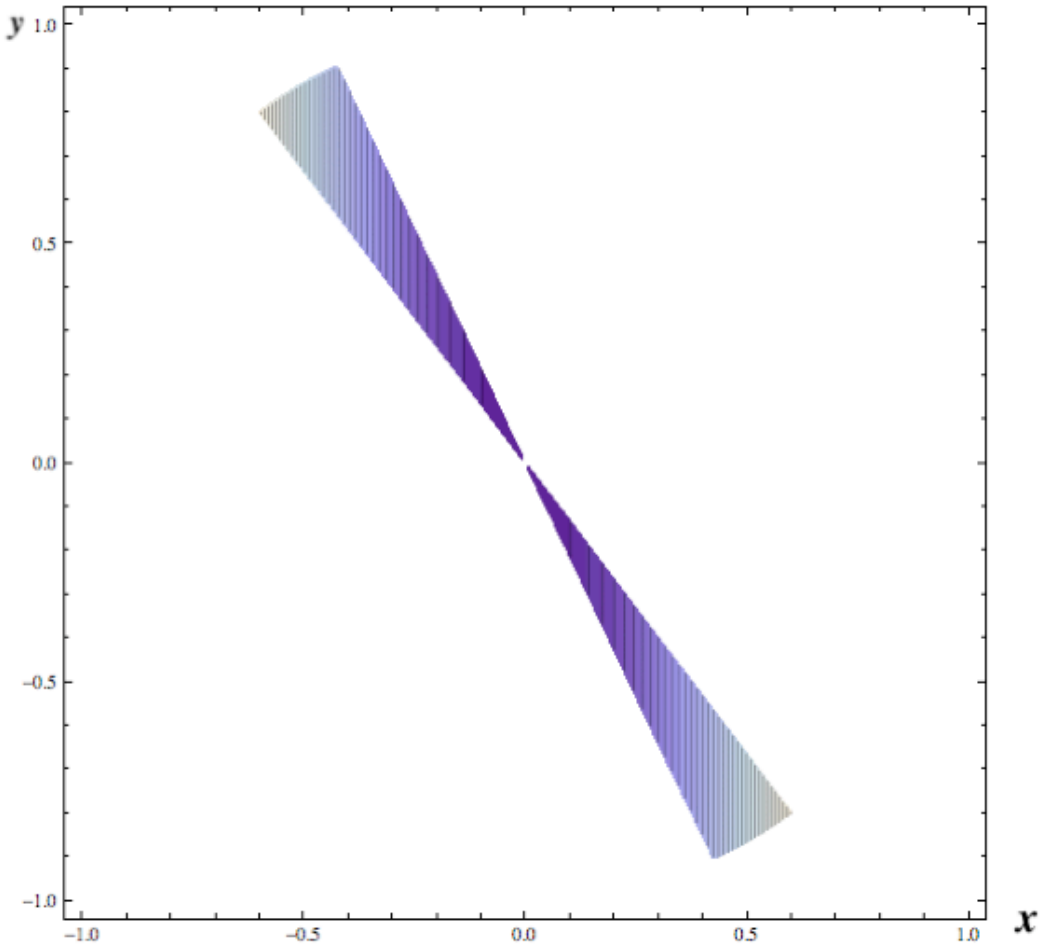

Figure 3.5a This is the same feasible region as in Figure 3.3a, with $a = 5, b = 10, \theta = \frac{\pi}{6}$. The lighter colors indicate higher objective function values. The two highest values occur in the bottom right and top left corners. These two locations have the exact same function value, and the two weight vectors are related by a constant phase difference of exactly π radians.

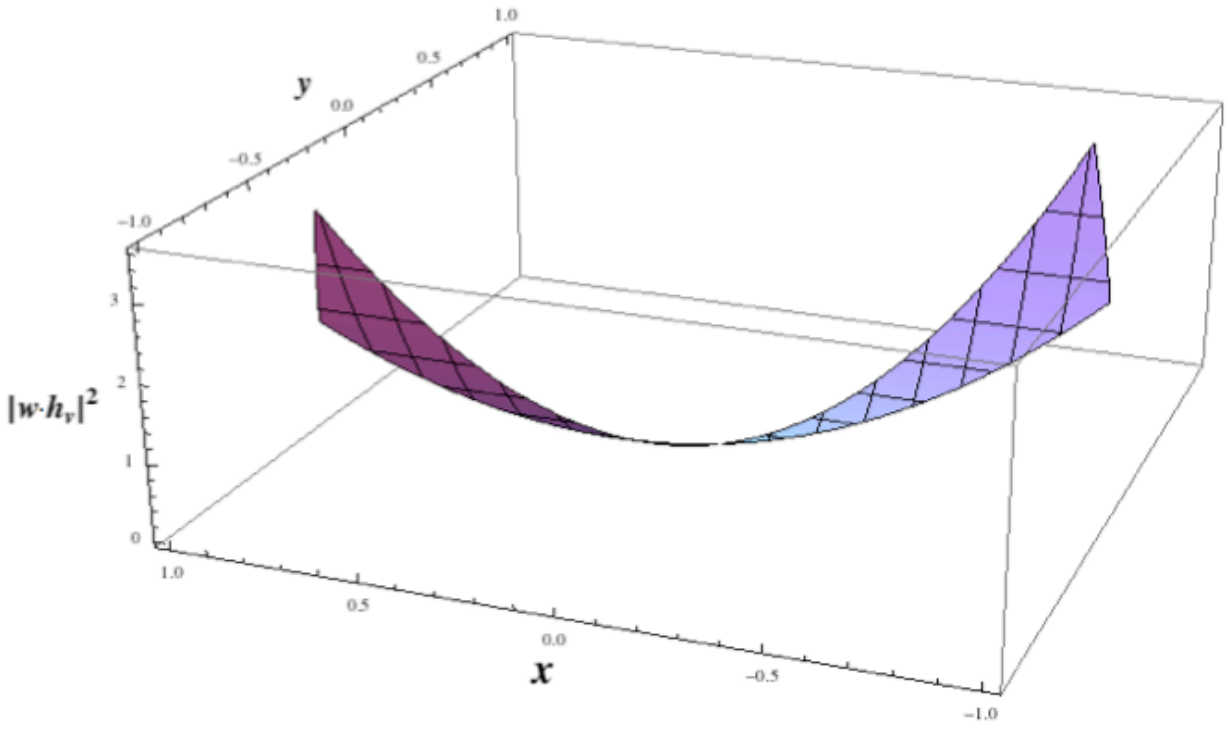

Figure 3.5b This is the same feasible region as in Figure 3.3a, with $a = 5, b = 10, \theta = \frac{\pi}{6}$. The overall shape of the objective function in the feasible region is more evident here. The two peaks have the height.

We now derive an expression for the change in the intensity at the receiver caused by a change in angle between $\overrightarrow{\boldsymbol{h_v}}$ and $\vec{\boldsymbol{w}}$. We first show how ϕ change as θ changes, i.e. how the angle between $\overrightarrow{\boldsymbol{h_v}}$ and $\vec{\boldsymbol{w}}$ changes with the angle between $\overrightarrow{\boldsymbol{h_v}}$ and $\overrightarrow{\boldsymbol{h_u}}$. Although we cannot solve the suppression constraint exactly for ϕ in terms of θ, we can find the derivative $\frac{d\phi}{d\theta}$. We use this result to find $\frac{dq}{d\theta}$, where q denotes the intensity at the receiver.

$$\frac{d\phi}{d\theta} = \frac{\partial\phi}{\partial R}\frac{\partial R}{\partial\theta}$$

$$\frac{\partial R}{\partial\theta} = \frac{a^2}{b^2\cos^2\phi}\frac{d}{d\theta}\cos^2(\phi-\theta)$$

$$= \frac{-2a^2\cos(\phi-\theta)\sin(\phi-\theta)}{b^2\cos^2\phi}$$

$$\frac{\partial R}{\partial\phi} = \frac{b^2\cos^2\phi\,(-2a^2\cos(\phi-\theta)\sin(\phi-\theta)) - a^2\cos^2(\phi-\theta)\,(2b^2\sin\phi\cos\phi)}{(b^2\cos^2\phi)^2}$$

$$= -2a^2b^2\frac{(\cos^2\phi\cos(\phi-\theta)\sin(\phi-\theta) + \cos^2(\phi-\theta)\sin\phi\cos\phi)}{b^4\cos^4\phi}$$

$$\frac{\partial\phi}{\partial R}\frac{\partial R}{\partial\theta} = \frac{b^4\cos^4\phi\,(-2a^2\cos(\phi-\theta)\sin(\phi-\theta))}{-2a^2b^2(\cos^2\phi\cos(\phi-\theta)\sin(\phi-\theta) + \cos^2(\phi-\theta)\sin\phi\cos\phi)b^2\cos^2\phi}$$

$$= \frac{\cos\phi\sin(\phi-\theta)}{\cos\phi\sin(\phi-\theta) + \cos(\phi-\theta)\sin\phi}$$

$$= \frac{\cos\phi\sin(\phi-\theta)}{\sin(2\phi-\theta)}$$

$$= \frac{1}{2}\frac{(\sin(2\phi-\theta) - \sin\theta)}{\sin(2\phi-\theta)}$$

$$\boxed{\frac{d\phi}{d\theta} = \frac{1}{2} - \frac{\sin\theta}{2\sin(2\phi - \theta)}}$$

Let q represent the intensity at the receiver.

$$q = |h_v w|^2 = b^2 x^2 = b^2 \cos^2\phi$$

$$\frac{dq}{d\theta} = \frac{dq}{d\phi}\frac{d\phi}{d\theta} = -b^2 \cos\phi \sin\phi \left(1 - \frac{\sin\theta}{\sin(2\phi - \theta)}\right)$$

$$\boxed{\frac{dq}{d\theta} = -\frac{b^2}{2}\sin 2\phi \left(1 - \frac{\sin\theta}{\sin(2\phi - \theta)}\right)}$$

For this expression to be useful to us, we must show that, at least in this example, θ has an approximately linear relationship with the distance u between the receiver and the eavesdropper. We cannot directly compute $\frac{dq}{du}$, but we can use $\frac{dq}{d\theta}$ to analyze $\frac{dq}{du}$.

We now expand the components of $\overrightarrow{\boldsymbol{h_v}}$ and $\overrightarrow{\boldsymbol{h_u}}$ using the Fraunhofer diffraction pattern of square apertures. d is the half-width of the apertures; the receiver is a distance L away from the transmitter array.

$$\overrightarrow{\boldsymbol{h_v}} = \begin{bmatrix} e^{j\left(kL-\frac{\pi}{2}+\frac{k}{2L}(x_1^2+y_1^2)\right)} 4d^2 \dfrac{1}{\lambda L} \operatorname{sinc}\left(\dfrac{2dx_1}{\lambda L}\right) \operatorname{sinc}\left(\dfrac{2dy_1}{\lambda L}\right) \\ \\ e^{j\left(kL-\frac{\pi}{2}+\frac{k}{2L}(x_2^2+y_2^2)\right)} 4d^2 \dfrac{1}{\lambda L} \operatorname{sinc}\left(\dfrac{2dx_2}{\lambda L}\right) \operatorname{sinc}\left(\dfrac{2dy_2}{\lambda L}\right) \end{bmatrix}$$

$$\overrightarrow{\boldsymbol{h_u}} = \begin{bmatrix} e^{j\left(kL-\frac{\pi}{2}+\frac{k}{2L}\left((x_1-u_x)^2+(y_1-u_y)^2\right)\right)} 4d^2 \dfrac{1}{\lambda L} \operatorname{sinc}\left(\dfrac{2d(x_1-u_x)}{\lambda L}\right) \operatorname{sinc}\left(\dfrac{2d(y_1-u_y)}{\lambda L}\right) \\ \\ e^{j\left(kL-\frac{\pi}{2}+\frac{k}{2L}\left((x_2-u_x)^2+(y_2-u_y)^2\right)\right)} 4d^2 \dfrac{1}{\lambda L} \operatorname{sinc}\left(\dfrac{2d(x_2-u_x)}{\lambda L}\right) \operatorname{sinc}\left(\dfrac{2d(y_2-u_y)}{\lambda L}\right) \end{bmatrix}$$

where (x_1, y_1) and (x_2, y_2) represent the positions of the two apertures and (u_1, u_2) represent the suppression point position. Let $y_1 = 0$, $y_2 = 0$, and $u_y = 0$. If $\overrightarrow{\boldsymbol{h_v}}$ and $\overrightarrow{\boldsymbol{h_u}}$ were both in $\mathbb{R}^2$, we could use the following expression to find the angle between the two vectors.

$$\cos\theta = \frac{\boldsymbol{h_v} \cdot \boldsymbol{h_u}}{\|\boldsymbol{h_v}\|\|\boldsymbol{h_u}\|}$$

Instead, we consider the dot product of the two vectors as a measurement of their parallelism.

$$\boldsymbol{h_v h_u} = \left(\frac{4d^2}{\lambda L}\right)^2 e^{j\left(kL-\frac{\pi}{2}+\frac{k}{2L}x_1^2\right)}\mathrm{sinc}\left(\frac{2dx_1}{\lambda L}\right)e^{j\left(kL-\frac{\pi}{2}+\frac{k}{2L}(x_1-u)^2\right)}\mathrm{sinc}\left(\frac{2d(x_1-u)}{\lambda L}\right)$$

$$+\left(\frac{4d^2}{\lambda L}\right)^2 e^{j\left(kL-\frac{\pi}{2}+\frac{k}{2L}x_2^2\right)}\mathrm{sinc}\left(\frac{2dx_2}{\lambda L}\right)e^{j\left(kL-\frac{\pi}{2}+\frac{k}{2L}(x_2-u)^2\right)}\mathrm{sinc}\left(\frac{2d(x_2-u)}{\lambda L}\right)$$

$$= \left(\frac{4d^2}{\lambda L}\right)^2 e^{j\left(2kL-\pi+\frac{k}{2L}(x_1^2+(x_1-u)^2)\right)}\mathrm{sinc}\left(\frac{2dx_1}{\lambda L}\right)\mathrm{sinc}\left(\frac{2d(x_1-u)}{\lambda L}\right)$$

$$+\left(\frac{4d^2}{\lambda L}\right)^2 e^{j\left(2kL-\pi+\frac{k}{2L}(x_2^2+(x_2-u)^2)\right)}\mathrm{sinc}\left(\frac{2dx_2}{\lambda L}\right)\mathrm{sinc}\left(\frac{2d(x_2-u)}{\lambda L}\right)$$

$$= \frac{16d^4}{(\lambda L)^2}e^{j(2kL-\pi)}\left[e^{j\frac{k}{2L}(2x_1^2-2x_1u+u^2)}\mathrm{sinc}\left(\frac{2dx_1}{\lambda L}\right)\mathrm{sinc}\left(\frac{2d(x_1-u)}{\lambda L}\right)\right.$$

$$\left.+\, e^{j\frac{k}{2L}(2x_2^2-2x_2u+u^2)}\mathrm{sinc}\left(\frac{2dx_2}{\lambda L}\right)\mathrm{sinc}\left(\frac{2d(x_2-u)}{\lambda L}\right)\right]$$

Let $x_1 = -x_2$ so the two apertures are equidistant around the origin along the x-axis and thus also centered with respect to the receiver. Let $H = \boldsymbol{h_v} \cdot \boldsymbol{h_u}$.

$$H = \boldsymbol{h_v} \cdot \boldsymbol{h_u} = \frac{16d^4}{(\lambda L)^2} e^{j\left(2kL - \pi + \frac{k}{2L}u^2\right)} \operatorname{sinc}\left(\frac{2dx_1}{\lambda L}\right) \left[e^{j\frac{k}{L}(x_1(x_1-u))} \operatorname{sinc}\left(\frac{2d(x_1-u)}{\lambda L}\right) + e^{j\frac{k}{L}(x_2(x_2-u))} \operatorname{sinc}\left(\frac{2d(x_2-u)}{\lambda L}\right) \right]$$

$$= \frac{16d^4}{(\lambda L)^2} e^{j\left(2kL - \pi + \frac{k}{2L}u^2\right)} \operatorname{sinc}\left(\frac{2dx_1}{\lambda L}\right) \left[e^{j\frac{k}{L}(x_1(x_1-u))} \operatorname{sinc}\left(\frac{2d(x_1-u)}{\lambda L}\right) + e^{j\frac{k}{L}(x_1(x_1+u))} \operatorname{sinc}\left(\frac{2d(x_1+u)}{\lambda L}\right) \right]$$

$$= \frac{16d^4}{(\lambda L)^2} e^{j\left(2kL - \pi + \frac{k}{2L}u^2 + \frac{k}{L}x_1^2\right)} \operatorname{sinc}\left(\frac{2dx_1}{\lambda L}\right) \left[e^{-j\frac{k}{L}x_1 u} \operatorname{sinc}\left(\frac{2d(x_1-u)}{\lambda L}\right) + e^{j\frac{k}{L}x_1 u} \operatorname{sinc}\left(\frac{2d(x_1+u)}{\lambda L}\right) \right]$$

$$\frac{dH}{du} = \frac{1}{L^3\lambda^2} 8d^4 e^{j\frac{k}{2L}(4L^2+u^2-2ux_1+2x_1^2)} \mathrm{sinc}\left(\frac{2dx_1}{\lambda L}\right) \left(L \left(\frac{2\cos\left(\frac{2d(x_1-u)}{\lambda L}\right)}{x_1-u} \right.\right.$$

$$+ \frac{2e^{2j\frac{k}{L}ux_1}\cos\left(\frac{2d(x_1+u)}{\lambda L}\right)}{x_1+u}$$

$$\left. + \frac{L\lambda}{d}\left(-\frac{\sin\left(\frac{2d(x_1-u)}{\lambda L}\right)}{(u-x_1)^2} + \frac{e^{2j\frac{k}{L}ux_1}\sin\left(\frac{2d(x_1+u)}{\lambda L}\right)}{(u+x_1)^2} \right) \right)$$

$$\left. - 2jk(u-x_1)\mathrm{sinc}\left(\frac{2d(x_1-u)}{\lambda L}\right) - 2je^{2j\frac{k}{L}ux_1}k(x_1+u)\mathrm{sinc}\left(\frac{2d(x_1+u)}{\lambda L}\right) \right)$$

Within a certain range of the receiver (i.e. within the main lobe), the dot product of $\boldsymbol{h_u}$ and $\boldsymbol{h_v}$ decreases with increasing distance u between the receiver and the suppression point. The arccosine of the absolute value of this dot product increases linearly within that range. (See Figure 3.6 for example plots of these relationships.) This indicates the analysis in terms of θ in our toy example is probably a good approximation of the behavior of a physical system as u increases.

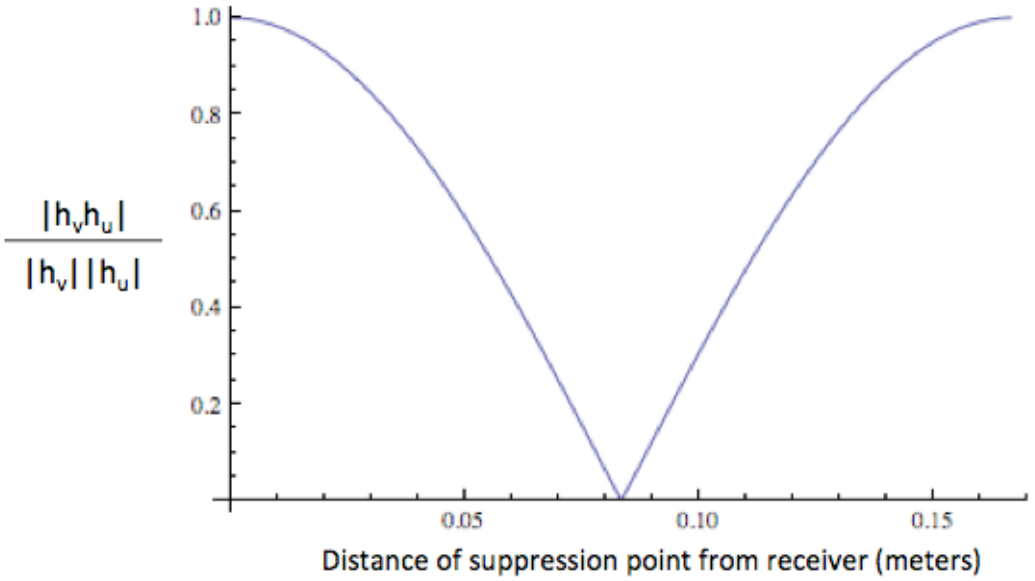

Figure 3.6a Plot of $\frac{\boldsymbol{h_v \cdot h_u}}{|\boldsymbol{h_v}||\boldsymbol{h_u}|}$ versus u for $L = 10000\ m, d = 0.01\ m, x_1 = 0.03\ m, x_2 = -0.03$.

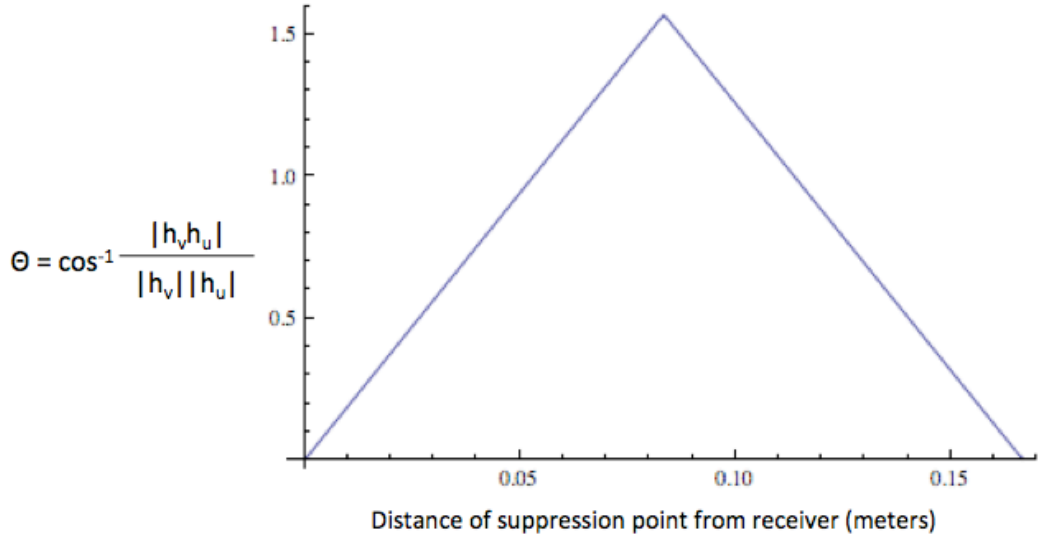

Figure 3.6b Plot of $\cos^{-1}\left(\frac{|\boldsymbol{h_v \cdot h_u}|}{|\boldsymbol{h_v}||\boldsymbol{h_u}|}\right)$ versus u for the same parameters. The relationship is approximately linear.

Returning to our toy example, we can use our calculated $\frac{dq}{d\theta} = \frac{b^2}{2}\sin 2\phi\left(1 - \frac{\sin\theta}{\sin(2\phi-\theta)}\right)$, where $\frac{a^2\cos^2(\phi-\theta)}{Rb^2} = \cos^2\phi$ to get a general idea of how q varies with u. As expected, $\frac{dq}{d\theta} = 0$ in Case 1 when $\phi = 0$. Increasing u in this case does not change the power at the receiver. Figure 3.7 shows how the intensity at the receiver varies with the angle θ. Figure 3.8 plots $\frac{dq}{d\theta}$ versus θ.

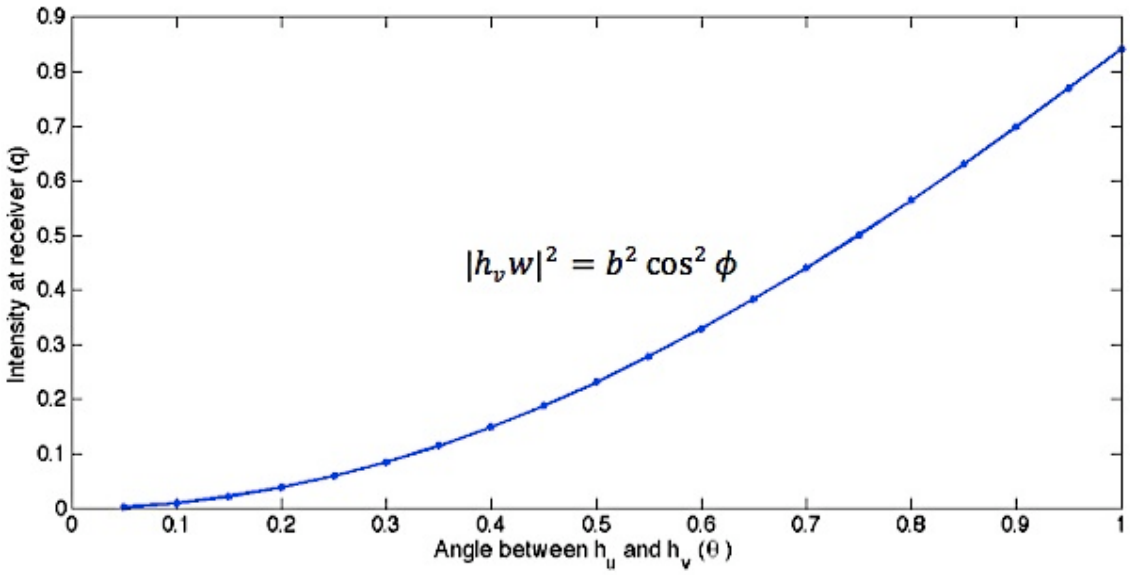

Figure 3.7 Plot of the intensity at the receiver as the angle θ between $\overrightarrow{\boldsymbol{h_u}} = \begin{bmatrix}\cos\theta \\ \sin\theta\end{bmatrix}$ and $\overrightarrow{\boldsymbol{h_v}} = \begin{bmatrix}\sqrt{2} \\ 0\end{bmatrix}$, for $\frac{1}{R} = 10$.

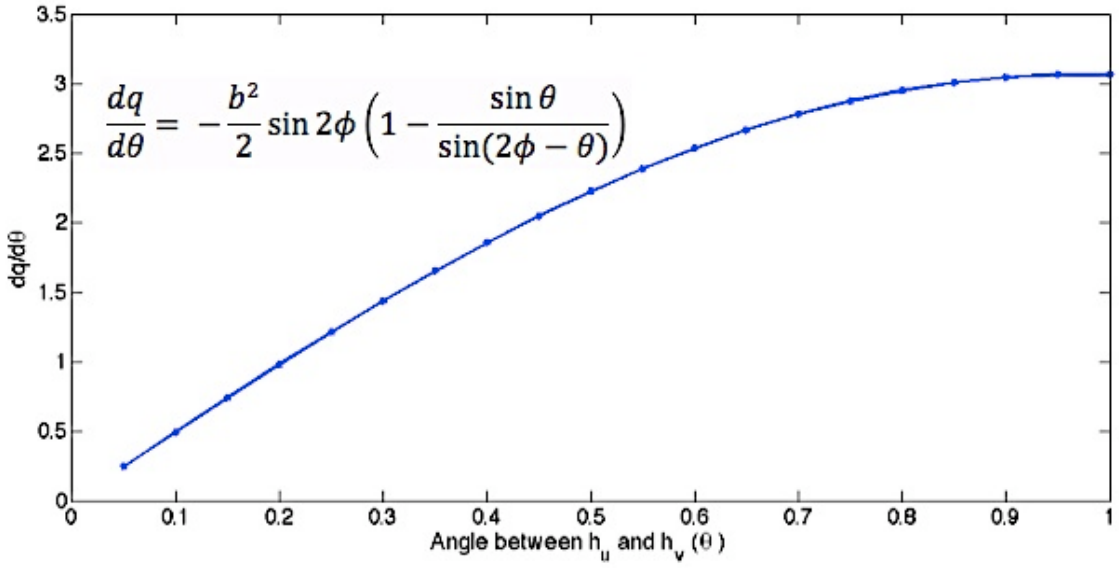

Figure 3.8 Plot of $\frac{dq}{d\theta}$ between $\overrightarrow{\boldsymbol{h_u}} = \begin{bmatrix}\cos\theta \\ \sin\theta\end{bmatrix}$ and $\overrightarrow{\boldsymbol{h_v}} = \begin{bmatrix}\sqrt{2} \\ 0\end{bmatrix}$, for $\frac{1}{R} = 10$. From this plot, we observe that the intensity at the receiver shows quadratic growth with θ for small θ and approximately linear growth as θ approaches $\frac{\pi}{2}$.

We now show how the signal-to-suppression region power ratio behaves in the region directly around the desired suppression point. We also show how this behavior changes with increasing angle θ. Suppose $m = \frac{|h_v \cdot w|^2}{|h_u \cdot w|^2}$ is the signal to suppression ratio at point u. Let $\tilde{m} = \frac{|h_v \cdot w|^2}{|h_{\tilde{u}} \cdot w|^2}$ be the signal to suppression ratio at a point $\tilde{u}$ near u.

$$\tilde{m} = \frac{|h_v \cdot w|^2}{|h_{\tilde{u}} \cdot w|^2} = \frac{b^2 x^2}{a\cos\phi\cos(\theta+\tilde{\theta}) + a\sin\phi\sin(\theta+\tilde{\theta})}$$

$$= \frac{b^2\cos^2\phi}{a^2\cos^2(\theta+\tilde{\theta}-\phi)}$$

$$\boxed{\frac{d\tilde{m}}{d\tilde{\theta}} = -\frac{2b^2}{a^2}\frac{\cos^2\phi\sin(\phi-\theta-\tilde{\theta})}{\cos^3(\phi-\theta-\tilde{\theta})}}$$

$$\boxed{\frac{d^2\tilde{m}}{d\tilde{\theta}d\theta} = \frac{-2b^2\cos^2\phi\left(-2+\cos\left(2(\phi-\theta-\tilde{\theta})\right)\right)}{a^2\cos^4(\phi-\theta-\tilde{\theta})}}$$

As θ increases, the variation in the signal-to-suppression region power ratio at $\theta+\tilde{\theta}$ decreases, and thus the minimum suppression ratio in the suppression region increases as well. Thus we generally expect to be able to achieve the same suppression ratio with fewer suppression points if the suppression region is further away from the receiver. This is supported by the example plots in Figure 3.9.

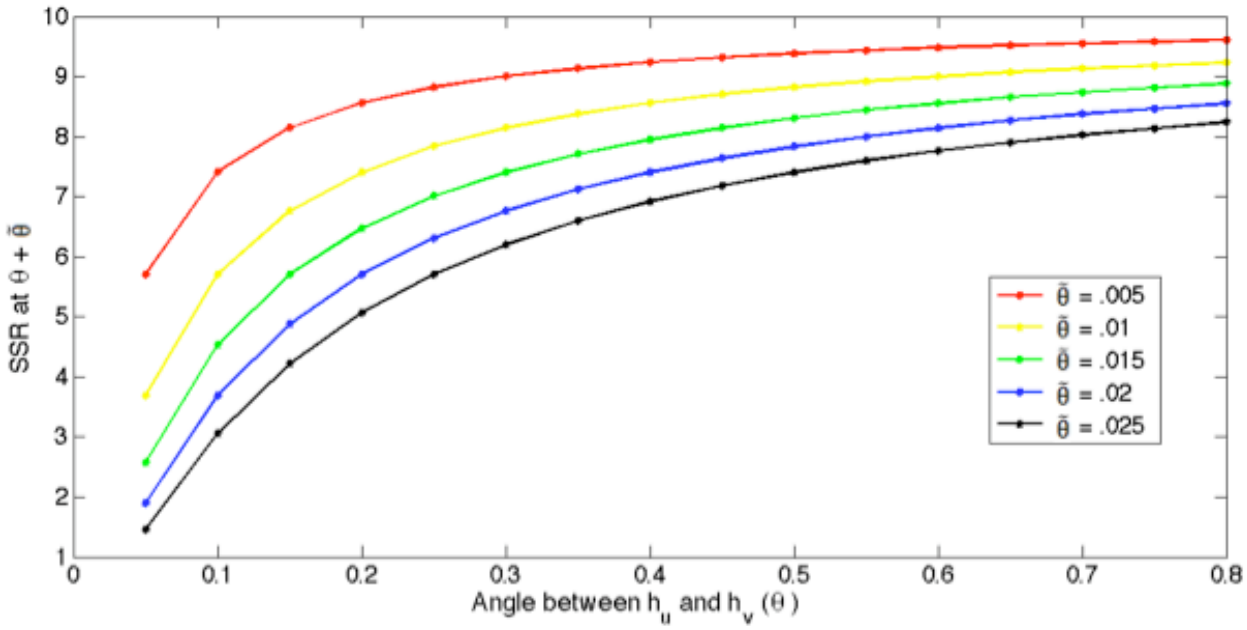

Figure 3.9 As in previous example, $\overrightarrow{\boldsymbol{h_u}} = \begin{bmatrix}\cos\theta \\ \sin\theta\end{bmatrix}$, $\overrightarrow{\boldsymbol{h_v}} = \begin{bmatrix}\sqrt{2} \\ 0\end{bmatrix}$, and $\frac{1}{R} = 10$. Each plot shows the value of the signal-to-suppression-region power ratio at a point $\theta + \tilde{\theta}$ as θ increases. The suppression ratio at θ is exactly 10 in each case.

The expressions for $\frac{d\tilde{m}}{d\tilde{\theta}}$ and $\frac{d^2\tilde{m}}{d\tilde{\theta}d\theta}$ suggest a relationship between our lowest achievable signal-to-suppression-region power ratio within a suppression region and both the width and number of suppression points in the suppression region. Figure 3.10 shows plots of these relationships. In general, the maximum $\tilde{\theta}$ we must consider when determining the minimum signal-to-suppression-region power ratio increases with the distance between two successive suppression points. As the width of the suppression region increases, this distance increases, and the value of $\tilde{\theta}$ at which we must evaluate the suppression ratio increases. Thus we expect the achievable suppression ratio to decrease with suppression region width. As θ approaches 0, the suppression ratio changes more rapidly with $\tilde{\theta}$, so smaller changes in overall suppression width are likely to have a much greater impact on the suppression ratio. Increasing the number of

suppression points has the opposite effect. This results in a smaller maximum $\tilde{\theta}$, and thus we would expect the achievable suppression ratio to increase. However, increasing the number of suppression points is countered by the additional constraints placed on the objective function. Because there will be fewer degrees of freedom with which to maximize the intensity at the receiver, increasing the number of suppression points will tend to decrease the suppression ratio.

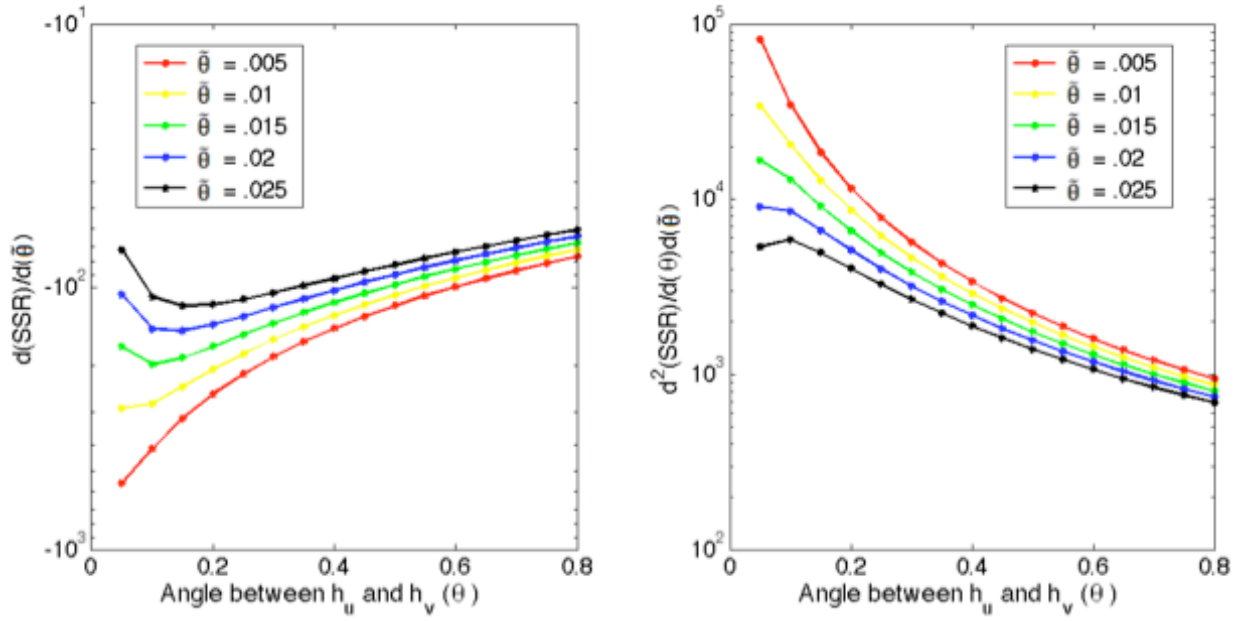

Figure 3.10 As in Figure 3.9, $\overrightarrow{\boldsymbol{h_u}} = \begin{bmatrix}\cos\theta \\ \sin\theta\end{bmatrix}$, $\overrightarrow{\boldsymbol{h_v}} = \begin{bmatrix}\sqrt{2} \\ 0\end{bmatrix}$, and $\frac{1}{R} = 10$. Each plot on the left shows the value of $\frac{d\tilde{m}}{d\tilde{\theta}}$ at a point $\theta + \tilde{\theta}$ as θ increases. Each plot on the right shows the value of $\frac{d^2\tilde{m}}{d\tilde{\theta}d\theta}$ at a point $\theta + \tilde{\theta}$ as θ increases. The signal-to-suppression-region power ratio at θ is exactly 10 in each case.

Finally, we show how the receive power varies with the fill factor pre-suppression. In Chapter 7, we will compare this to the relationship between receive power and fill factor after suppression. Let the fill factor of an N-aperture linear array be f.

The maximum intensity at receiver is

$$\left| h_v \cdot \frac{h_v}{|h_v|} \right|^2 = \sqrt{\sum_{i=1}^{N} h_{vi}^* h_{vi}}$$

$$h_{vi}^* h_{vi} = \frac{16d^4}{\lambda L} \operatorname{sinc}^2 \left(\frac{2dx_i}{\lambda L} \right)$$

$$\frac{\partial}{\partial f} \left(\sqrt{\sum_{i=1}^{N} h_{vi}^* h_{vi}} \right) = \frac{1}{2\sqrt{\sum_{i=1}^{N} h_{vi}^* h_{vi}}} \frac{\partial}{\partial f} \sum_{i=1}^{N} h_{vi}^* h_{vi} = \frac{1}{2\sqrt{\sum_{i=1}^{N} h_{vi}^* h_{vi}}} \sum_{i=1}^{N} \frac{\partial}{\partial f} h_{vi}^* h_{vi}$$

If d is the half-width of an aperture, $d = \frac{Df}{2N}$, where D is the length of the array.

$$\frac{\partial}{\partial f} h_{vi}^{*} h_{vi} = \frac{\partial}{\partial f}\left[\frac{16d^4}{(\lambda L)^2}\operatorname{sinc}^2\left(\frac{2dx_i}{\lambda L}\right)\right]$$

$$\frac{\partial}{\partial f} h_{vi}^{*} h_{vi} = \frac{\partial}{\partial f}\left[\frac{1}{(\lambda L)^2}\left(\frac{Df}{N}\right)^4 \operatorname{sinc}^2\left(\frac{Dfx_i}{N\lambda L}\right)\right]$$

$$= \frac{2f^2D^3 \operatorname{sinc}\left(\frac{Dfx_i}{N\lambda L}\right)\left(Dfx_i \cos\left(\frac{Dfx_i}{N\lambda L}\right) - LN\lambda \sin\left(\frac{Dfx_i}{N\lambda L}\right) + 2Dfx_i \operatorname{sinc}\left(\frac{Dfx_i}{N\lambda L}\right)\right)}{L^2N^4x_i\lambda^2}$$

$$= \frac{2f^2D^3}{L^2N^4x_i\lambda^2}\operatorname{sinc}\left(\frac{Dfx_i}{N\lambda L}\right)\left(Dfx_i \cos\left(\frac{Dfx_i}{N\lambda L}\right) - LN\lambda \sin\left(\frac{Dfx_i}{N\lambda L}\right) + 2Dfx_i \operatorname{sinc}\left(\frac{Dfx_i}{N\lambda L}\right)\right)$$

$$\sum_{i=1}^{N} h_{vi}^{*} h_{vi} = \sum_{i=1}^{N} \frac{16d^4}{(\lambda L)^2}\operatorname{sinc}^2\left(\frac{2dx_i}{\lambda L}\right) = \frac{16d^4}{(\lambda L)^2}\sum_{i=1}^{N} \operatorname{sinc}^2\left(\frac{2dx_i}{\lambda L}\right)$$

$$\sum_{i=1}^{N} \frac{\partial}{\partial f} h_{vi}^{*} h_{vi} = \frac{2f^2D^3}{L^2N^4\lambda^2}\sum_{i=1}^{N} \frac{1}{x_i}\operatorname{sinc}\left(\frac{Dfx_i}{N\lambda L}\right)\left(Dfx_i \cos\left(\frac{Dfx_i}{N\lambda L}\right) - LN\lambda \sin\left(\frac{Dfx_i}{N\lambda L}\right)\right.$$

$$\left. + 2Dfx_i \operatorname{sinc}\left(\frac{Dfx_i}{N\lambda L}\right)\right)$$

We substitute this expression into $\frac{1}{2\sqrt{\sum_{i=1}^{N} h_{vi}^{*} h_{vi}}} \sum_{i=1}^{N} \frac{\partial}{\partial f} h_{vi}^{*} h_{vi}$ and find that

$$\frac{\partial}{\partial f}\left(\sqrt{\sum_{i=1}^{N} h_{vi}^{*} h_{vi}}\right)$$

$$= \frac{D}{\lambda L N^2 \sqrt{\sum_{i=1}^{N} \operatorname{sinc}^2\left(\frac{2dx_i}{\lambda L}\right)}} \sum_{i=1}^{N} \frac{1}{x_i} \operatorname{sinc}\left(\frac{Dfx_i}{N\lambda L}\right)\left(Dfx_i \cos\left(\frac{Dfx_i}{N\lambda L}\right)\right.$$

$$\left. - LN\lambda \sin\left(\frac{Dfx_i}{N\lambda L}\right) + 2Dfx_i \operatorname{sinc}\left(\frac{Dfx_i}{N\lambda L}\right)\right)$$

Let $\lambda = 10^{-6}$, $L = 10^4$, $D = 10^{-1}$, $N = 2$, and $x_i = \pm\frac{D}{2}$.

$$\frac{\partial}{\partial f}\left(\sqrt{\sum_{i=1}^{N} h_{vi}^{*} h_{vi}}\right) = \frac{\sqrt{2}}{f^2 \operatorname{sinc}\left(\frac{f}{4}\right)} f^2 \operatorname{sinc}\left(\frac{f}{4}\right)\left(\frac{f}{4}\cos\left(\frac{f}{4}\right) - \sin\left(\frac{f}{4}\right) + \frac{f}{2}\operatorname{sinc}\left(\frac{f}{4}\right)\right)$$

$$\boxed{\frac{\partial}{\partial f}\left(\sqrt{\sum_{i=1}^{2} h_{vi}^{*} h_{vi}}\right) = \sqrt{2} f\left(\frac{1}{4}\cos\left(\frac{f}{4}\right) + \frac{1}{2}\operatorname{sinc}\left(\frac{f}{4}\right)\right) - \sqrt{2}\sin\left(\frac{f}{4}\right)}$$

For $0 < f \leq 1$, $\frac{\partial}{\partial f}\left(\sqrt{\sum_{i=1}^{N} h_{vi}^{*} h_{vi}}\right)$ is approximately linear, suggesting that the maximum intensity at the receiver $\sqrt{\sum_{i=1}^{N} h_{vi}^{*} h_{vi}}$ shows approximately quadratic growth with increasing fill factor. Indeed, in this example $\sqrt{\sum_{i=1}^{2} h_{vi}^{*} h_{vi}} = \frac{1}{2\sqrt{2}} f^{2} \operatorname{sinc}\left(\frac{f}{4}\right)$. As N increases, the quadratic approximation of the increase in receiver intensity will be more accurate.

Chapter 4

Numerical Methods

The nonlinear optimization problem defined in Chapter 2 was solved numerically using NLopt, a software package containing open-source implementations of nonlinear optimization algorithms [9]. We used an implementation of an evolutionary global optimization algorithm (ISRES) and an implementation of a sequential quadratic programming local optimization algorithm (SLSQP). Since the goal of this thesis was to analyze the physical potential for suppressing power to a defined region, the algorithms we chose may not have the optimum run time for our specific problem. We briefly summarize the two algorithms that we used and our reasons for choosing them below.

4.1 Improved Stochastic Ranking Evolution Strategy

Because the problem is a non-convex global optimization problem with disjoint feasible regions (due to a singularity at $\vec{w} = \vec{0}$) and nonlinear inequality constraints, we used the stochastic evolutionary algorithm described in [10]. It is referred to in [9] as the Improved Stochastic Ranking Evolution Strategy (ISRES). ISRES stochastically ranks a population of potential solutions and mutates the best of these to locate the best solution. We used the NLopt default for the population size, resulting in a population of $20\times(N+1)$ individuals, for an N-aperture array [9]. The stochastic ranking is the "bubble-sort-like procedure" described in [12], which with some probability P_f compares two potential solutions based on their objective function values and with probability $1-P_f$ compares them according to a penalty function that

accounts for the inequality constraints. The top-ranked individuals are each mutated multiple times through the evolution strategy described in [10] to form a new population. The step size for each mutation is determined through a log-normal update rule on the parent step size; random fluctuations from this expected median are reduced via exponential smoothing of previous step sizes in the same lineage. Each parent has one mutation generated by a step towards the individual ranked immediately below the parent.

ISRES is not guaranteed to converge, but it can potentially escape non-optimum local maxima. The time the algorithm takes to reach an acceptable solution is dependent on the problem dimension and the number of constraints (i.e. the number of apertures and the number of suppression points, respectively), as well as on the distance of the suppression region from the receiver. The time to convergence generally increases with additional apertures and suppression points and generally decreases as the suppression region moves further away. The latter dependence could be more accurately attributed to the pre-suppression SSR for a particular suppression region, which tends to decrease with increasing suppression region.

There is no clear heuristic for determining that the algorithm has converged; the documentation in [9] suggests that the algorithm should be run for as long as possible in order to achieve the best practical result. One issue with this algorithm for our problem is that if all of the local optima have the same objective function value, the algorithm would waste computation time by searching through multiple feasible regions to find effectively the same solution as in all the other feasible regions.

4.2 Sequential Least Squares Quadratic Programming

The local optimization algorithm we used was the sequential quadratic programming algorithm detailed in [13] and summarized below. This algorithm uses an iterative search algorithm, where the start vector $\overrightarrow{\boldsymbol{w_0}}$ is successively updated by steps $\alpha_k \vec{\boldsymbol{d}}_k$ at each step k. The search direction $\overrightarrow{\boldsymbol{d_k}}$ at each step is determined by solving the quadratic programming problem:

$$\min_{d \in \mathbb{R}^N} \left(\frac{1}{2} \boldsymbol{d}^* \boldsymbol{B_k} \boldsymbol{d} + \nabla f(\boldsymbol{w_k}) \boldsymbol{d} \right)$$

subject to

$$\nabla g_j(\boldsymbol{w_k}) \boldsymbol{d} + g_j(\boldsymbol{w_k}) \geq 0$$

where $g_j(\boldsymbol{w})$ for $1 \leq j \leq m$ are the inequality constraints (including the relaxed weight constraint). $\boldsymbol{B_k}$ is the Hessian matrix of the Lagrange function

$$L(\boldsymbol{w}, \lambda) = f(\boldsymbol{w}) - \sum_{j=1}^{m} \lambda_j g_j(\boldsymbol{w})$$

Instead of evaluating each $\boldsymbol{B_k}$ at each step k, the algorithm uses the Wilson-Han-Powell Method (a treatment of this method is found in [14]) to approximate the Hessian matrix using only first order information and to determine the step size α_k. $\boldsymbol{B_k}$ is approximated using Broyden-Fletcher-Goldfarb-Shanno updates, which, according to [15], can be used to approximate the Hessian for "general nonquadratic function of modest dimensions." It is suggested in [13] that the problem dimension be less than 200; the documentation in [9] suggests that up to a few thousand parameters would be feasible. In this thesis, we do not consider any aperture arrays (or suppression point arrays) of greater than $N = 100$.

We ran this algorithm using MATLAB until it was unable to continue due to roundoff errors. We then considered the algorithm to have converged to a solution if the resultant weight

vector caused the inequality constraints to be within a 10^{-10} relative tolerance (that is, $g_j(\boldsymbol{w}) \leq 10^{-10}$ for convergence).

4.3 Comparison of Algorithms

Because we did not prove that each local optimum of the problem had an equal objective function value, we first employed the global algorithm to find numerical solutions. However, because of the stochastic nature of the global algorithm, convergence was not guaranteed. Additionally, the time to convergence required by the global algorithm was several orders of magnitude greater than the time to convergence required by the local algorithm (hours versus seconds). It is unclear that the benefits of using the global algorithm outweighed the costs, especially since symmetry of the problem suggested that the local optima were equivalent. When we compared the results of running the global algorithm with running the local algorithm with random start vectors on the same systems, we found that provided we specified appropriate termination criteria and constraint tolerances for the local algorithm, we were able to get as good or better results from SLSQP as from ISRES on the linear aperture array. The weight vectors we obtained from SLSQP with varying start vectors were different from each other, but they differed by constant phase factors, and were therefore functionally equivalent.

We therefore chose to use only the local algorithm for the two-dimensional case. The run-time was much faster, the trends seen were comparable to those seen in the linear case with the global algorithm, and the suppression constraints were successfully met.

4.4 Simulated System Specifications

Before we present our numerical results in the following chapters, we make precise the details of the systems we analyze.

4.4.1 Linear Aperture Array

In Chapter 5, we analyze a linear aperture array. Due to the complexity of solving the nonlinear optimization problem – especially with the global algorithm – for a large number of apertures, we consider first the case of a linear transmit array to shed light on the issues involved in using the general problem formulation to suppress power to a desired area. Parameters such as fill factor or number of suppression points in the linear aperture formulation can be varied independently of many other parameters. The trends we observe in the linear case may be generalizable to more complex models. We conduct most of our analysis on the linear array system with the global optimization algorithm ISRES. This algorithm takes too long to converge when we extend our consideration to the 2D array in Chapter 6, but we use it with the linear apertures and show that the local optimization algorithm SLSQP converges to a weight vector within the same equivalence class.

Our system model, shown in a generalized form in Figure 4.1, comprises a 0.48 meter by 0.01 meter linear aperture array centered at $\xi = 0$ in the transmit plane. The height of each aperture in the array is constrained to 0.01 meters, but the width can vary with the desired fill factor. The fill factor is defined as the total summed widths of the apertures in the array divided by 0.48 meters, the total width of the array. The optical wavelength is 10^{-6} meters and the receive plane is a distance of 10000 meters from the transmitter. The position of intended receiver is taken to be at $x = 0$.

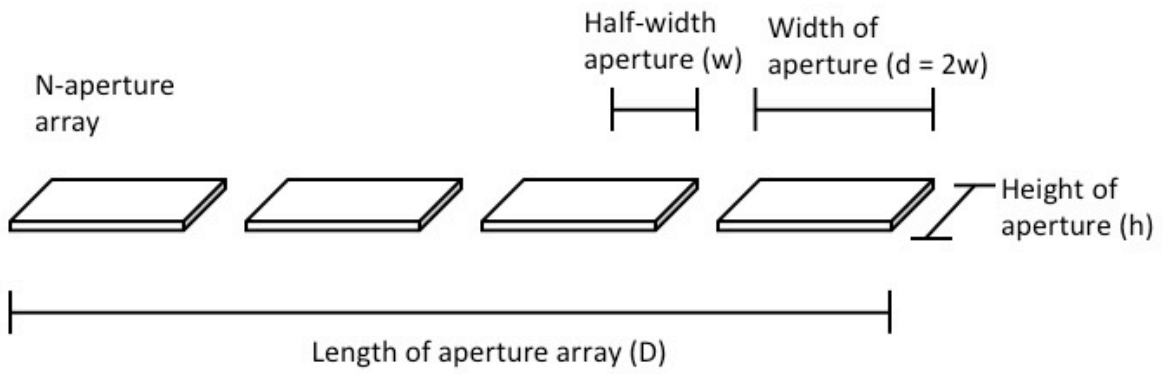

Figure 4.1 Linear aperture array with variable parameters labeled. In our numerical examples in Chapter 5, $D = 0.48$ m and $h = 0.01$ m. d and w vary with the number of apertures and the specified fill factor.

The desired SSR at each suppression point is 10. We define the suppression region by a sequence of suppression points equally spaced on a line in the receive plane. The first and last suppression points mark the edges of our desired suppression region. The distance of the suppression region from the receiver is measured by the distance along the x-axis from the receiver to the closest suppression point. Figure 4.2 shows a desired suppression region for a linear aperture array.

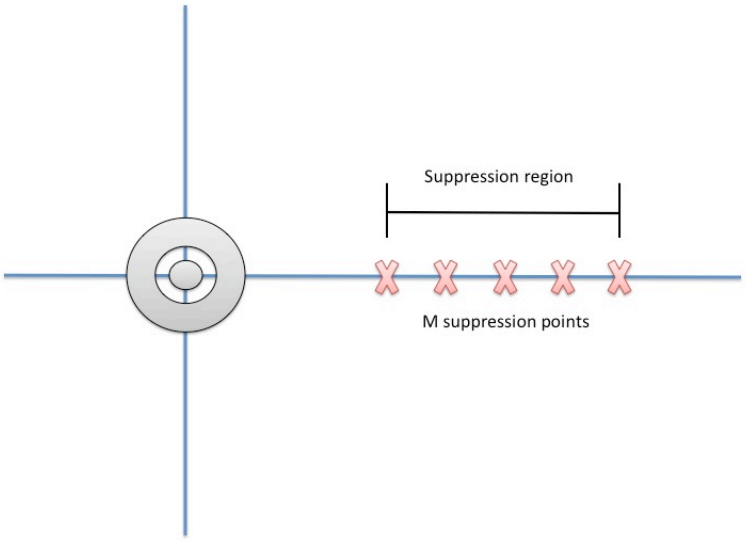

Figure 4.2 One dimensional suppression region with equally spaced suppression points. The receiver is at the origin.

We measure distance along the x axis in approximate beam widths of 0.0208 meters, calculated from the total array length of 0.48 meters. We begin by analyzing the system with a filled aperture array: we vary the number of abutted apertures that fill the 0.48 meters array. The apertures all have the same height, but their width varies in order to maintain the overall dimensionality of the array. Later, we decrease the fill factor and accordingly decrease the aperture widths.

4.4.2 Two-Dimensional Aperture Array

In Chapter 6, we present results for the two-dimensional aperture array. This is a more complex model, and therefore we choose to perform our numerical calculations with the local optimization algorithm SLSQP to speed up computation. We use a square transmit aperture array centered at the origin and suppress a square region in the receive plane. We populate the

array with a perfect square number of apertures, such that each corner of the array contains an aperture. The suppression region is likewise comprised of a perfect square of suppression points, centered around the x-axis. The distance of the suppression region from the receiver is measured by the distance along the x-axis from the receiver to the closest suppression point. Figure 4.3 shows the two-dimensional aperture array, and Figure 4.4 shows the two-dimensional suppression region.

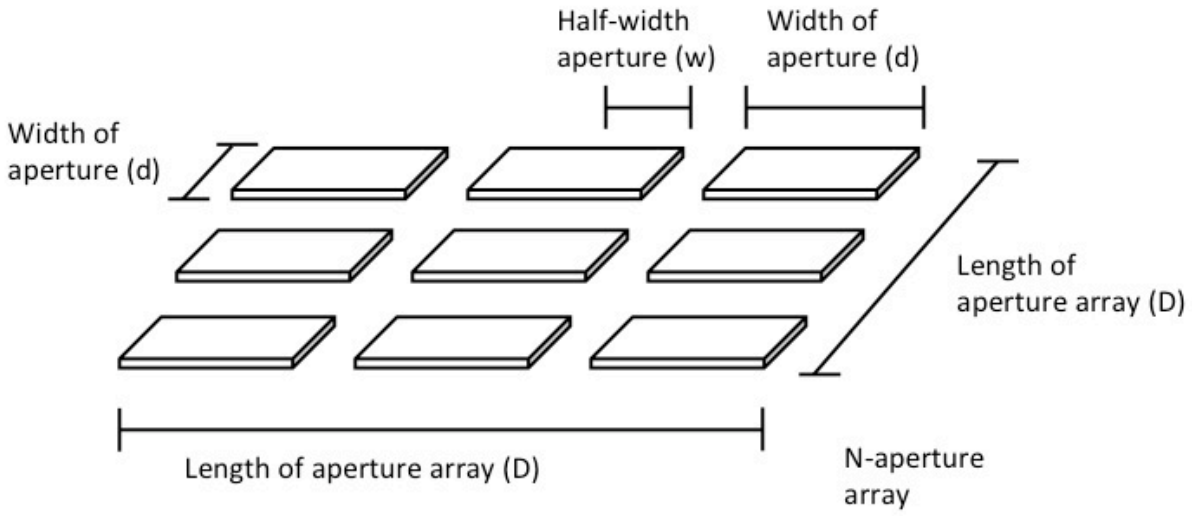

Figure 4.3 2D aperture array with parameters labeled. In our calculations in Chapter 6, we take $D = 100$ and define d based on the number of apertures N and the fill factor.

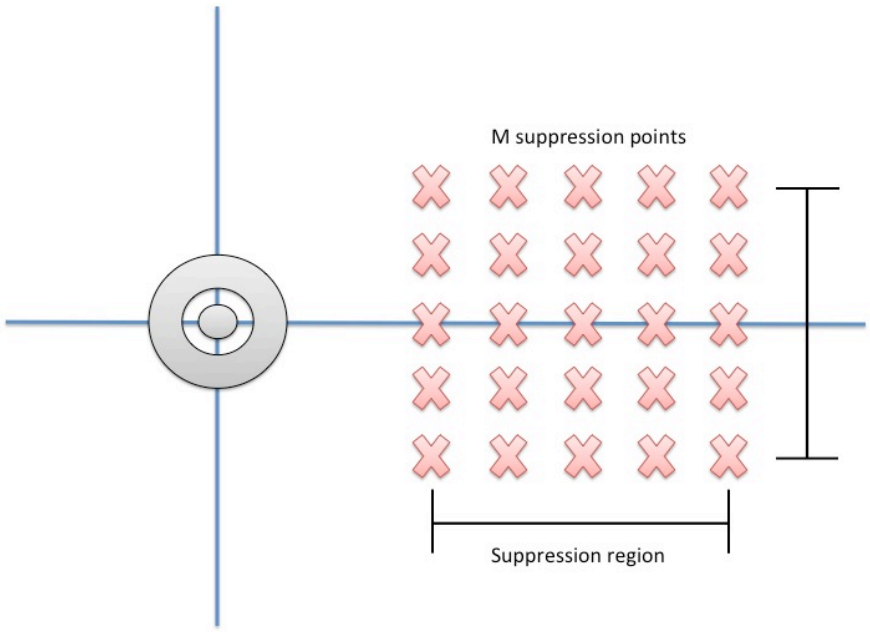

Figure 4.4 Two-dimensional suppression region. The suppression points are equally spaced in the x- and y- directions such that they form a square pattern. The receiver is located at the origin.

Our transmitter model comprises a 0.1 meter by 0.1 meter square aperture array centered at $(\xi, \eta) = (0,0)$ in the transmit plane. The width of each square aperture varies with the specified number of apertures and the fill factor. The fill factor is defined as the total summed area of the apertures in the array divided by 0.01 square meters, the total area of the array. The optical wavelength is still 10^{-6} meters and the receive plane is a distance of 10000 meters from the transmitter. The position of intended receiver is taken to be at $(x, y) = (0,0)$.

The desired SSR at each suppression point is 10. We define the suppression region by a square array of suppression points equally spaced in the x- and y- directions in the receive plane. The suppression points at the corners of the square array mark the edges of our desired suppression region. The distance of the suppression region from the receiver is measured by the distance along the x-axis from the receiver to the closest suppression point. The width between

suppression points, i.e. the separation between adjacent points along the x-axis is determined by the specified number of suppression points and the size of the suppression region.

We measure distance along the x- and y- axes in approximate beam widths of 0.1 meters, calculated from the total array size of 0.1 by 0.1 meters.

4.4.3 Adjustable Parameters

In all of our calculations, we keep the wavelength fixed at 10^{-6} meters and the distance between the transmit plane and the receive plane at 10000 meters. The total size of the linear aperture array is kept constant at 0.48 meters; the total size of the square aperture array is kept constant at 0.1 by 0.1 meters. The number of apertures and the number of fill factors is specified for each calculation; these parameters determine the size of the apertures. The size of the suppression region and the number of suppression points used to approximate it can also be specified for each calculation; these parameters determine the spacing between the suppression points. Lastly, the distance of the suppression region from the receiver (along the x-axis) and the desired signal to suppression ratio can be specified.

If the number of suppression points exceeds the number of apertures, the problem is over-constrained and the optimization algorithm may have no solution to converge to – except in special cases, e.g. if some of the suppression points are in a region smaller than one null width. Additionally, the number of parameters affects the amount of time the algorithms take to converge; since the global algorithm takes significantly longer than the local algorithm to find a solution, the aggregate number of apertures and suppression points is very relevant in choosing the type of algorithm to use. This is why we choose to use the global algorithm only for the linear aperture array case, which is computationally simpler to solve.

Chapter 5

Suppression Via Linear Aperture Array

As described in Chapter 4 (Section 4.4.1), our example linear array system model comprises a 0.48 meter by 0.01 meter linear aperture array centered at $x = 0$ in the transmit plane. The height of each aperture in the array is constrained to 0.01 meters, but the width can vary with the desired fill factor. The fill factor is defined as the total summed widths of the apertures in the array divided by 0.48 meters, the total width of the array. The optical wavelength is 10^{-6} meters and the receive plane is a distance of 10000 meters from the transmitter. The position of the intended receiver is at $x = 0$ in the receive plane. The desired signal-to-suppression-region power ratio (defined as the signal power at the user divided by the maximum power in the suppression region) is 10.

We measure distance along the x-axis in approximate beamwidths of 0.0208 meters, calculated from the total array length of 0.48 meters. This is the approximate half-width of the main lobe of the transmission at the receiving plane. Figure 5.1a demarcates this beamwidth in a plot of the output radiation pattern for a filled array with 24 apertures, with maximum possible power transmitted to the receiver. For sparse arrays, i.e. those with small fill factors, the sub-apertures within the array define an envelope of grating lobes, but the width of the total array defines the width of each of these grating lobes and the width of the main lobe of the transmission. The approximate half-width of these lobes is our 0.0208 meter beamwidth approximation. The significant grating lobes that we may want to suppress power to occur within the main lobe of the sub-aperture envelope, i.e. the main lobe of the transmission of a

single aperture within the array. Figure 5.1b shows a plot of the output radiation pattern for a sparse array with 24 apertures, with maximum possible power transmitted to the receiver.

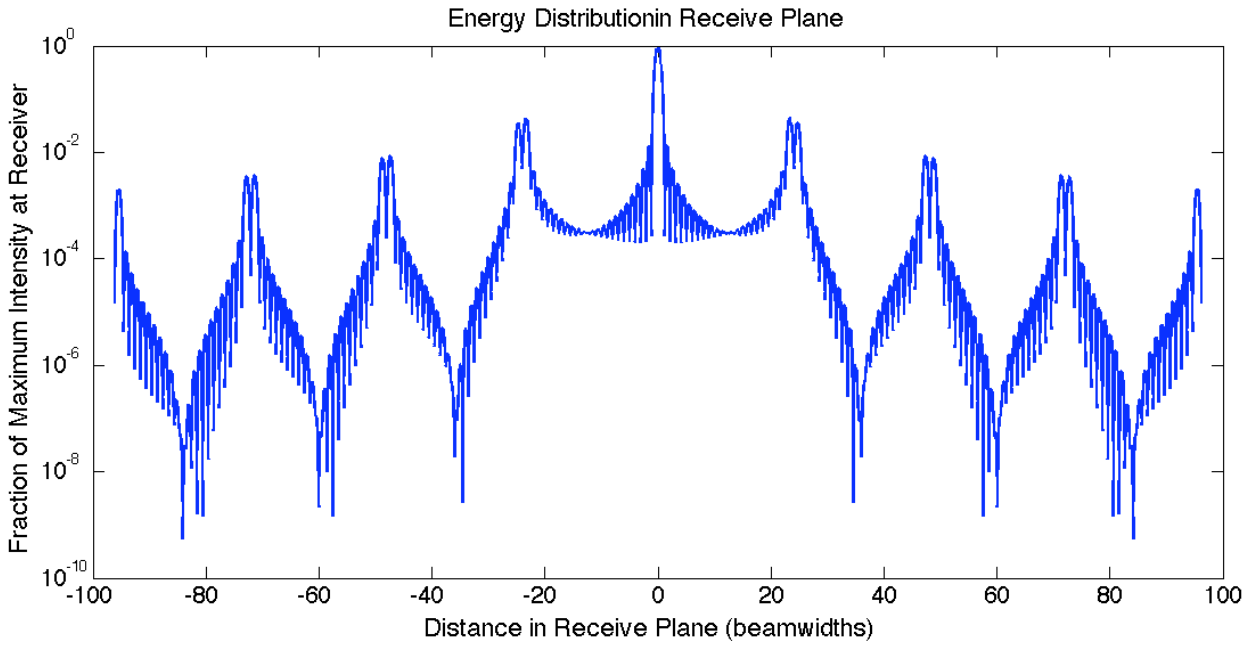

Figure 5.1a Radiation pattern in receive plane from a filled 24-aperture linear array, with maximum intensity at the receiver.

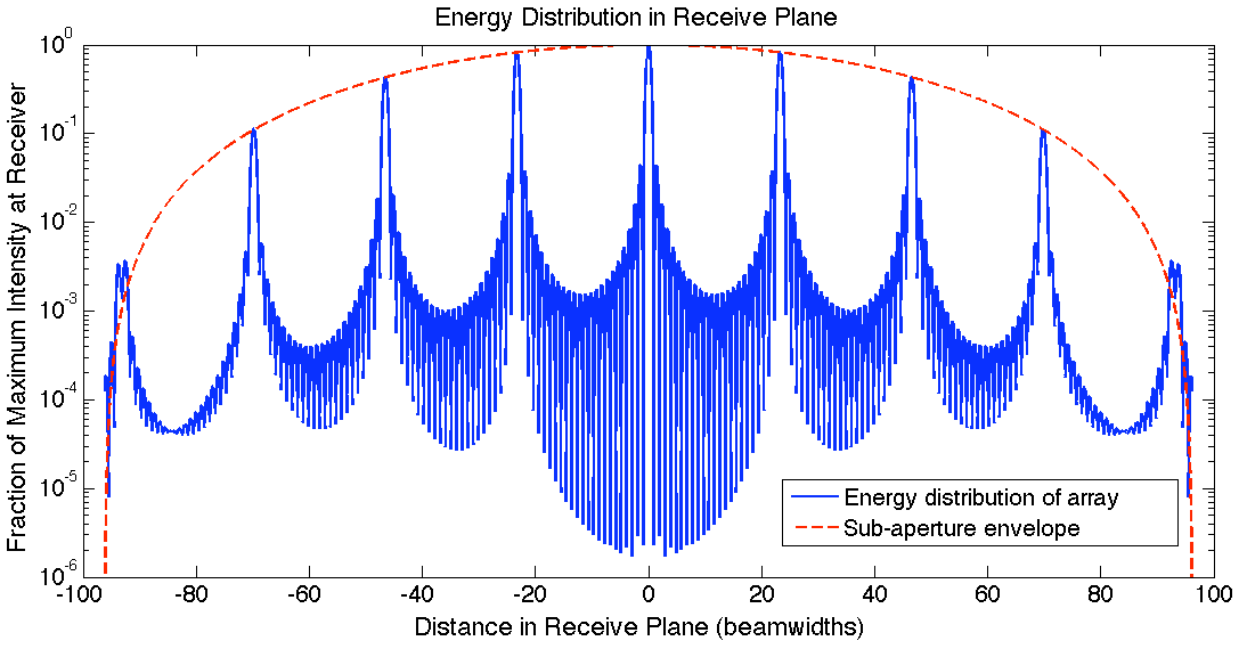

Figure 5.1b Radiation pattern in receive plane from a 24-aperture sparse linear array of fill factor = 0.1, with maximum intensity at the receiver.

In our analysis below, we consider two different normalizations of the intensity in the receive plane. First, we consider how much the intensity at the receiver decreases after suppression; this term is calculated as the fraction of the maximum possible intensity at the intended user that remains after suppression. This is a useful statistic because it indicates the extent to which different parameters affect the signal at the user after suppression. We also consider the intensity at the receive power assuming the total transmitted power $\sum_{i=1}^{N} A_i |w_i|^2$ is normalized to 1, where N is the number of apertures, A_i is the area of aperture i, and w_i is the weight of that aperture. This value allows us to better see the tradeoff between certain parameters, whereby changing one parameter could increase the absolute power at the receiver at the cost of making the system more sensitive to changes in other parameters.

5.1 Comparison of ISRES and SLSQP for Linear Aperture Array

We use both ISRES and SLSQP in our analysis of the linear aperture array. As discussed in Chapter 4, neither of these algorithms is guaranteed to converge to the global optimum weight vector. However, our results suggest that ISRES does find a reasonable solution after no more than a few million iterations, and SLSQP converges to a similar solution regardless of the choice of start vector. Figure 5.2 shows an example plot for which ISRES and SLSQP both converge to equivalent weight vectors.

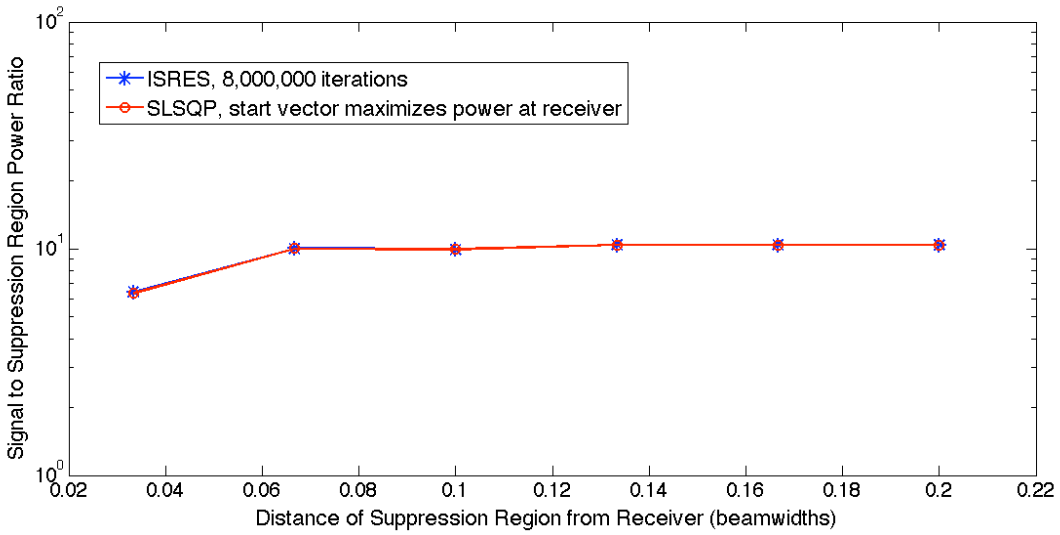

Figure 5.2 The signal to suppression region power ratio versus the distance of the suppression region from the receiver for an example aperture configuration. ISRES and SLSQP both converge to the same values.

Since we did not prove that a local optimization algorithm would be sufficient to solve this problem, using ISRES or another global algorithm would be preferable to SLSQP – although even ISRES is not ideal (discussed in the documentation of [9]) because it has no satisfactory termination criterion. To get a rough estimate of the time to convergence of ISRES, we chose a maximum number of iterations of 4 million and determined the algorithm had "converged"

sooner, i.e. at l iterations, if the SSR for greater than l iterations was within 2% of the SSR at 4 million iterations, and if the corresponding decrease in receive power was within 5% of the decrease at 4 million iterations.

The time for convergence of ISRES, approximately proportional to the number of iterations required, was heavily dependent on number of apertures. Running on a dual core 3.07 GHz Intel processor, and optimizing for 12 apertures, 2 suppression points, and a suppression region 0.2 beamwidths away from the intended receiver, the algorithm took approximately 1.2 minutes to converge. The same setup with 24 apertures took approximately 4.6 minutes to converge. For a specific set of system parameters, the time to converge remained nearly constant as the suppression region moved further than 0.2 beamwidths away. However, as the suppression region moved closer to the intended receiver, the time to convergence increased dramatically; a system with 24 apertures and a suppression region 0.1 beamwidths away took approximately 11.0 minutes to converge.

Running SLSQP was dramatically faster, as is evident in Figure 5.3, which compares the run time of SLSQP under two different start vectors to the run time of ISRES under 8 million iterations. For suppression region distances as close as 0.0333 beamwidths to the receiver, such a high number of iterations may be necessary for convergence. SLSQP was run until roundoff errors prevented the algorithm from continuing. From Figure 5.3, we see that the SLSQP run time remains fairly constant for differing suppression region distances and is on the order of seconds.

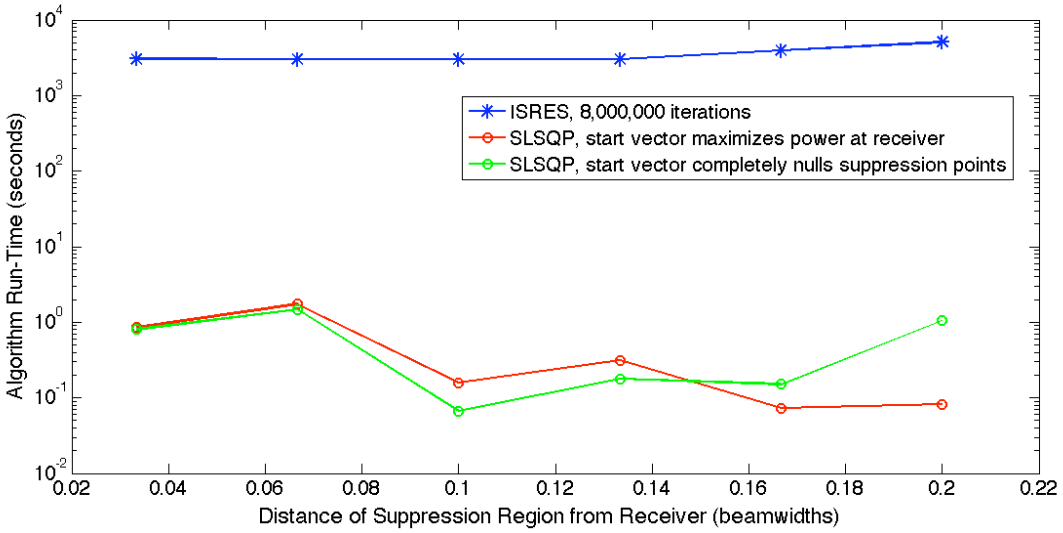

Figure 5.3 The run time for ISRES at 8 million iterations is three or four orders of magnitude the run time of SLSQP.

While most of the data in the analysis below was found using ISRES, we chose to use SLSQP to speed up calculation for plots with more data points or systems with more dimensions. Figure 5.2, and other similar test cases, suggest that SLSQP finds as good or better results as ISRES.

5.2 Transmit Array Characteristics

5.2.1 Number of Apertures

We begin by analyzing the system with a filled aperture array: we vary the number of abutted apertures that fill the 0.48 meters array. The apertures all have the same height, but their width varies in order to maintain the overall dimensionality of the array. Figure 5.4 shows how the post-to-pre-suppression receiver power ratio varies with the number of apertures comprising a full array. As the number of apertures increases, the power at the receiver is less affected by suppressing power to a region 0.1667 beamwidths away. Since the number of suppression points is kept constant in this example, increasing the number of apertures provides the system with

more degrees of freedom with which to maximize the receive power after suppressing the desired suppression points. This plot asymptotically approaches the performance of the continuous filled aperture- where we can adjust the amplitude and phase of each point in the array.

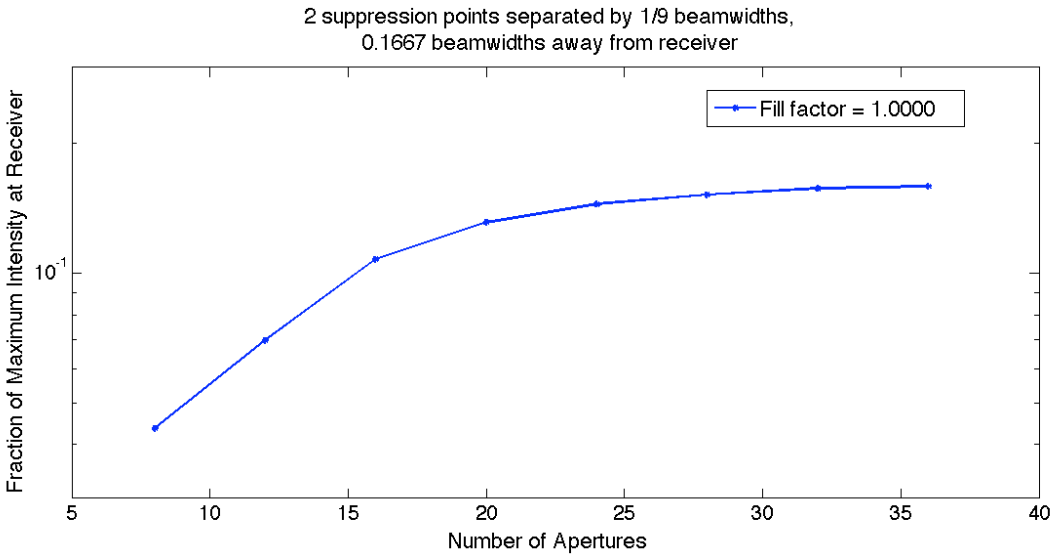

Figure 5.4 Fraction of maximum user power received after suppression versus number of apertures.

5.2.2 Fill Factor

Our analysis of the effect of the array fill factor on system performance is complicated by the effects of other system parameters – namely the width and distance between apertures – on the signal in the receive plane. The post-suppression power at the intended user is generally proportional to the pre-suppression signal to suppression region power ratio. If the signal power at the receiver is much higher than the power in the suppression region before the input weight vector is optimized, the fraction of the maximum received power sent to the intended user after optimization is higher than if the original power received by the user were closer to the original suppression region power. Since that original power ratio is directly related to the transmit

aperture parameters, it follows that the power received by the user after suppression is also affected by the geometry of the transmit apertures. As the width of the apertures decreases, the pre-suppression power distribution widens, and thus the pre-suppression power ratio decreases. As the distance between the apertures decreases, the pre-suppression power distribution also widens, and thus the pre-suppression power ratio decreases as well.

In Figure 5.5, we observe two counterintuitive trends regarding the post-suppression power at the receiver that we explain by analyzing the aperture geometry of the transmit array. However, we first must emphasize that Figure 5.5 shows the relative decrease in power at the receiver after suppression, not the absolute power at the receiver (see Figure 5.6 to compare the post-suppression power at the receiver given a fixed transmitter power.) We assume that for each array configuration, the amount of transmitter power is scaled such that the power at the receiver before suppression is constant. We then plot the fraction of this power that remains at the receiver after suppression of a 1/9 beamwidth suppression region 5/30 beamwidths away from the receiver. The first trend we observe is that the fraction of the pre-suppression maximum user power received by the intended user after suppression decreases with increasing fill factor. The effect is much more pronounced for smaller number of apertures. Second, for smaller fill factors, the post-to-pre-suppression receiver power ratio appears to decrease as the number of apertures increase, which contradicts what we observe for a filled aperture array.

Both of our observations are a direct result of keeping the overall array dimensions constant while varying the internal parameters. Decreasing the fill factor requires decreasing the width of each aperture and simultaneously increasing the distance between the apertures. Since the distance between apertures affects the modulation of the radiation pattern whereas the width of the aperture affects the external envelope, the distance between apertures is the dominant

parameter within the main lobe. Here, as the distance between apertures increases for smaller fill factors, the pre-suppression signal-to-suppression-region power ratio increases, and the receiver power ratio likewise increases. For a constant fill factor, increasing the number of apertures decreases both the width of the apertures and the distance between them. This should decrease the pre-suppression signal-to-suppression-region power ratio, and therefore decrease the post-to-pre-suppression receiver power ratio. However, this decrease is countered by the added optimization control of having more apertures. For larger fill factors, this last parameter dominates and the receiver power ratio increases with more apertures. For smaller fill factors, where the area of the apertures is very small, increasing the number of apertures does not counteract the effects of decreasing the width of and distance between the apertures.

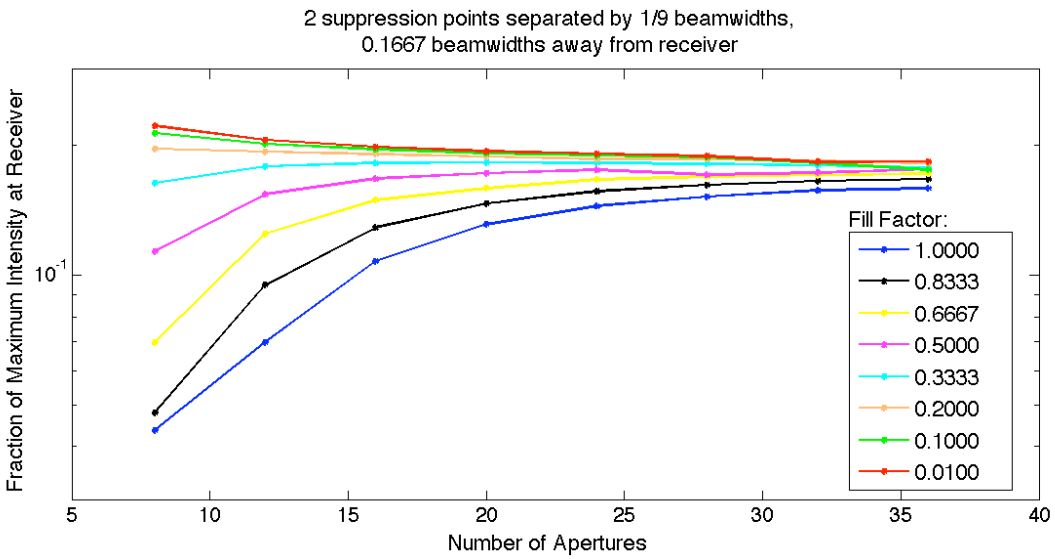

Figure 5.5 Fraction of maximum user power received after suppression versus number of apertures, for varying fill factors.

The data shown in Figure 5.6 is similar to that of Figure 5.5, although with almost twice as many data points. In Figure 5.6, however, the intensity after suppression is normalized such that each point corresponds to a system with the same transmit power. The curves in this plot can be used to compare the absolute intensity at the receiver after suppression for different aperture and fill factor combinations. Here, the effect of increasing the number of apertures for a constant fill factor appears less dramatic.

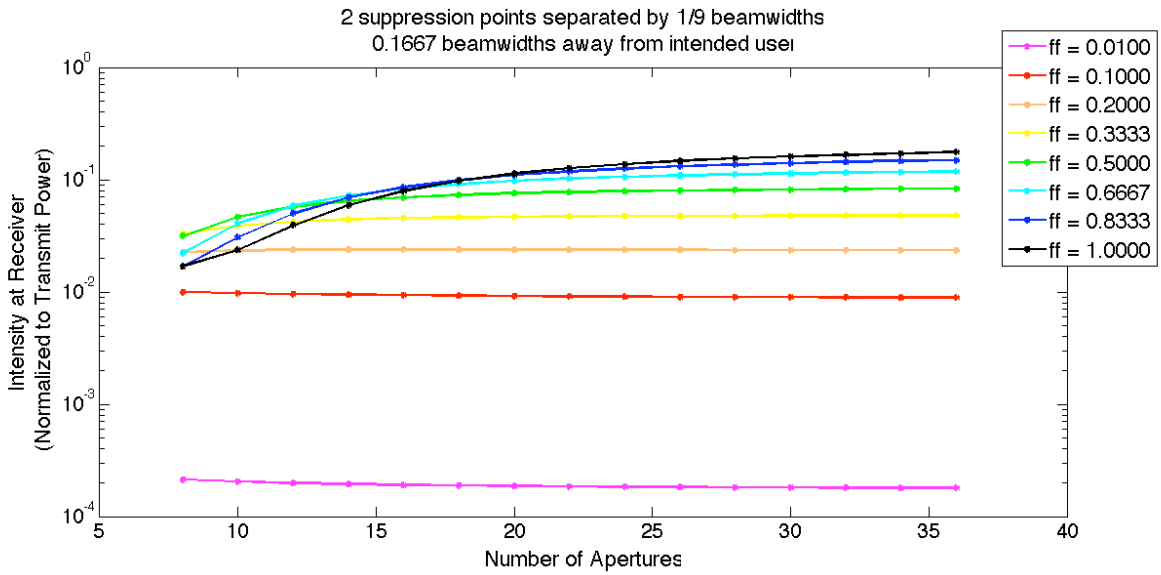

Figure 5.6 Intensity at the receiver after suppression versus number of apertures, for varying fill factors. The intensity is normalized such that the transmit power $\sum_{i=1}^{N} A_i|w_i|^2 = 1$, where N is the number of apertures, A_i is the area of aperture i, and w_i is the weight of that aperture.

The best results are obtained with large fill factors and many apertures, but the fill factor appears to have a more significant impact on receiver power than the number of apertures. This is especially clear in Figure 5.7, where the intensity versus fill factor curves for 16, 24 and 36 apertures are not easily distinguishable until the fill factor is greater than 0.5. Although for smaller fill factors, the receiver intensity does decrease with increased number of apertures, the

added optimization control almost entirely counters that effect and the resulting intensity is approximately the same regardless of the number of apertures. For small fill factors, arrays with fewer apertures are in fact doubly desirable, since these systems require less computational effort for suppression and are less physically expensive.

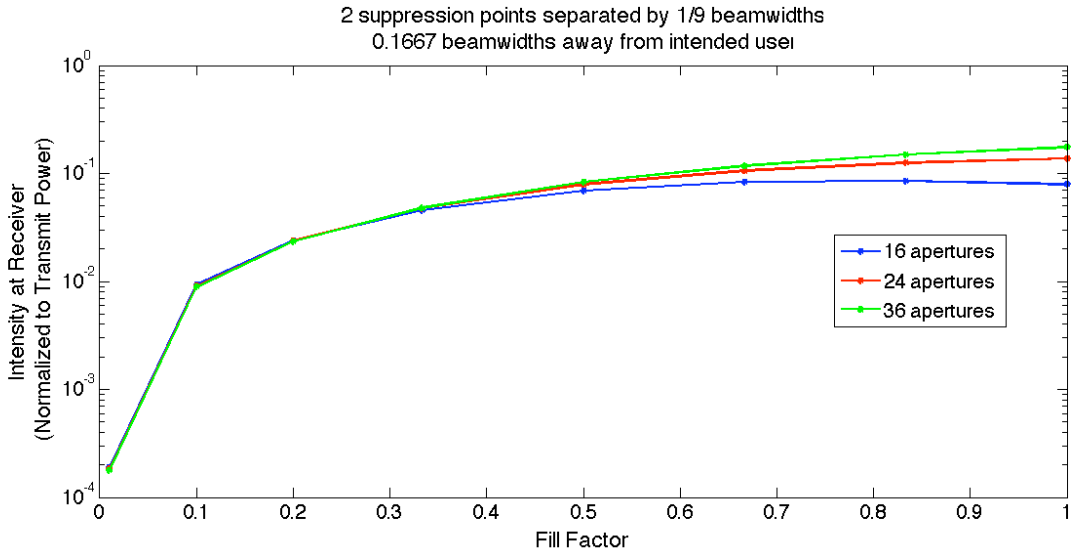

Figure 5.7 Intensity at the receiver after suppression versus fill factor, for varying apertures. The intensity is normalized such that the transmit power $\sum_{i=1}^{N} A_i |w_i|^2 = 1$, where N is the number of apertures, A_i is the area of aperture i, and w_i is the weight of that aperture.

In order to take advantage of spatial diversity to mitigate turbulence, we desire arrays with smaller fill factors and a greater number of apertures. Figures 5.6 and 5.7 reveal the tradeoffs that must be considered when choosing these transmitter parameters.

5.3 Suppression Region Characteristics

We now turn to the characteristics of the suppression region that impact the success of suppressing a desired region to a specified ratio.

5.3.1 Separation of Suppression Points

The separation of suppression points is a significant parameter when the length of the suppression region grows large. If the suppression points used to approximate the suppression region are too far from each other, there might be energy spikes in the suppression region between the suppression points, thus decreasing the overall signal-to-suppression-region power ratio. We calculate this ratio based on the maximum intensity in the suppression region, so the further apart the suppression points are, the smaller the ratio will be. Using a larger number of suppression points to approximate the suppression region may result in a better signal-to-suppression-region ratio but requires more time to converge to a solution and could require more apertures. In Figures 5.8-5.10, we show that the required separation between the suppression points varies based on the distance of the suppression region from the intended receiver and the acceptable decrease in power at the receiver. We find that the signal-to-suppression-region ratio is less sensitive than the receiver power to suppression point separation; however, a decrease in signal-to-suppression-region ratio is worse than a decrease in receive power, since the latter can be accommodated with an appropriately scaled transmitter power.

Figure 5.8 shows the effect the distance between suppression points can have on the optimized radiation pattern. In Figure 5.8, we see that the decrease in user power after suppression remains constant until the separation between the suppression points exceeds the distance between the suppression region and the intended receiver. If the distance between the

two points becomes too large, not only will the power to the intended user be overly limited, but the desired signal-to-suppression-region ratio threshold may not be satisfied for the entire region between the suppression points. Figure 5.9 shows that the achievable signal-to-suppression-region ratio remains fairly constant until the separation between the suppression points is twice the distance between the suppression region and the receiver. This indicates that there is a range of suppression point separation for which the desired signal-to-suppression-region ratio can be achieved, but at a cost of decreasing intensity at the receiver.

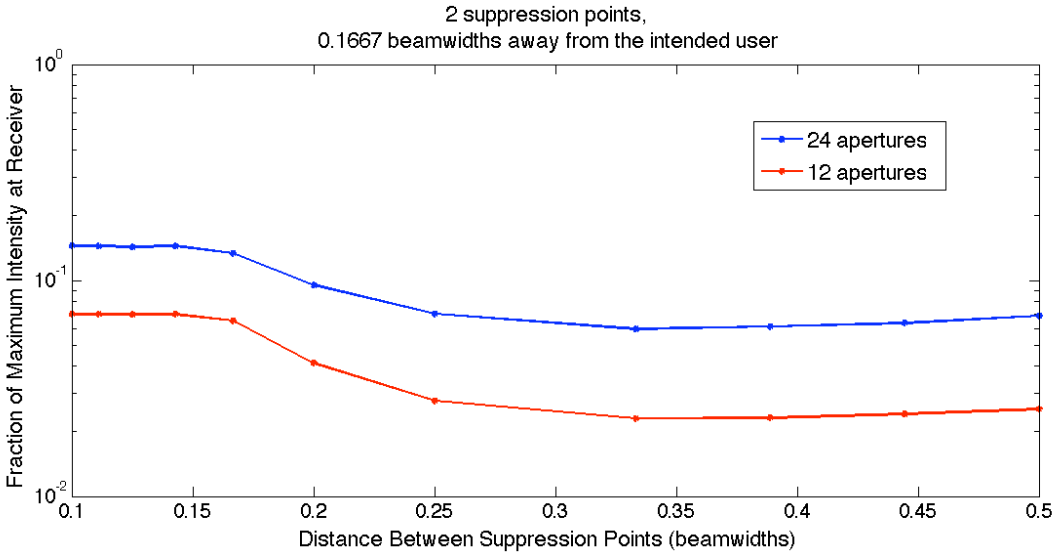

Figure 5.8 Fraction of maximum user power received after suppression versus distance between suppression points, for varying number of apertures. The first suppression point is located 0.1667 beamwidths away from the receiver.

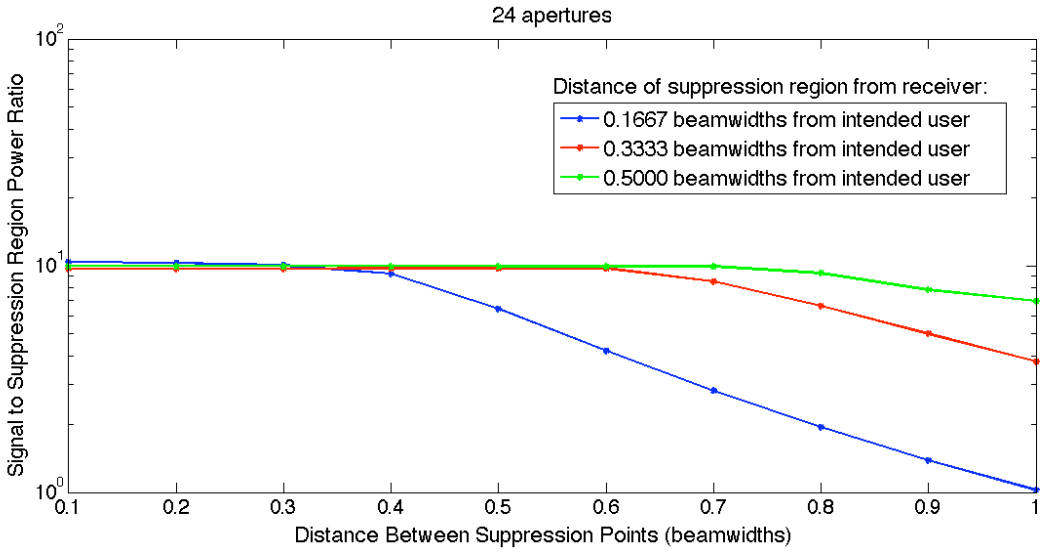

Figure 5.9 Signal to suppression region power ratio versus distance between suppression points, for various suppression region positions.

Figure 5.10 shows that the effect on the achievable signal-to-suppression-region ratio caused by increasing the separation between suppression points is worse with more apertures, but we see in Figure 5.8 that the effect on the receiver power is worse with fewer apertures. This is a result of our method of approximating the suppression region, through which we enforce the desired signal-to-suppression-region ratio only at the specified suppression points. Thus when the suppression points are farther apart, the power to those points is suppressed exactly, but the power to the region between them is not deliberately limited. With more apertures, the algorithm has more degrees of freedom with which to maximize the receiver power, but in doing so, it may create intensity peaks in between the spread suppression points.

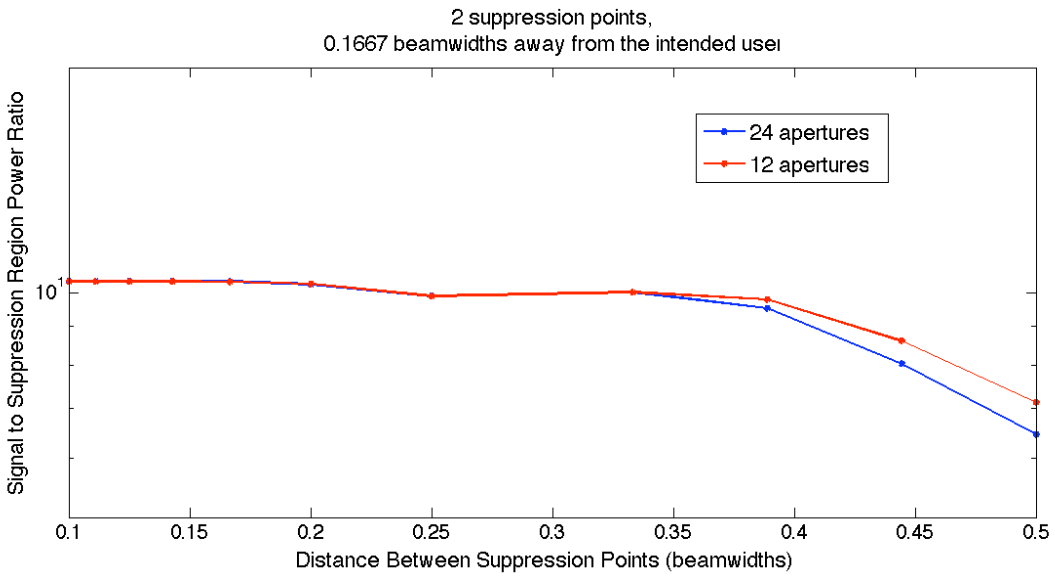

Figure 5.10 Signal to suppression region power ratio versus distance between suppression points, for varying number of apertures.

Although we claim that the achievable signal-to-suppression-region ratio is more important than the corresponding decrease in user power, the decrease in received power at the user is important for two reasons. One, the number of iterations required for ISRES to reach a solution increases as the post-suppression power at the intended receiver decreases. Two, the transmitter power required to ensure successful transmission to the intended receiver increases linearly with the decrease in receive power. While a 10 dB increase in required transmit power might be acceptable, a 30 dB increase might not be. Thus, it is useful to note what parameters affect the post-suppression receive power.

5.3.2 Distance and Length of Suppression Region

This section discusses how the power received by the intended user after suppression varies with the distance of the suppression region from the receiver. The distance of the suppression region from the receiver is measured from the first point in the suppression region. We noted earlier that for a filled array, increasing the number of apertures increases the fraction of the maximum user power received after suppression. Figure 5.11 highlights the difference in this receive power ratio between a filled 12 aperture array and a filled 24 aperture array, with a 1-beamwidth long suppression region. The receive power ratio from the 24 aperture array is consistently higher than that of the 12 aperture array, but the difference in the ratio grows smaller as the suppression region moves further away from the receiver.

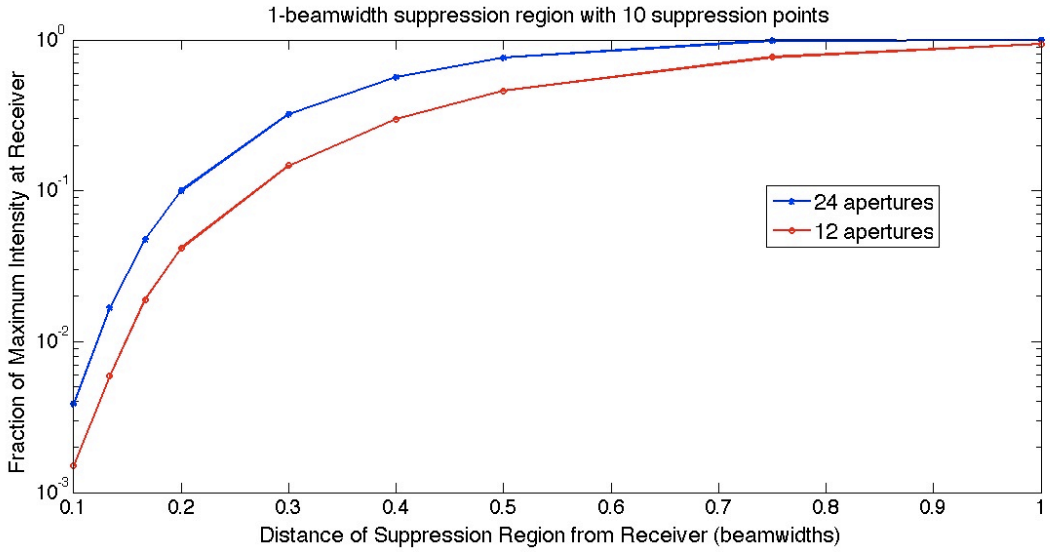

Figure 5.11 Fraction of maximum user power received after suppression versus distance of suppression region, for varying number of apertures.

Figures 5.12 and 5.13 compare the effect of different suppression region lengths on the power received by the intended user after suppression as the distance of the suppression region moves from the receiver for different suppression region lengths. We increase the length of the suppression region by increasing the number of suppression points; the distance between the suppression points is kept constant at 0.1111 beamwidths. Each curve represents a suppression region of a different length. Figure 5.12 shows that regardless of suppression region length, the user power after suppression increases with the distance of the suppression region from the intended receiver. Figure 5.13 shows that the decrease in received user power after suppression is on the order of 20 dB when the suppression region is within a fifth of a beamwidth from the receiver. This indicates that although an signal-to-suppression-region ratio of 10 can be achieved when the suppression region is as close as a tenth of a beamwidth away from the intended user, the necessary increase in transmit power might be too expensive, depending on the length of the suppression region. Both plots indicate that when the suppression region is very close to the receiver, the length of the suppression region has a much greater effect on the post-suppression power at the receiver.

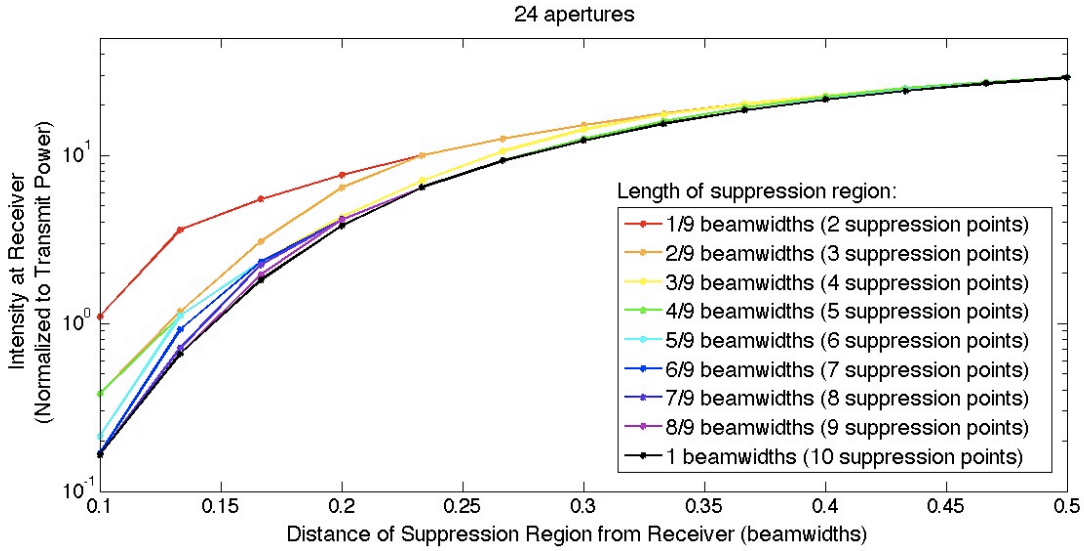

Figure 5.12 Intensity at the receiver after suppression versus distance of suppression region from receiver, for various suppression region lengths. The intensity is normalized such that the transmit power $\sum_{i=1}^{N} A_i |w_i|^2 = 1$, where N is the number of apertures, A_i is the area of aperture i, and w_i is the weight of that aperture.

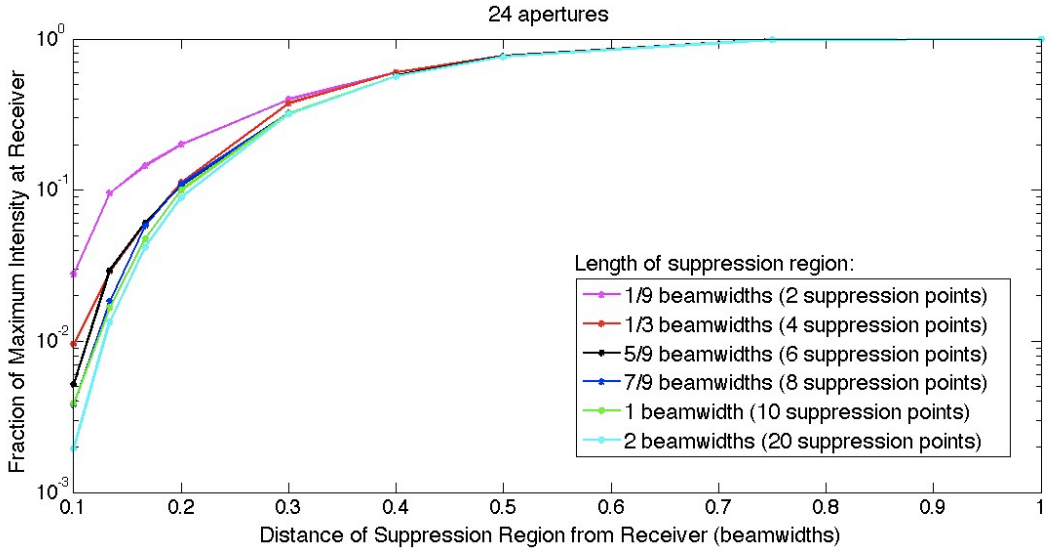

Figure 5.13 Fraction of maximum user power received after suppression versus distance of suppression region, for various suppression region lengths.

Figure 5.14 shows how the length of the suppression region affects the power at the intended user after suppression. A longer suppression region is necessary when there is significant uncertainty as to an eavesdropper's or another user's position. It is clear from the figure that the location of the first point in the suppression region is much more significant than the length of the suppression region itself. The first point has the highest received power prior to suppression and is closest to the intended receiver; therefore it is the hardest to suppress without pulling down the intended user's received power. Points further out in the suppression region are successively easier to suppress. For a suppression region 0.5 beamwidths away, changing the length of the suppression region has a negligible effect. However, for a close-in suppression region 0.1 beamwidths away from the from receiver, the length of the suppression region has a significant impact on the post-suppression user power. Figure 5.14 indicates that if an eavesdropper is close to the receiver, in order to achieve adequate suppression with a reasonable transmit power, the uncertainty as to his position must be smaller than if the eavesdropper were further away.

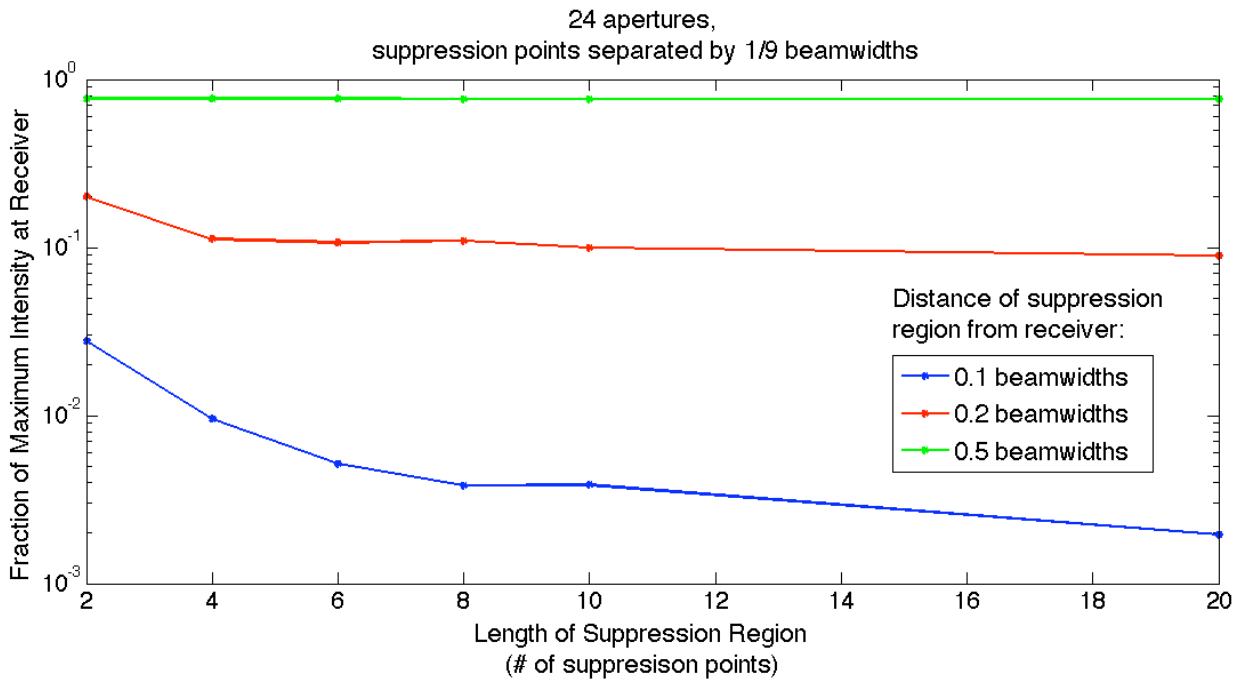

Figure 5.14 Fraction of maximum user power received after suppression versus length of suppression region, for various suppression region positions.

5.4 Summary of Trends

- It is possible to suppress the power to a broadly defined region in the receive plane without compromising the ability of the intended user to receive the signal.
- The amount of time the stochastic evolutionary algorithm takes to converge to the optimum weight vector is approximately constant if the suppression region is 0.2 beamwidths or more away from the intended user.
- The sequential quadratic programming local algorithm is about three orders of magnitude faster than the evolutionary global algorithm. For our calculations in this chapter, both algorithms converge to equivalent solutions.

- The separation between suppression points in the suppression region must be smaller than the distance between the user and the suppression region to prevent a significant decrease in post-suppression power at the receiver. If we assume the closest region we will suppress power to is 0.1 beamwidths away from the receiver, then the distance between the suppression points must be no more than 0.1 beamwidths.

- The separation between suppression points must be less than twice the distance between the user and the suppression region in order for an SSR of 10 to be achieved through optimization.

- The required transmit power increases as the suppression region moves closer to the intended user. Closer than 0.2 beamwidths, scaling the transmit power to maintain the integrity of the signal at the user becomes rapidly expensive.

- The distance of the first suppression point is much more significant than the length of the suppression region. However, suppressing more points does decrease the power received by the intended user.

- For smaller fill factors, the number of apertures is much less significant than the width and distance between apertures. The receive power ratio can even decrease with increasing number of apertures. Additionally, as the fill factor gets smaller, the grating lobes become potentially damaging, allowing interference and interception much further away than just within the main lobe. However, smaller fill factors with more apertures are best at mitigating the effects of turbulence via spatial diversity.

Chapter 6

Suppression Via Two-Dimensional Aperture Array

As described in Chapter 4 (Section 4.4.2), our example two-dimensional array system model comprises a 0.1 meter by 0.1 meter square aperture array centered at $(x, y) = (0, 0)$ in the transmit plane. Each aperture in the array is square, but its width can vary with the desired fill factor. The fill factor is defined as the total summed area of the apertures in the array divided by 0.01 square meters, the total area of the array. The optical wavelength is 10^{-6} meters and the receive plane is a distance of 10000 meters from the transmitter. The position of the intended receiver is at $(x, y) = (0, 0)$ in the receive plane. The desired signal-to-suppression-region power ratio (defined as the signal power at the user divided by the maximum power in the suppression region) is 10 dB until Section 6.3.

We measure distance along the x- and y- axes in approximate beamwidths of 0.1 meters, calculated from the array width of 0.1 meters. This is the approximate half-width of the main lobe of the transmission in the receive plane. Figure 6.1 demarcates a 1x1 beamwidth region in a plot of the output radiation pattern for a sparse array with 16 apertures, with maximum possible power transmitted to the receiver. For arrays with small fill factors, this beamwidth is also the approximate half-width of grating lobes. We can see several grating lobes in both the x- and y-directions in Figure 6.1. In Figure 6.2, we show the same plot in 3D, with the z-axis representing the relative intensity at the receiver.

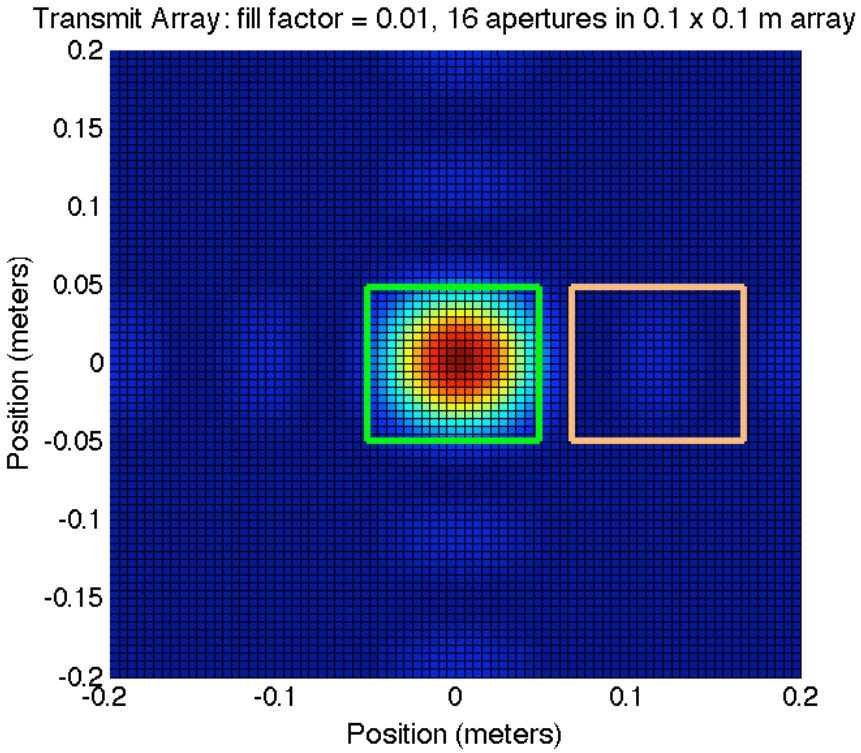

Figure 6.1a Radiation pattern in the far field from a 16-aperture transmit array with maximum power at the receiver. The intensity is represented by color; red represents the greatest intensity value and blue represents the lowest. The green square demarcates a 1×1 beamwidth region in the receive plane. The orange square shows the location of a grating lobe. Figures 6.1b and 6.1c below show 3D representations of this plot.

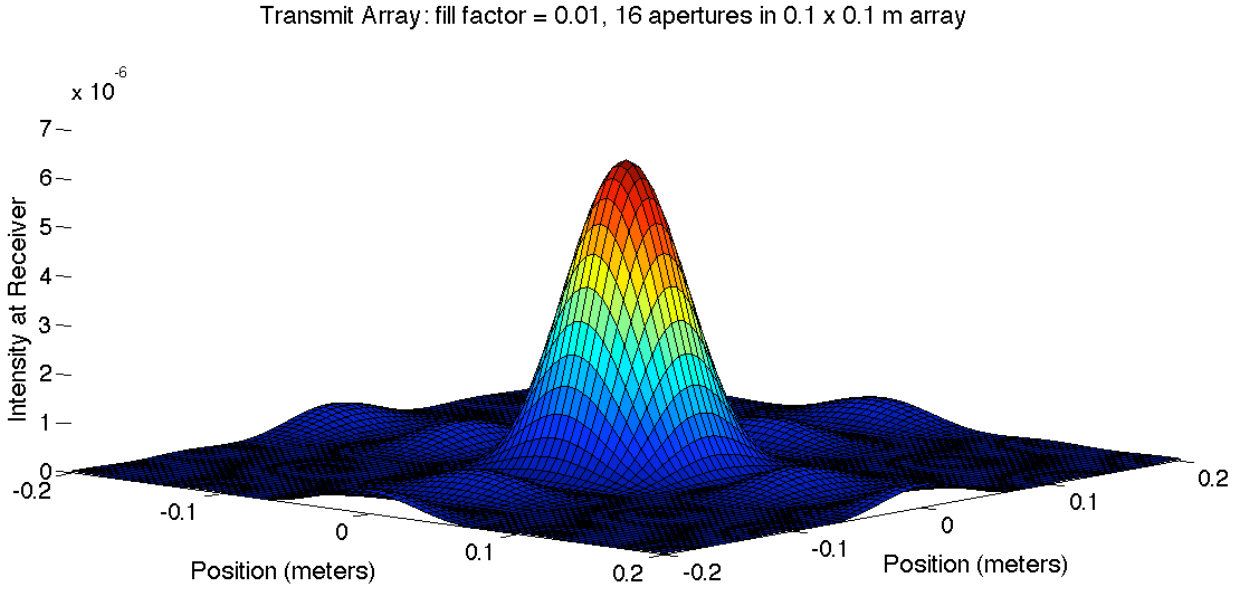

Figure 6.1b Radiation pattern in the far field from a 16-aperture transmit array with maximum power at the receiver, where the z-axis represents the intensity on a linear scale.

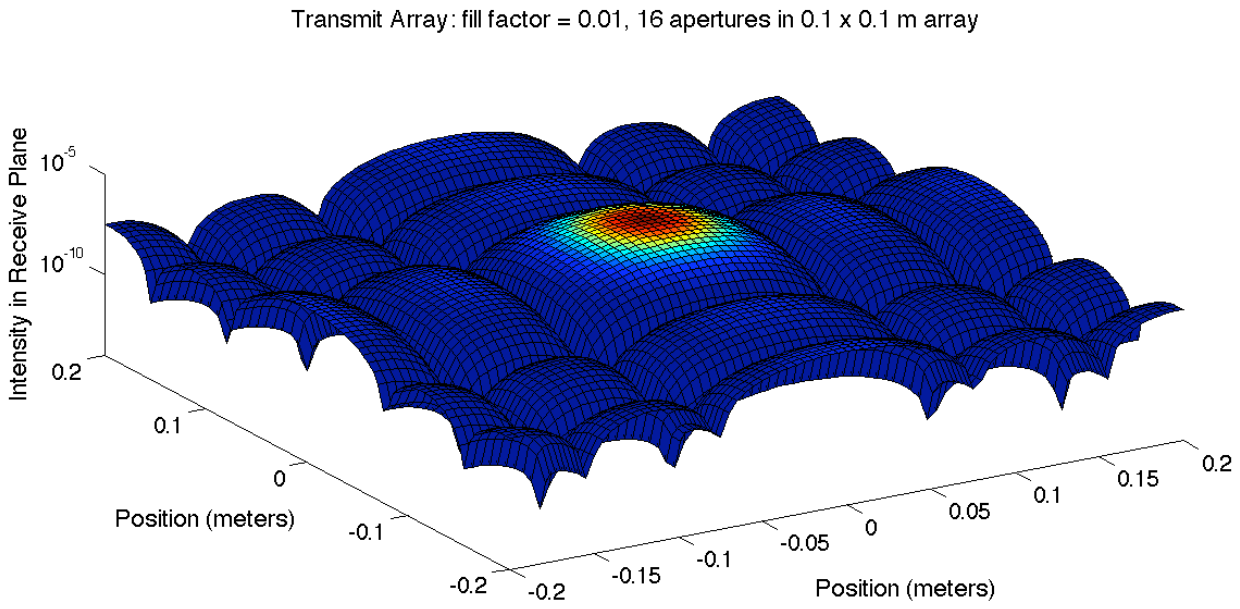

Figure 6.1c Radiation pattern in the far field from a 16-aperture transmit array with maximum power at the receiver, where the z-axis represents the intensity on a logarithmic scale. The existence of grating lobes is made clear by this representation of the intensity in the receive plane.

In this chapter, we always normalize the intensity at the receiver such that the total transmitted power $\sum_{i=1}^{N} A_i|w_i|^2$ is 1, where N is the number of apertures, A_i is the area of aperture i, and w_i is the weight of that aperture. Due to the increased complexity of the two-dimensional system compared to the linear array, we solve each system for the optimum weight vector using SLSQP to avoid the unreasonably long run times of ISRES.

6.1 Transmit Array Characteristics

In Figure 6.2, we vary the number of apertures and the fill factor of the transmit array, and plot the signal-to-suppression-region power ratio in a ½ × ½ beamwidth region as the suppression region moves away from the receiver. We constrain the power at the 4 corners of the square suppression region to less than one tenth of the power at the receiver. The plotted

signal-to-suppression-region power ratio is the ratio of the maximum intensity within the suppression region (bounded by the 4 suppression points) to the intensity at the receiver. As the suppression region moves away from the receiver, the intensity inside the suppression region decreases relative to the intensity at the receiver, and the ratio for the whole region approaches 10 dB.

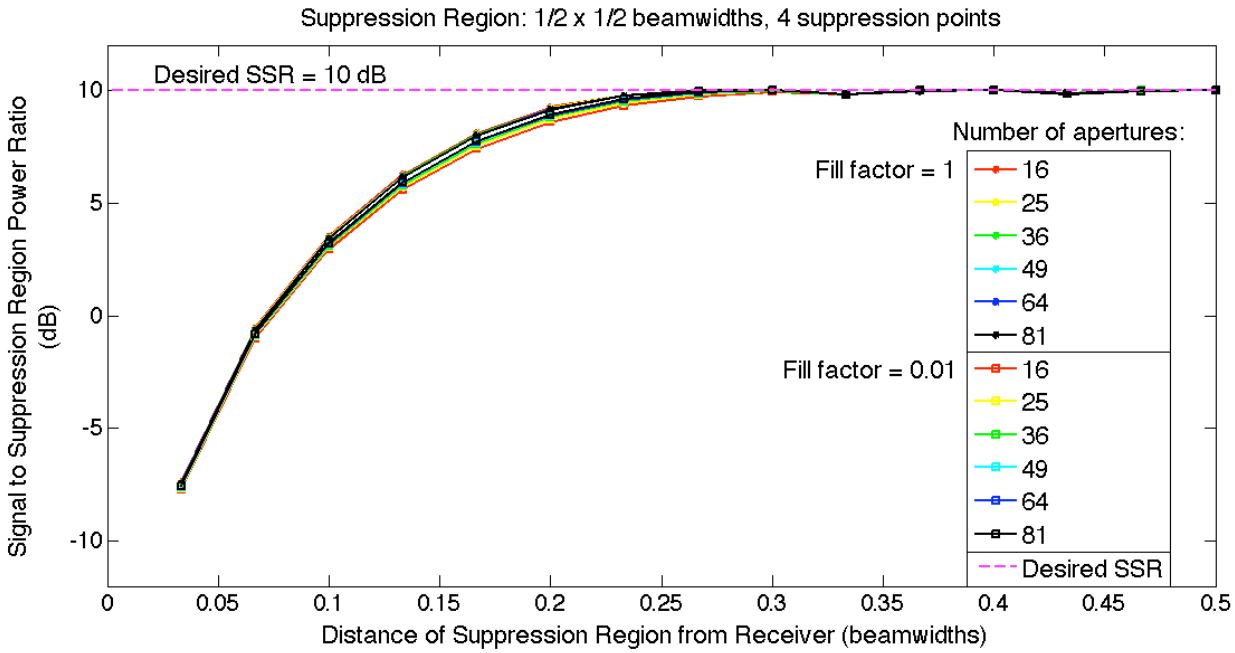

Figure 6.2 Achievable signal-to-suppression-region power ratio in a ½ × ½ beamwidth region versus distance of suppression region from receiver. The desired SSR of at least 10 dB is enforced only at the 4 suppression points at the corners of the suppression region. We vary the number of apertures and plot results for a fill factor of 1 and a fill factor of 0.01.

Figure 6.2 also indicates that for a two-dimensional array, the number of apertures and the fill factor of the array have very little effect on the achievable signal to suppression ratio. Increasing the fill factor improves the achievable ratio, but this improvement is slight. When the suppression region is between 0.0667 beamwidths and 0.3 beamwidths away from the receiver,

there is less than a 1 dB difference between the achievable signal-to-suppression-region power ratios of arrays with fill factors 0.01 and 1. When the suppression region is more than 0.3 beamwidths or less than 0.0667 beamwidths away from the receiver, the difference in ratios between the different transmit array configurations is effectively negligible, less than 0.2 dB. Changing the number of apertures has a similarly small effect. For a sparse array, the achievable suppression ratio is less than 0.5 dB greater for 81-aperture array than for a 16-aperture sparse array. Figure 6.2 therefore indicates that achieving some desired signal-to-suppression-region power ratio need not be a factor in the choice of the number of apertures and the fill factor for a transmit array. However, the choice of fill factor will be influenced by the signal strength required by the intended user and the available transmitter power. Additionally, if the suppression area is wider than a beamwidth, then the grating lobes resulting from small fill factors may make the problem of achieving the specified suppression ratio more difficult.

Figure 6.3 shows the intensity at the receiver versus the distance of suppression region for the same transmit arrays as in Figure 6.2. From this figure, we see that the power received by the intended user increases as the suppression region moves away from the intended receiver. The rate of this increase appears to be approximately the same for both fill factors. We also note that the number of apertures does not have a significant impact on the post-suppression intensity at the receiver. However, it is clear from this figure that increasing the fill factor significantly increases the intensity at the receiver after suppression, even if the total transmit power is the same. Given equal transmitter power, the intensity with the filled array is 20 dB greater than with the sparse array of fill factor 0.01. This is because the filled array can better direct the power towards the receiver. In Figure 6.4, we examine this effect more closely.

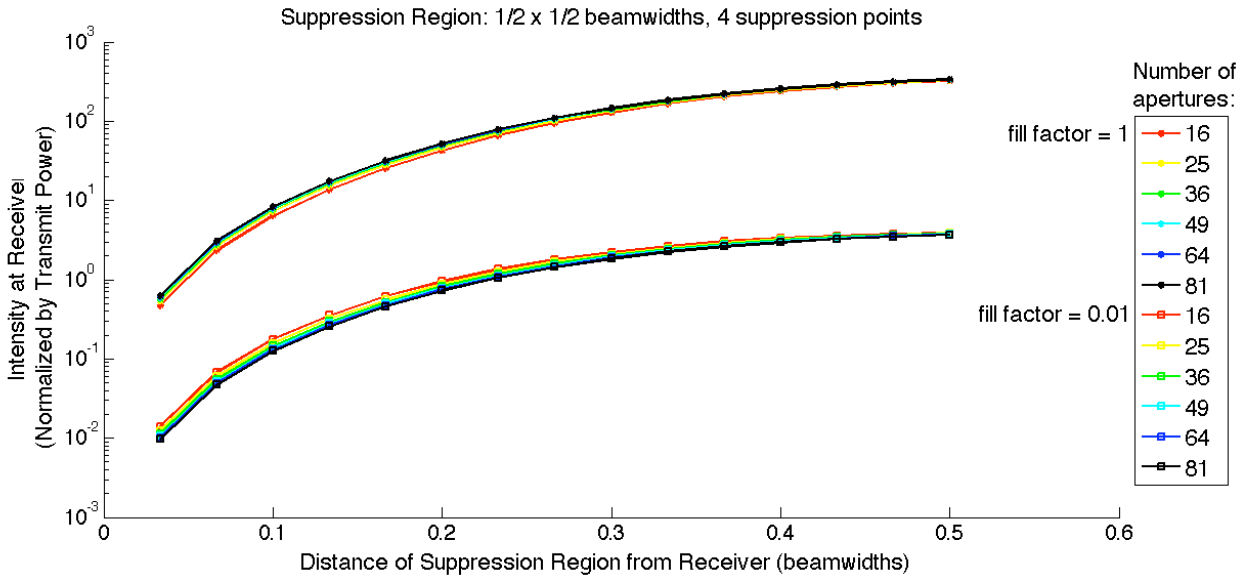

Figure 6.3 Intensity at receiver versus distance from suppression region. We vary the number of apertures and plot results for a fill factor of 1 and a fill factor of 0.01.

Figure 6.4 shows how the intensity at the receiver varies with fill factor. The effect of increasing the fill factor decreases as the fill factor approaches 1. It is clear that a fill factor of 1 achieves the best intensity at the receiver. We also note that the area of the suppression region does not change the effect of increasing the fill factor. However, it does appear to affect the absolute intensity at the receiver for each fill factor. Generally, increasing the area of the suppression region decreases the power at the receiver. Thus, in the plot below, the receiver intensity with the ¼ × ¼ beamwidth suppression region is greater than that with the ½ × ½ beamwidth suppression region. Exceptions occur only if the distance between the suppression points becomes large enough that the power to the region between these points is not very suppressed. In Figure 6.4, although the receiver intensity with a 1 × 1 beamwidth suppression region is greater than that with the ½ × ½ beamwidth suppression region, we note that for a fill factor of 0.1, the achievable suppression ratio for the 1 × 1 beamwidth region is only 4.41 dB,

much smaller than the achievable ratio of 9.81 dB for the ½ × ½ beamwidth region. Since achieving the desired signal-to-suppression-region power ratio is our primary objective, and maximizing the receive power is secondary to that goal, we do not need to consider the receiver power for systems for which the desired suppression is not possible.

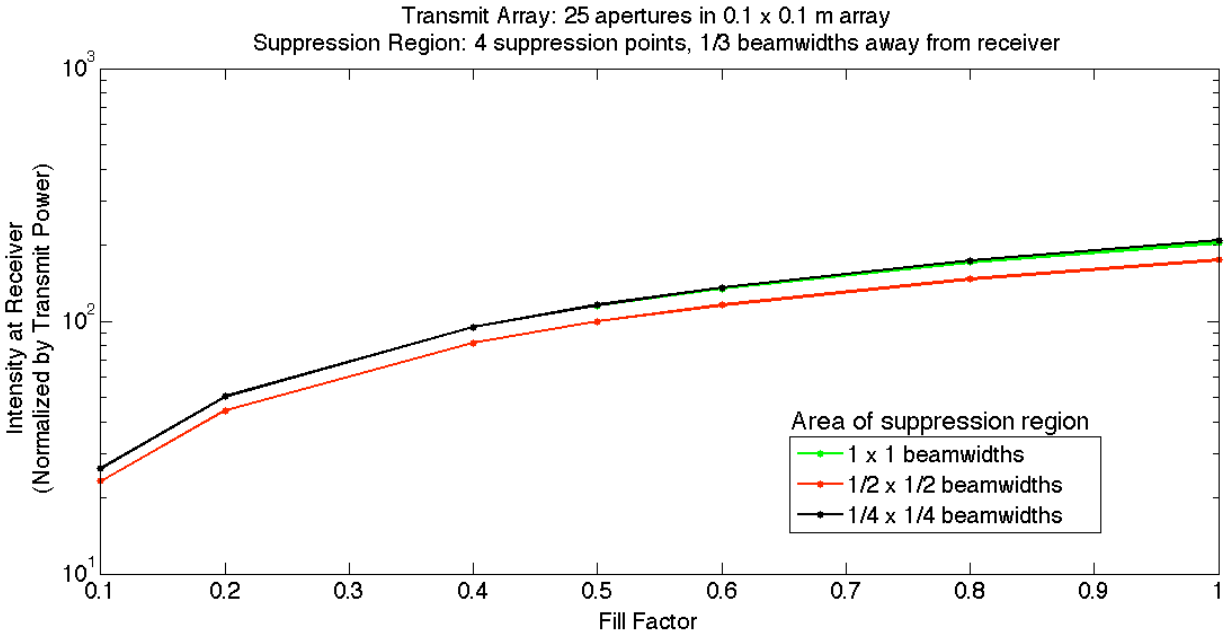

Figure 6.4 Intensity at receiver versus fill factor. We vary the area of the suppression region. There are 4 suppression points in this area to which the desired signal-to-suppression-region power ratio (SSR) of 10 dB is enforced. We want the intensity at the receiver to be as high as possible, but not at the cost of a lower SSR. As predicted, the received intensity for the ¼ × ¼ beamwidth suppression region is greater than the ½ × ½ beamwidth suppression region. Both of these regions can be suppressed to the desired 10 dB SSR. The 1 × 1 beamwidth suppression region does not match the expected pattern because the 4 suppression points that approximate the region are spaced too far apart for the 10 dB SSR to be achieved.

Before we address the effects of various suppression region characteristics, we comment on two counterintuitive results that are evident in Figures 6.2 and 6.3, in which increasing the number of apertures has opposite effects for the two different fill factors. [2]

1.) Increasing the number of apertures increases the achievable signal-t-suppression-region power ratio for small fill factors and decreases this ratio for large fill factors.

2.) Conversely, increasing the number of apertures decreases the intensity at the receiver for the sparse array; for the filled array, increasing the number of apertures increases the intensity at the receiver.

These results are related to the ratio between the power at the receiver and the power in the suppression region before suppression, an effect we discussed in the context of a linear array in Section 5.2.2, and now discuss for the two-dimensional array. Recall that our overall array has a fixed size. This means that for any given fill factor, we cannot independently consider the number of apertures or the size of the apertures.

For maximum diversity, we desire a small fill factor and a large number of apertures. As noted in Chapter 5, to increase the number of apertures in a sparse array with both a fixed fill factor and fixed dimensions, we must decrease both the distance between apertures and the size of the apertures. Thus, the energy in the far field is more spread out, and the intensity at the receiver decreases, while the intensity in the suppression region (before suppression) increases. For a filled array, the distance between the apertures is irrelevant, and the effect of decreasing the size of the aperture is countered by the additional degrees of freedom apertures from the

[2] Recall that in our system model, the sub-apertures are identical and uniformly spaced along the x- and y- axes of the array. Therefore our results do not reflect the effect on the system of adding additional apertures in other locations in the array (e.g. adjacent to the existing apertures in a sparse array) or of using apertures of varying size.

additional apertures. Thus the intensity at the receiver increases with more apertures, while the pre-suppression intensity in the suppression region decreases.

We can now explain the effect on the signal-to-suppression-region ratio of increasing the number of apertures. For the sparse array, as the number of apertures increases, the intensity at the receiver decreases due to the wider energy distribution, and the pre-suppression signal-to-suppression-region ratio decreases. Achieving the desired suppression ratio of 10 dB is correspondingly difficult, and the post-suppression ratio is smaller. For the filled array, the opposite occurs. The intensity at the receiver increases due to the higher-dimensional weight vector, and the pre-suppression signal-to-suppression-region ratio increases. Here, achieving the desired suppression ratio of 10 dB is easier, and the post-suppression ratio is closer to 10 dB as the number of apertures increases.

6.2 Suppression Region Characteristics

We now look more closely at the effect of changing the area of the suppression region. Figure 6.5 depicts the achievable signal-to-suppression-region power ratio versus the distance of the suppression region. We consider square suppression regions of varying width, approximated via suppression points in the 4 corners. Because any square suppression region we consider will consist of a square number of such suppression regions regardless of the number of suppression points, the effect of varying the suppression region areas in Figure 6.5 could also be considered the effect of varying the distance between suppression points.

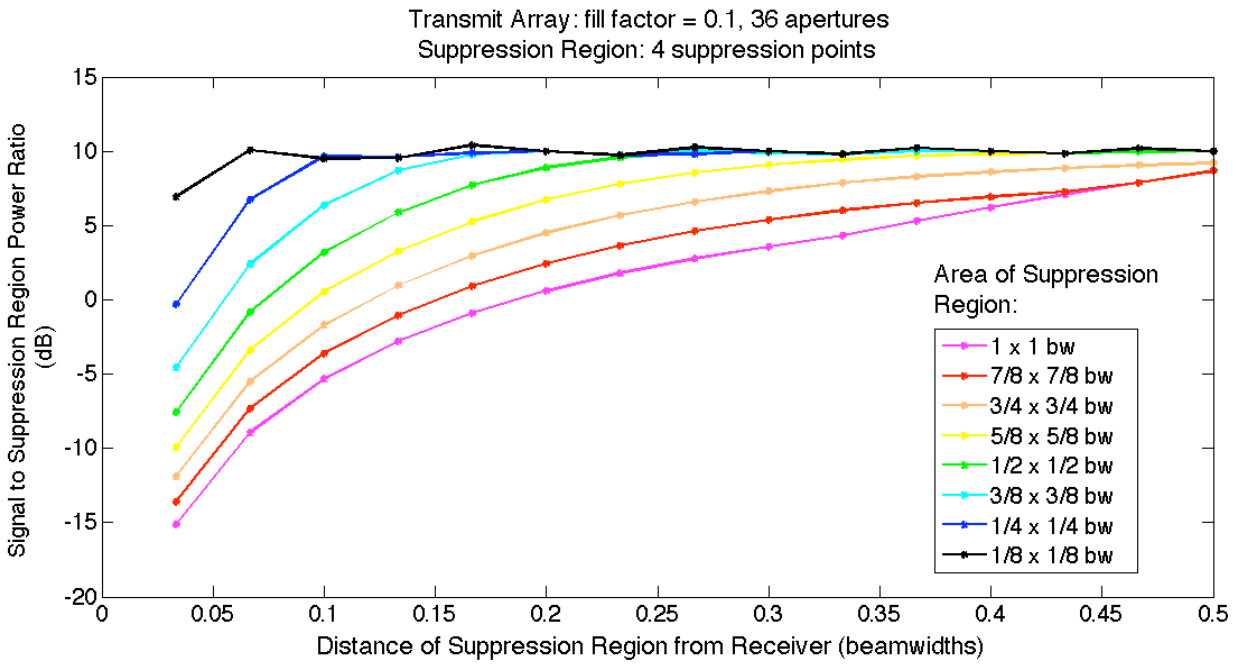

Figure 6.5 Achievable signal-to-suppression-region power ratio (SSR) versus distance of suppression region. We vary the area of the suppression region. There are 4 suppression points in this area to which the desired SSR of at least 10 dB is enforced. The plotted SSR is the ratio of the maximum power in the suppression region to the power at the receiver after suppression.

Figure 6.5 shows that the rate at which the achievable signal-to-suppression-region power ratio approaches the desired suppression of 10 dB increases with decreasing distance between suppression points. This figure depicts the two-dimensional analog of our claim in Chapter 5 that there is a tradeoff between the distance of another user or eavesdropper in the receive plane from the receiver and our uncertainty as to the user's exact position. If the other user is very close to the intended receiver, we must be significantly more certain as to his position in order to suppress all probable user locations to the desired ratio. As the user moves farther away, we can achieve the desired suppression ratio without having precise information about its position. If we want to suppress by 10 dB a region 0.1 beamwidths away from the receiver, the distance between the suppression points must be no more than 0.25 beamwidths.

Figures 6.6 and 6.7 compare the effects of increasing the width of the suppression region and increasing the number of suppression points. Figure 6.6 shows the closest distance a 10 dB suppression ratio is possible versus the width of the suppression region. This is plotted for three different approximations of each suppression region – with 4, 9, and 16 suppression points. Figure 6.7 shows the closest distance a 10 dB suppression ratio is possible versus the number of suppression points for three different sized suppression region. We define the closest distance suppression possible as the first location where the signal-to-suppression-region ratio exceeds 90% of the desired suppression ratio.

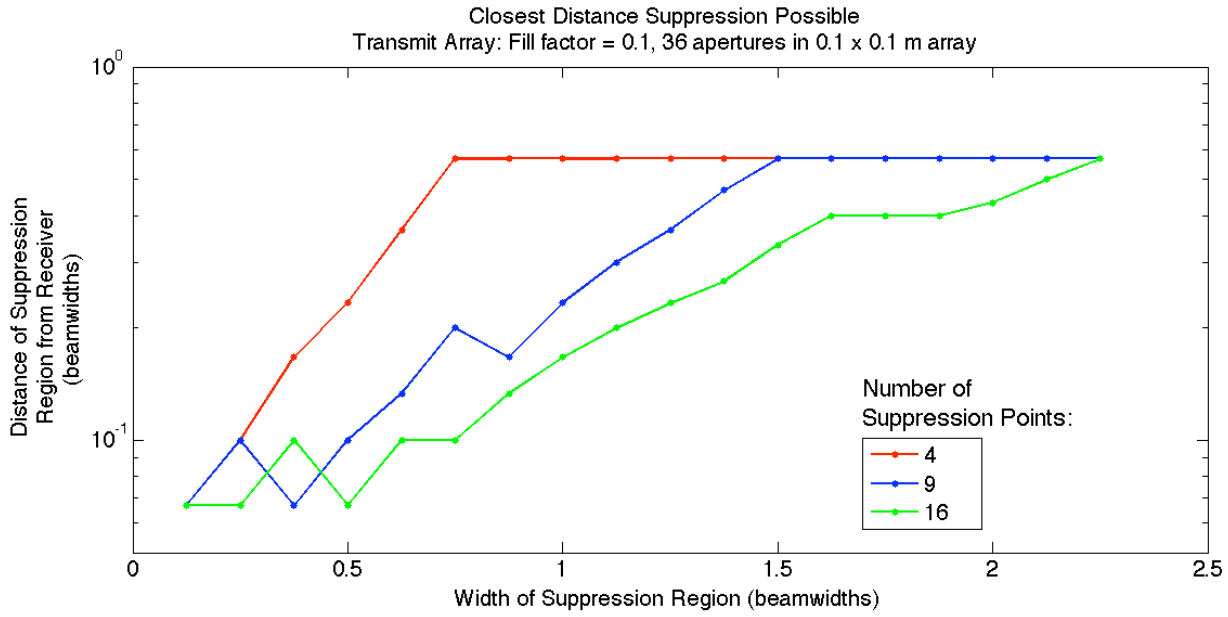

Figure 6.6 Closest distance suppression by 10 dB is possible for a given width of suppression region. We vary the number of suppression points to which the desired signal-to-suppression-region power ratio of 10 dB is enforced.

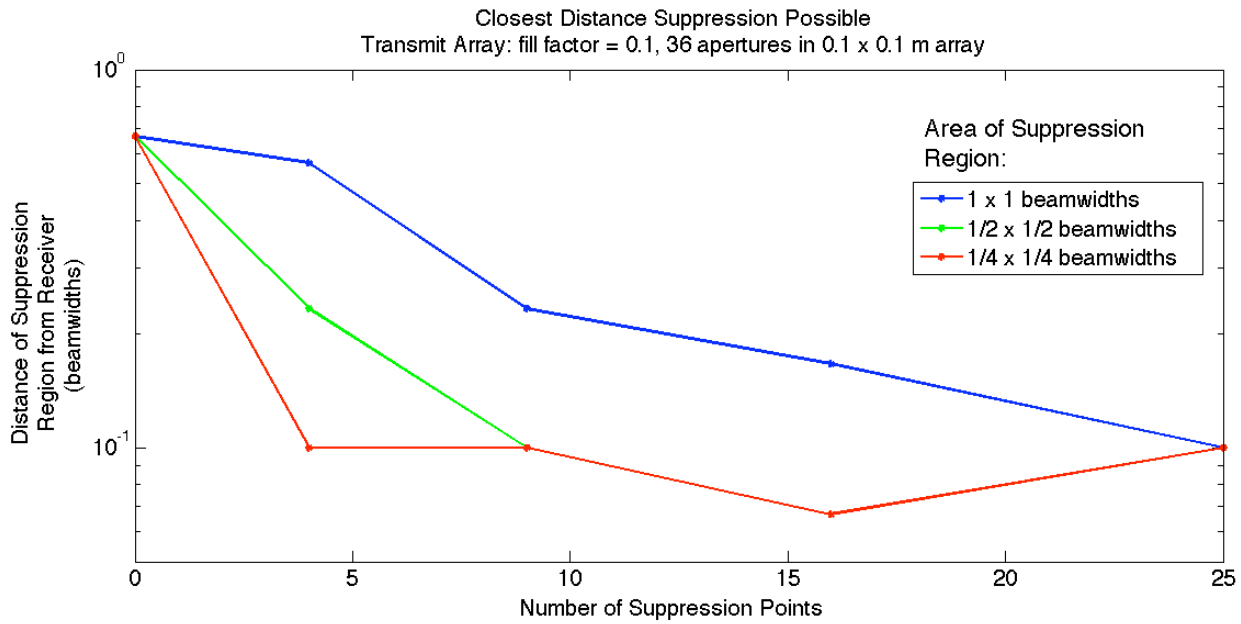

Figure 6.7 Closest distance suppression by 10 dB is possible for given number of suppression points. We vary the area of suppression region.

We observe two major trends: increasing the area of the suppression region increases the distance from the receiver at which suppression becomes possible, but increasing the number of suppression points decreases that distance. Both of these trends are a function of the inter-suppression-point spacing. As the area of the suppress region increases, the spacing between the points increases; as the number of suppression points increases, the spacing between the points decreases. Thus, we can compensate for uncertainty as to an eavesdropper's position by increasing the number of suppression points used to approximate its location.

We observe some kinks in the plots, particularly for larger number of suppression points. This may occur because as the number of suppression points increases, the optimization problem contains fewer degrees of freedom to maximize the intensity. If the intensity is lower, it becomes harder to increase the suppression ratio. This effect is intensified if the suppression points are very close together such that enforcing the suppression ratio at one point affects the ratio at another suppression point. Because of the complexity of the equations involved,

particularly the Fraunhofer diffraction pattern, many of the relationships between various parameters and the signal-to-suppression-region are not monotonically increasing or decreasing. However, since the kinks in the plots we observe are fairly small in both amplitude and beamwidth, the general trends we observe will still be useful when designing a system.

In Figure 6.6, the horizontal line to which all three of the plots converge is 0.5667 beamwidths. This suppression region position is 0.1 beamwidths closer to the receiver than the position at which the desired suppression ratio of 10 dB is achieved without suppression, when maximum power is directed at the intended receiver. At this point, it is unnecessary to have a suppression region that is much wider than 0.1 beamwidths, unless the suppression region is wide enough to extend to a grating lobe. Thus 4 suppression points are sufficient mainly for regions less than 0.75 beamwidths wide. However, much wider suppression regions can be successfully approximated by 4 points if they are located at least 0.5667 beamwidths away from the receiver. A 9-point suppression region is therefore useful only for regions less than 1.5 beamwidths wide, and a 16-point region is only useful for regions less than 2.25 beamwidths wide. For larger regions 4 suppression points could achieve the same signal-to-suppression-region power ratio.

We can use Figure 6.7 to find the closest distance suppression by 10 dB is possible for a given separation of suppression points. For instance, in order to suppress to 10 dB the power in a region 0.1 beamwidths away from the receiver, a ¼ × ¼ beamwidth region must have 4 suppression points, a ½ × ½ beamwidth region must have 9 points, and a 1 × 1 beamwidth region must have 25 suppression points. These all correspond to square regions with suppression points separated by ¼ beamwidths.

Figure 6.8 also shows how the number of suppression points affects the achievable signal-to-suppression ratio for a 1×1 beamwidth region varying distances from the receiver. As expected, increasing the number of suppression points decreases the distance at which a signal-to-suppression-region power ratio of 10 dB is achievable. Each curve in the figure reaches a suppression ratio of 10 dB when the distance between the suppression region and the receiver is approximately one half the distance between adjacent suppression points in the suppression region. This roughly corresponds to what we noted in Figure 6.7.

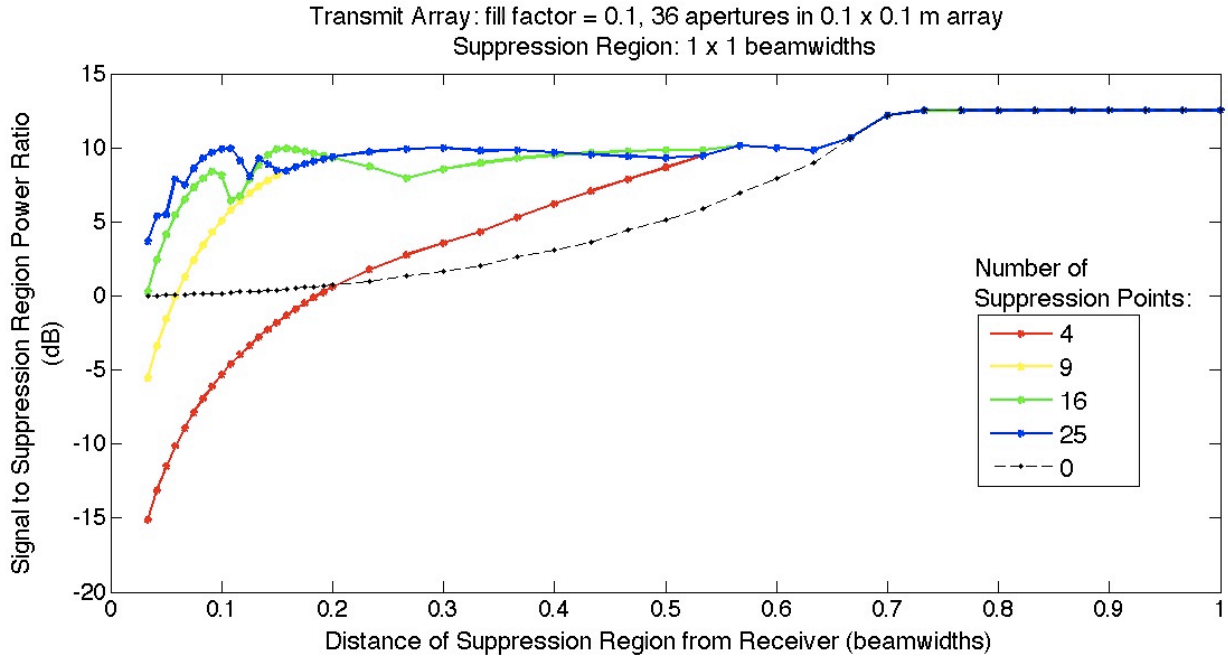

Figure 6.8 Achievable signal-to-suppression-region power ratio (SSR) for a 1×1 beamwidth region as it moves away from the receiver. We vary the number of suppression points to which the desired SSR of at least 10 dB is enforced.

6.3 Desired Signal-to-Suppression-Region Power Ratio

In this section, we vary the desired signal-to-suppression-region power ratio and show the effects on the intensity at the receiver and the distance at which various suppression ratios are achievable. Figure 6.9 shows the intensity at the receiver versus the desired suppression ratio for a suppression region 1/3 beamwidths away from the receiver. Each curve represents a suppression region of a different area. The figure shows that the post-suppression intensity at the receiver decreases as the signal-to-suppression ratio increases. The rate of decrease is slower for smaller suppression region areas, although the curves for the 1 x 1 beamwidth region and the ½ x ½ beamwidth region are very close.

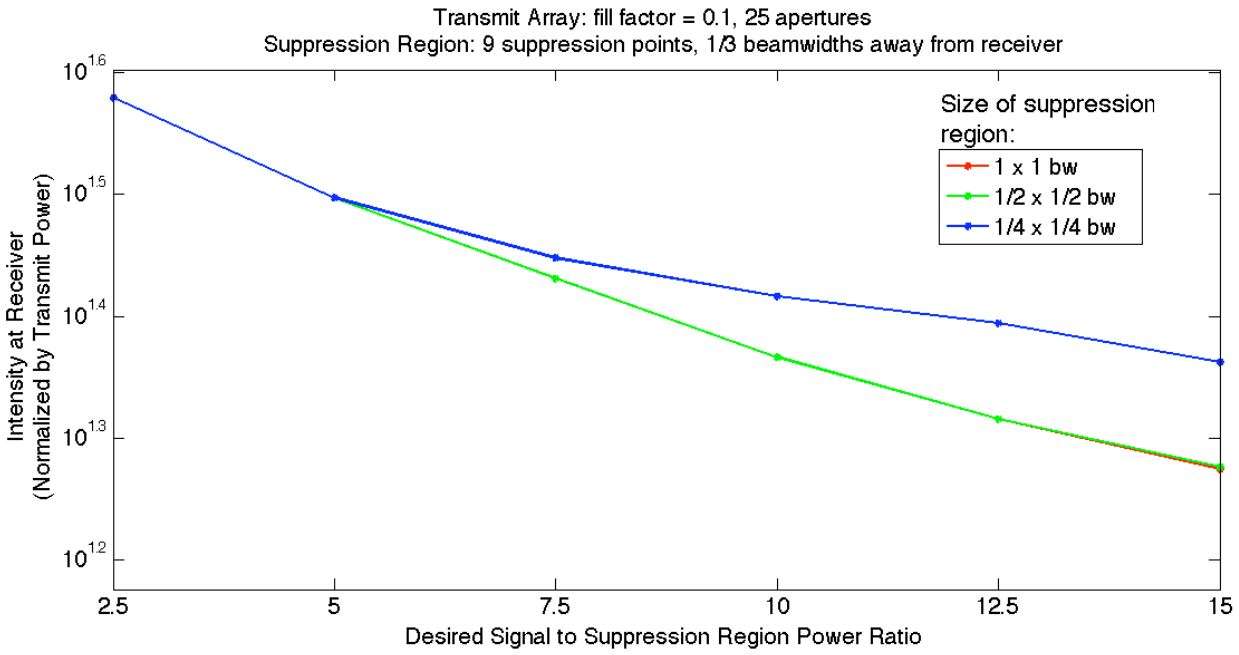

Figure 6.9 Intensity at receiver versus desired signal-to-suppression-region power ratio (SSR). We vary the area of the suppression region. There are 9 suppression points in this area to which the desired SSR is enforced.

Figure 6.10 reveals two trends. One, as the desired signal-to-suppression-region ratio increases, the distance at which such a ratio is achievable increases. The rate of this increase is fairly constant for different suppression region parameters. Two, as discussed in Section 6.2, the distance at which the desired suppression ratio is achievable is affected more by the separation between suppression points than by the area of the suppression region or the number of suppression points independently. As the distance between suppression points increases, the distance at which suppression is possible also increases, due too the unsuppressed energy spikes that occur between the suppression points of close-in suppression regions with widely spaced points.

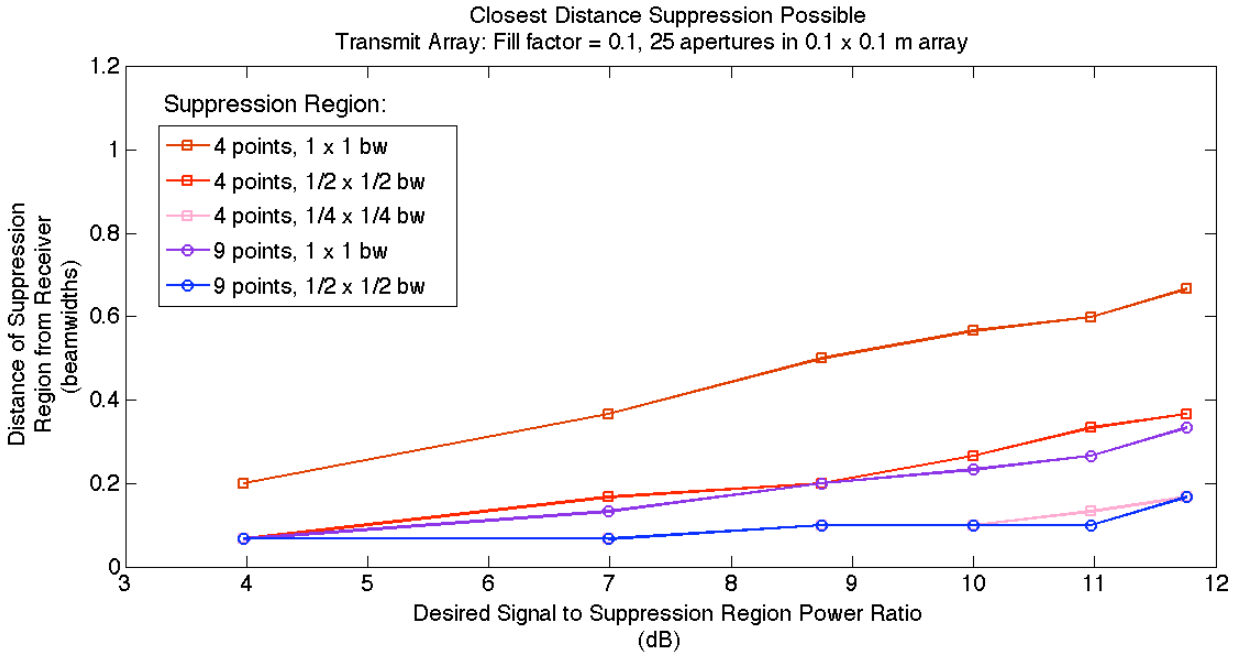

Figure 6.10 Closest distance a desired signal-to-suppression-region power ratio (SSR) can be achieved, based on the suppression region geometry. We vary both the area of the suppression region and the number of suppression points in this area to which the desired SSR is enforced.

Figure 6.11 shows four plots, each showing the signal-to-suppression-region power ratio versus distance of the suppression region from the receiver for six different desired suppression ratios. Each plot shows results for a different suppression region. Figure 6.11a shows results for a ½ × ½ beamwidth suppression region approximated by 4 suppression points. Figure 6.11b shows results for a ¼ × ¼ beamwidth suppression region approximated by 4 points. Figure 6.11c shows results for a ½ × ½ beamwidth suppression region approximated by 9 points. Figure 6.11d shows results for a ¼ × ¼ beamwidth suppression region approximated by 9 points. Figures 6.11b and 6.11c therefore show results for suppression regions with the same suppression point spacing.

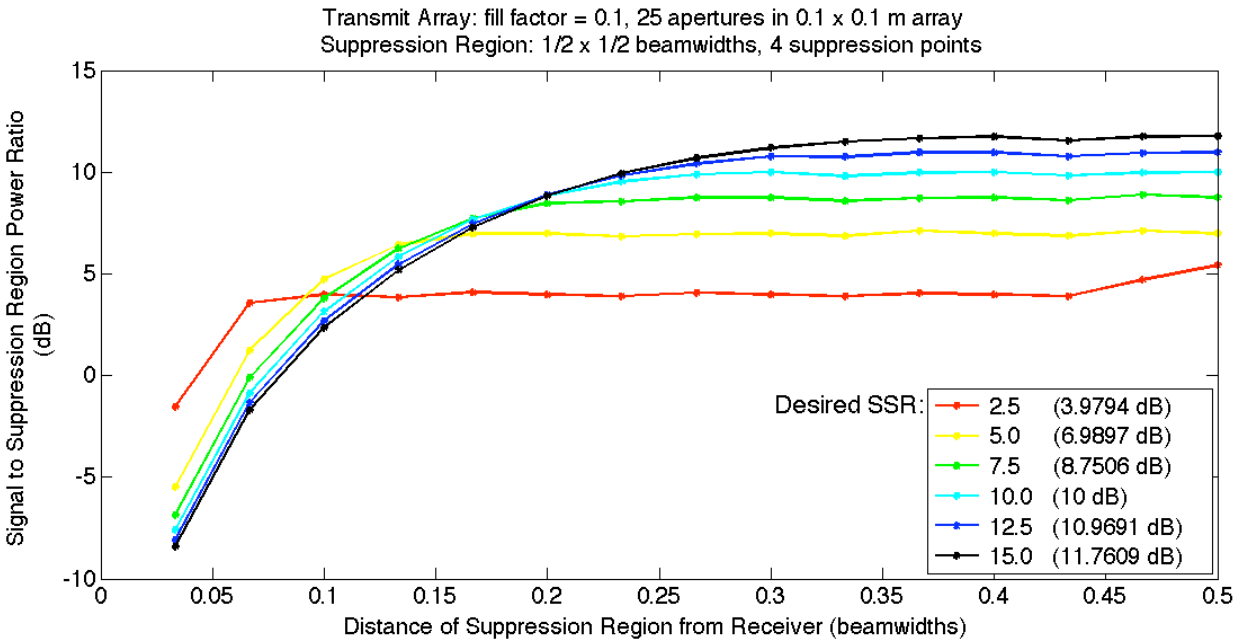

Figure 6.11a Achievable signal-to-suppression region ratio (SSR) for a ½ × ½ beamwidth suppression region as it moves away from the receiver. The desired SSR is only enforced at 4 suppression points.

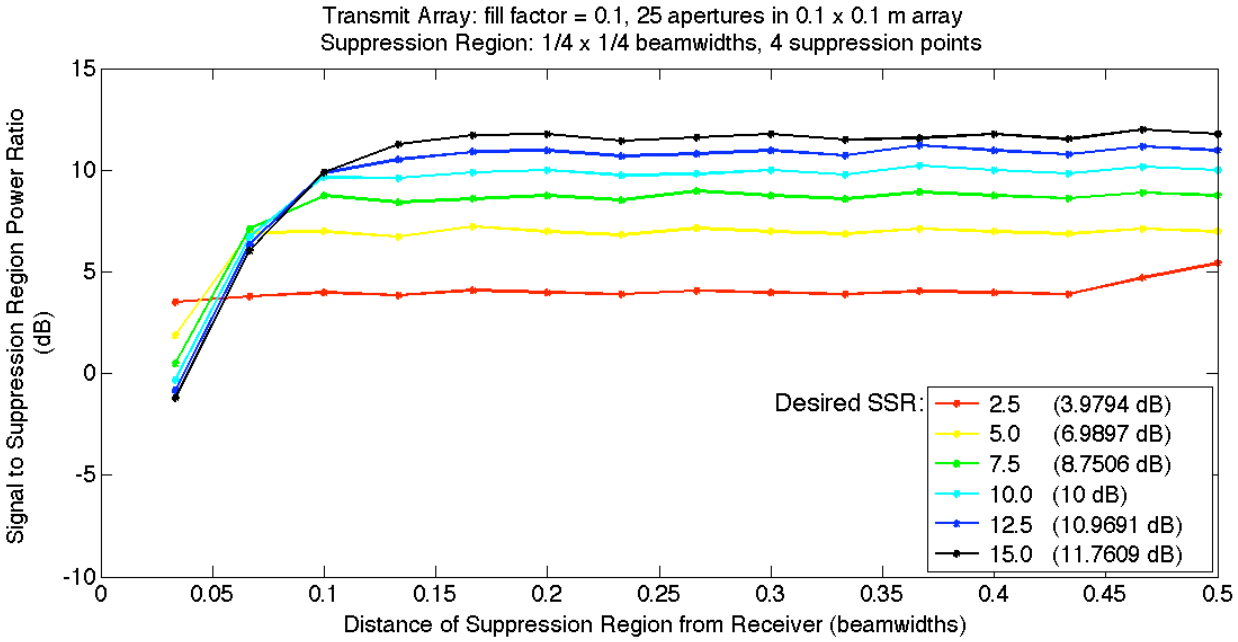

Figure 6.11b Achievable signal-to-suppression region ratio (SSR) for a ¼ × ¼ beamwidth suppression region as it moves away from the receiver. The desired SSR is only enforced at 4 suppression points.

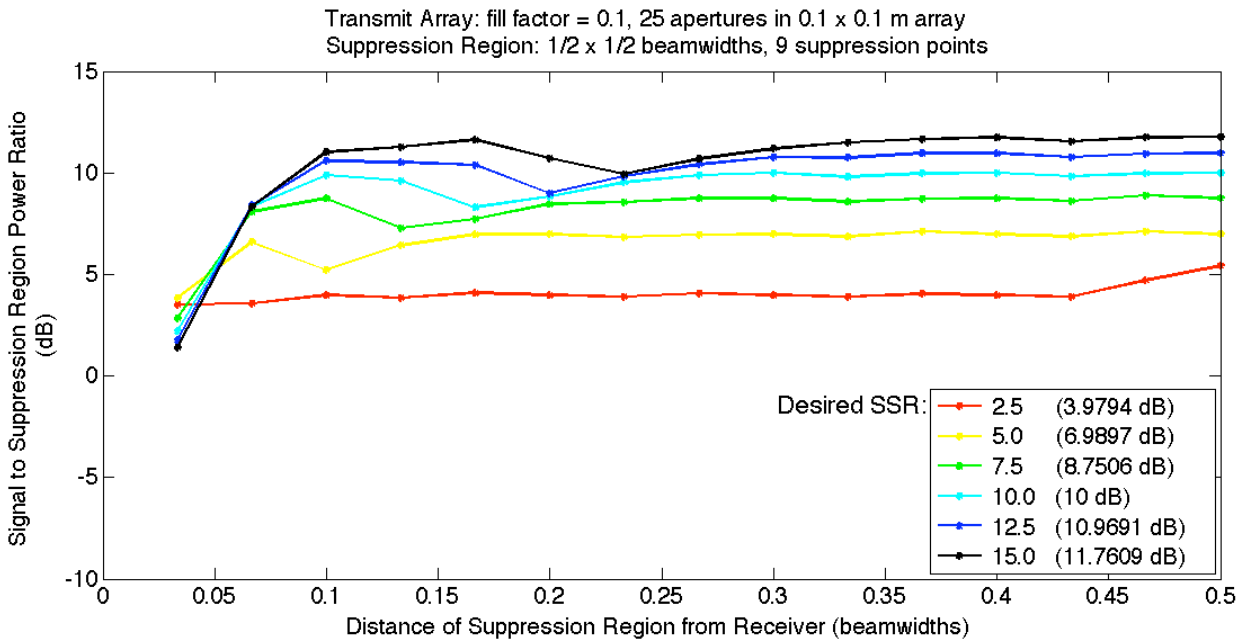

Figure 6.11c Achievable signal-to-suppression region ratio (SSR) for a ½ × ½ beamwidth suppression region as it moves away from the receiver. The desired SSR is only enforced at 9 suppression points.

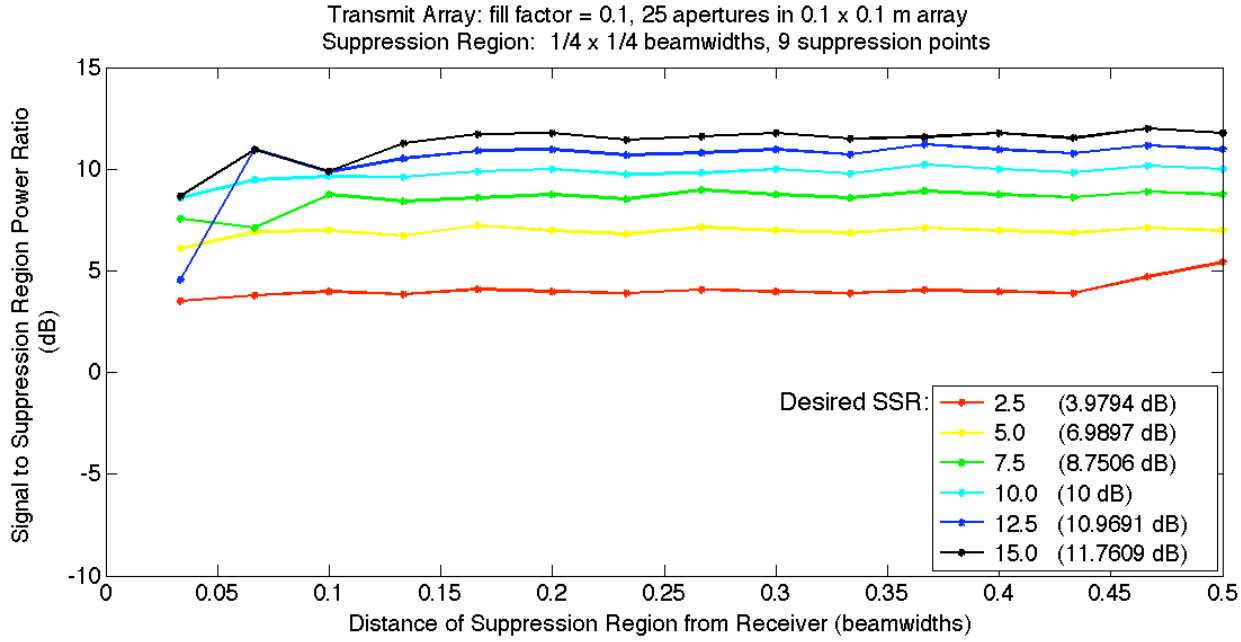

Figure 6.11d Achievable signal-to-suppression region ratio (SSR) for a ¼ × ¼ beamwidth suppression region as it moves away from the receiver. The desired SSR is only enforced at the 9 suppression points.

The results in Figure 6.11 are what we would expect from our previous analysis. In each case, increasing the desired signal-to-suppression-region power ratio increases the distance at which the desired suppression ratio is achieved. The achieved signal-to-suppression-region power ratio increases with increasing distance of the suppression region from the receiver until it reaches the desired ratio, at which point it remains approximately constant.

Comparing Figure 6.11a with Figure 6.11b, and Figure 6.11c with Figure 6.11d, we see that decreasing the area of the suppression region decreases the distance at which the desired suppression ratio is achieved. Comparing Figure 6.11a with Figure 6.11c, and Figure 6.11b with Figure 6.11d, we note that the increasing the number of suppression points in the suppression region has a similar effect to decreasing the area. Since increasing the number of suppression points will generally decrease the post-suppression power at the receiver and may not yield a feasible solution to the optimization problem, it is best to instead decrease the area of the suppression region. However, decreasing the area of the suppression region requires us to have more information about the position of the user or eavesdropper to whom we are suppressing power, which we may not be able to acquire.

6.4 Time to Convergence

The plots in Figure 6.12 illustrate the performance of the SLSQP algorithm in solving the optimization problem for a two-dimensional system. We compare the run time of the algorithm, the number of iterations, and the average time per iteration for the variable system parameters: number of apertures, suppression region position, fill factor, number of suppression points, and width of the square suppression region. We note that the run time and number of iterations

required are most affected by the number of suppression points; adjusting this parameter changes the number of inequality constraints that must be satisfied. Increasing the number of apertures also has a noticeable impact on the run time, but this parameter affects the dimensionality of the weight vector, and not the number of equations that must be solved. Increasing the width of the suppression region increases the necessary run time until the width becomes large enough that many of the inequality constraints become inactive.

Increasing the number of apertures or the number of suppression points increases the average time per iteration. Increasing the number of suppression points increases the number of iterations required, but increasing the number of apertures does not. This may be because the starting guess for SLSQP was the weight vector that maximized power at the receiver; this is closer to the optimum weight vector for transmitters with more apertures. On the whole, the convergence of SLSQP is on the order of seconds, so the differences shown below are of limited practical impact.

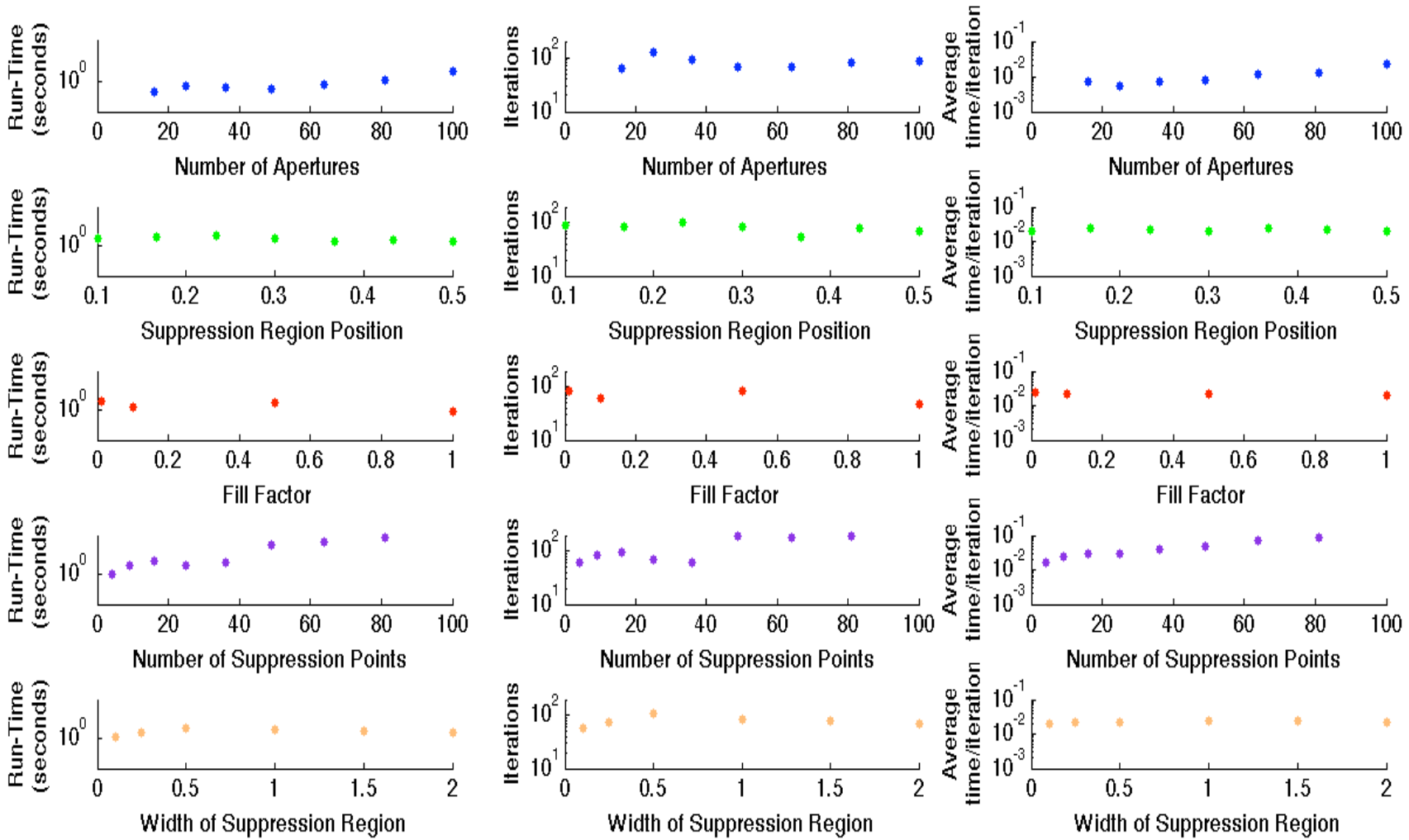

Figure 6.12 Performance metrics of solving for the optimum weight vector using SLSQP. Unless otherwise noted, the number of apertures is 100; the suppression region is located 5/30 beamwidths away from the receiver; the fill factor is 0.01; there are 9 suppression points, and the width of the suppression region is 1 beamwidth.

6.5 Redistribution of Energy in Receive Plane

As we discussed earlier, limiting the power to a desired suppression region also limits the power to the intended receiver. However, due to the conservation of energy, we know that the excess energy must be diverted elsewhere in the receive plane. Therefore, we now briefly consider the post-suppression energy distribution in the receive plane near – but not in – the desired suppression region. Specifically, we consider a semi-infinite region which consists of the desired suppression region and the region that extends infinitely beyond it along the x-axis, away from the receiver.[3] Figure 6.13 diagrams this region in relation to the suppression region.

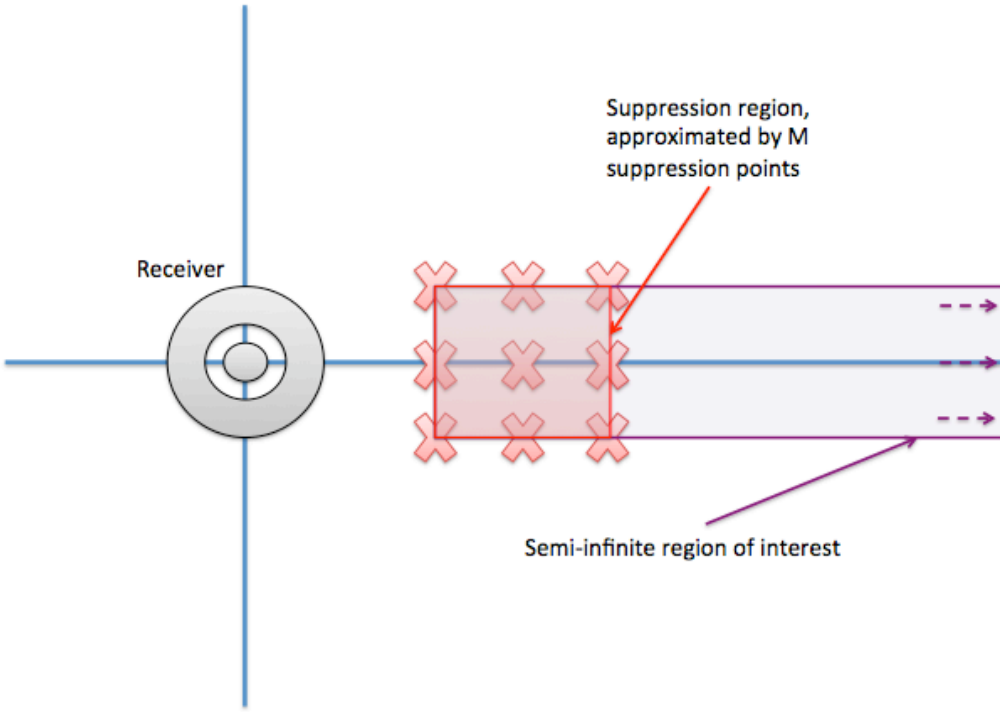

Figure 6.13 Diagram of the receive plane. The suppression region is marked by a red square; the suppression points that approximate this region are denoted by red X's. The semi-infinite region is marked in purple.

[3] For simplicity of computation, we only compute the radiation pattern within three beamwidths of the receiver. This is a reasonable simplification; we found that the integrals of the output radiation patterns we computed under various suppression conditions were approximately equal.

Our goal in considering this semi-infinite region is to examine whether limiting power to the specified suppression region might cause power to be diverted further from the receiver, such that the potential eavesdropper could move away from the receiver to detect the signal. We show below that if the desired suppression region is far from the intended receiver, the maximum power in the semi-infinite region is no more than the maximum power in the suppression region. In such a case, the eavesdropper would not benefit from moving away from the receiver. However, if the desired suppression region is very close to the intended receiver, then there may be significant power diverted to the semi-infinite region beyond the suppression region, such that an eavesdropper could achieve more success by moving away from the receiver.

We first consider the effect of the number of apertures (see Figure 6.14) and the fill factor (see Figure 6.15) of the transmit array on the maximum power inside the semi-infinite region. We find that increasing the number of apertures slightly increases the signal-to-semi-infinite-region power ratio; however, between a 36-aperture and a 100-aperture transmit array, this increase is no more than 3 dB. This implies that if the desired suppression region is close to the receiver, increasing the number of apertures may somewhat limit the power diverted further away from the receiver. From Figure 6.14, it is clear that the fill factor does not have any significant impact on the signal-to-semi-infinite-region power ratio.

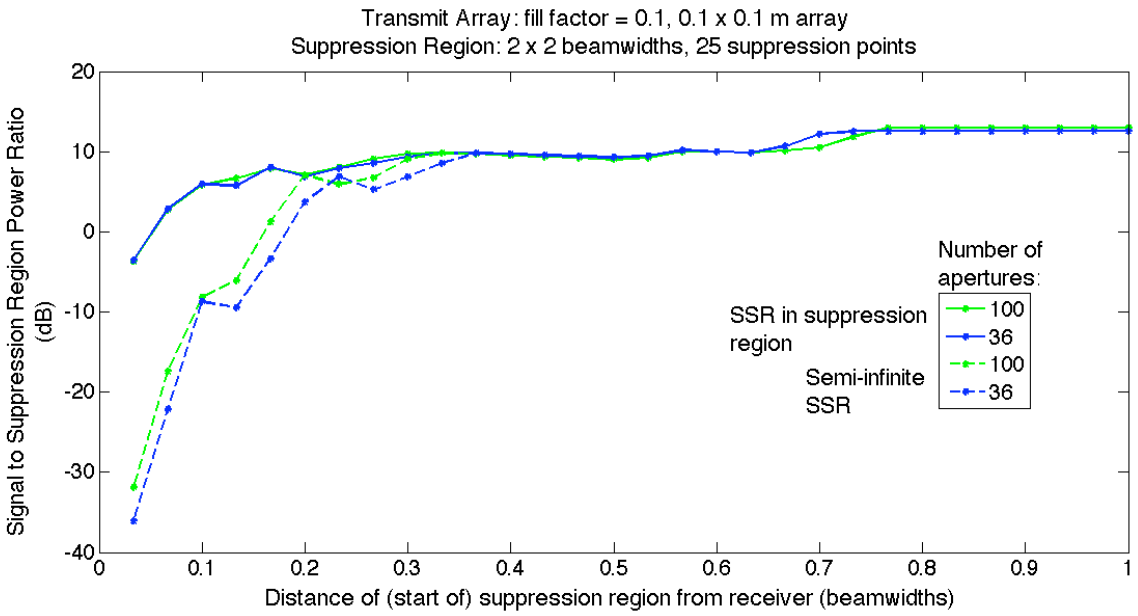

Figure 6.14 The solid curves show the minimum signal-to-suppression-region power ratio versus the distance of the suppression region from the receiver. The dashed curves show the minimum signal-to-semi-infinite-region power ratio versus the distance of the suppression region from the receiver. We vary the number of apertures.

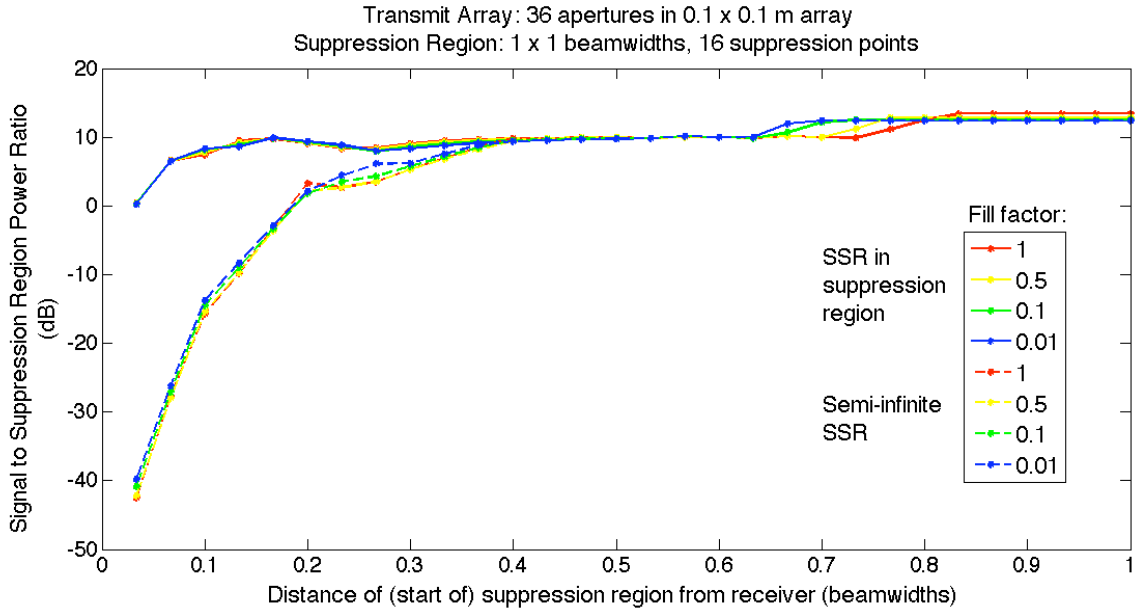

Figure 6.15 The solid curves show the minimum signal-to-suppression-region power ratio versus the distance of the suppression region from the receiver. The dashed curves show the minimum signal-to-semi-infinite-region power ratio versus the distance of the suppression region from the receiver. We vary the fill factor.

We next consider the effects of the size of the specified finite suppression region and the number of suppression points used to approximate this suppression region. The signal-to-semi-infinite-region power ratio does not seem to be affected by the number of suppression points used to approximate the suppression region. Increasing the number of suppression points increases the achievable signal-to-suppression-region power ratio but does not affect the signal-to-semi-infinite-region power ratio. From Figure 6.16, we see that the signal-to-semi-infinite-region power ratio is, however, dependent on the size of the desired suppression region. Given a constant number of suppression points, we can achieve a higher signal-to-suppression-region power ratio by decreasing the size of the suppression region; in contrast, we achieve a greater signal-to-semi-infinite-region power ratio by increasing the size of the suppression region. For determining the signal-to-suppression-region power ratio, the inter-spacing of the suppression points is the dominant factor; for determining the signal-to-semi-infinite-region power ratio, the size of the overall finite suppression region is the dominant factor.

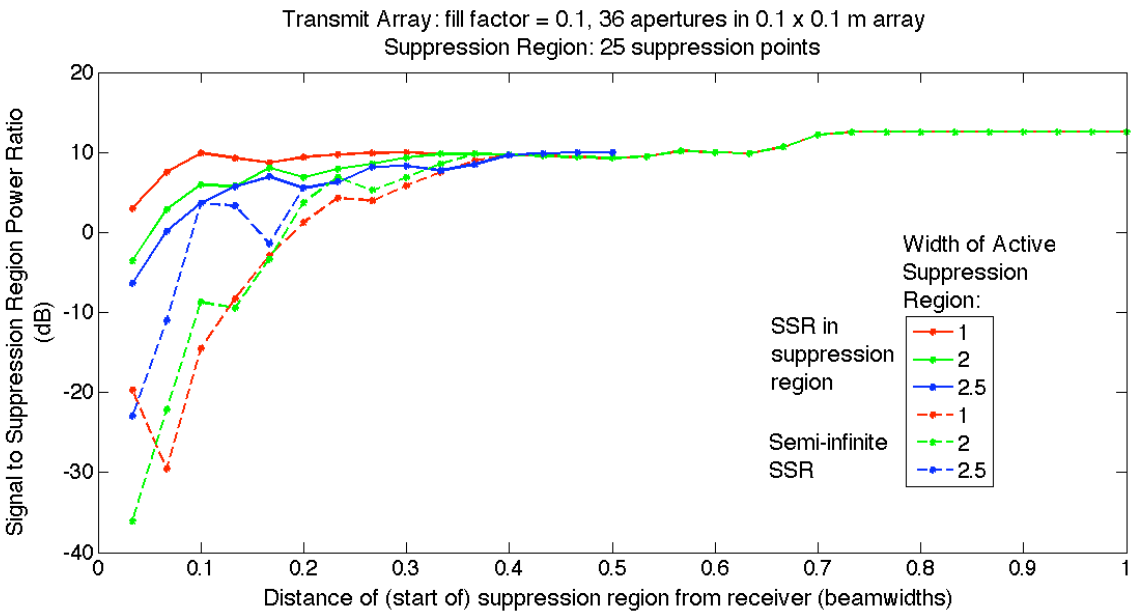

Figure 6.16 The signal-to-suppression-region power ratio versus the distance of the suppression region from the receiver. The solid curves show the minimum such ratio within the specified finite suppression region; the dashed curves show the minimum such ratio within the semi-infinite region that extends along the x-axis along the suppression region away from the receiver. We vary the width of the actively suppressed region.

Finally, we note that the real constraining factor in limiting interference and interception of the transmitted signal is that we must know precisely to which side of the receiver the eavesdropper or other user is. In order to limit power to a specified suppression region, we showed in this section that most of the power does not get diverted further away from the receiver. Instead, the excess power is directed towards the opposite side of the receiver. If we are trying to suppress a region located at some $x > 0$, most of the power in the receive plane is located at $x < 0$.

Chapter 7

Analysis of Suppression Capabilities

In this chapter, we analyze the numerical results we obtained for the two-dimensional aperture array system in Chapter 6. Although we were unable to find analytical expressions that explicitly define the dependence of the achievable signal-to-suppression-region ratio and the intensity at the receiver on various system characteristics, we can approximate the relationships between these parameters. In Section 7.1, we quantify these relationships for the particular system configurations we simulated in Chapter 6. In Section 7.2, we show how well our results matched our predictions from our toy example analysis in Chapter 3. Our overall goal is to get a sense of the considerations that will inform our system design for various suppression requirements. We summarize these design considerations in Section 7.3.

7.1 Best-Fit Equations for Observed Trends

In this section, we fit curves to our numerical results from the two-dimensional array simulations via MATLAB's curve fitting tool, which uses either the linear or nonlinear least squares method to minimize the summed squared error between the actual values and the model values. In Chapter 6, we presented the signal-to-suppression-region power ratios for various system configurations as dB ratios, but in this section we use the actual ratios to calculate the best fit equations. We do continue to plot the data using the dB suppression ratios; the best fit curves are adjusted accordingly in each figure. The normalized intensity at the receiver and other parameters are all plotted on a linear scale.

Figure 7.1 shows the relationship between the suppression region position and the achievable signal-to-suppression region ratio modeled as a cubic function. This relationship is very complex, and it was hard to find a function type that modeled it well. We recall from Chapter 6 that the achieved signal-to-suppression-region ratio is not monotonic with suppression region distance when there are a lot of suppression points in a suppression region close to the receiver. So the best fit curves for 16 and 25 suppression point regions are not very accurate for low suppression region positions.

The cubic function is the polynomial function of lowest order that could plausibly represent the relationship in this figure. The horizontal region at a suppression ratio of 10 dB corresponds to the distances from the receiver in which suppression is both achievable – in that the desired ratio can be satisfied throughout the desired suppression region – and also necessary – in that the desired signal-to-suppression-region ratio is not satisfied by the weight vector that maximizes the receiver intensity. A cubic function with a point of inflection in this horizontal region is therefore a good choice to approximate these curves. We considered a quartic function, but it was not a significantly better approximation of the data than the cubic function we show below.

The data points for each approximation of the suppression region are constant in two ranges along the x-axis: first, where a 10 dB suppression is achievable through suppression, and second where none of the suppression points need to be actively suppressed because the pre-suppression intensity in the suppression region is low enough. We discounted the region beyond 0.7 beamwidths when calculating the best fit, since suppression is unnecessary in this region. There is no clear relationship between the number of suppression points and the coefficients in the best fit cubic functions. However, the point of inflection in each plot could be used to

approximate the distance at which suppression is reasonably achievable. This point is approximately the same for 16 and 25-point suppression regions, but occurs at a more distant position for the 9-point suppression region.

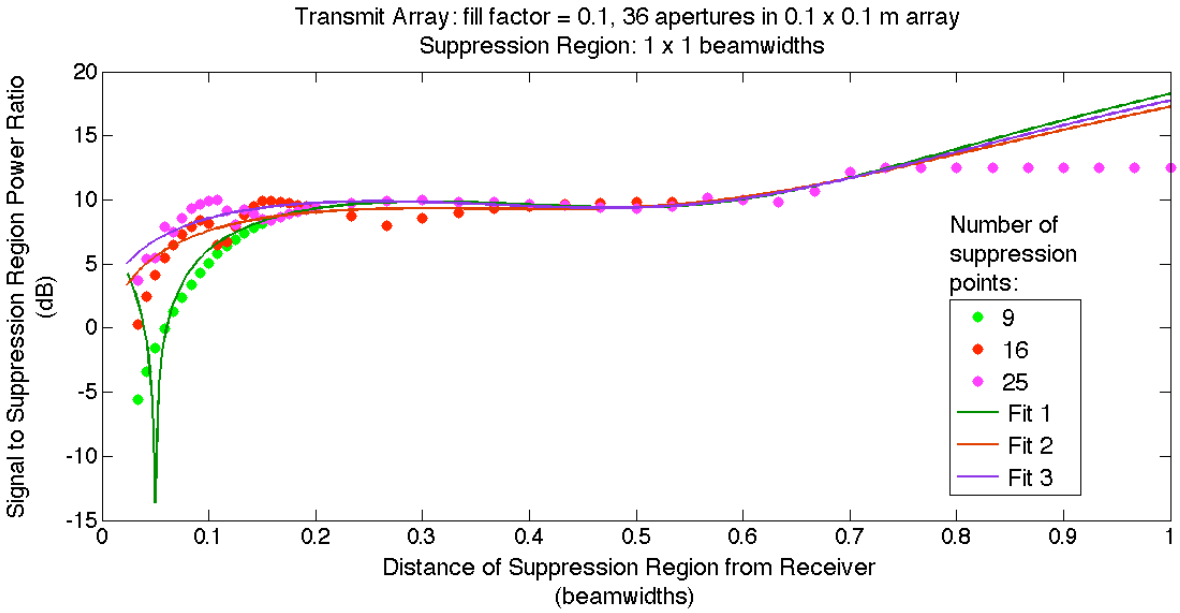

Figure 7.1 Best fit curves (polynomial, order 3) for the signal-to-suppression-region power ratio in terms of distance of a 1×1 beamwidth suppression region from the receiver, for varying number of suppression points. Table 7.1 shows the polynomial coefficients for each curve.

$y = a_1x^3 + a_2x^2 + a_3x + a_4$	$\boldsymbol{a_1}$	$\boldsymbol{a_2}$	$\boldsymbol{a_3}$	$\boldsymbol{a_4}$
Fit 1 (9 suppression points)	283.4	-336.7	125.9	-5.445
Fit 2 (16 suppression points)	176.7	-192.4	68.25	0.648
Fit 3 (25 suppression points)	214.9	-235.4	78.46	1.455

Table 7.1 Best fit cubic equations for the curves in Figure 7.1. The value of y in these equations is the actual signal-to-suppression-region power ratio (i.e. not expressed in dB). x is the is the distance of the suppression region from the receiver.

Figure 7.2 shows that the closest distance a 10 dB suppression region can be to the receiver varies exponentially with the width of the region until the closest distance becomes 0.5667 beamwidths. At this distance, any sized suppression region with at least 4 suppression points can be suppressed to 10 dB. From Table 7.2, we see that the coefficient $\boldsymbol{a_2}$ inside the exponential decreases approximately linearly with the number of suppression points used to approximate the suppression region.

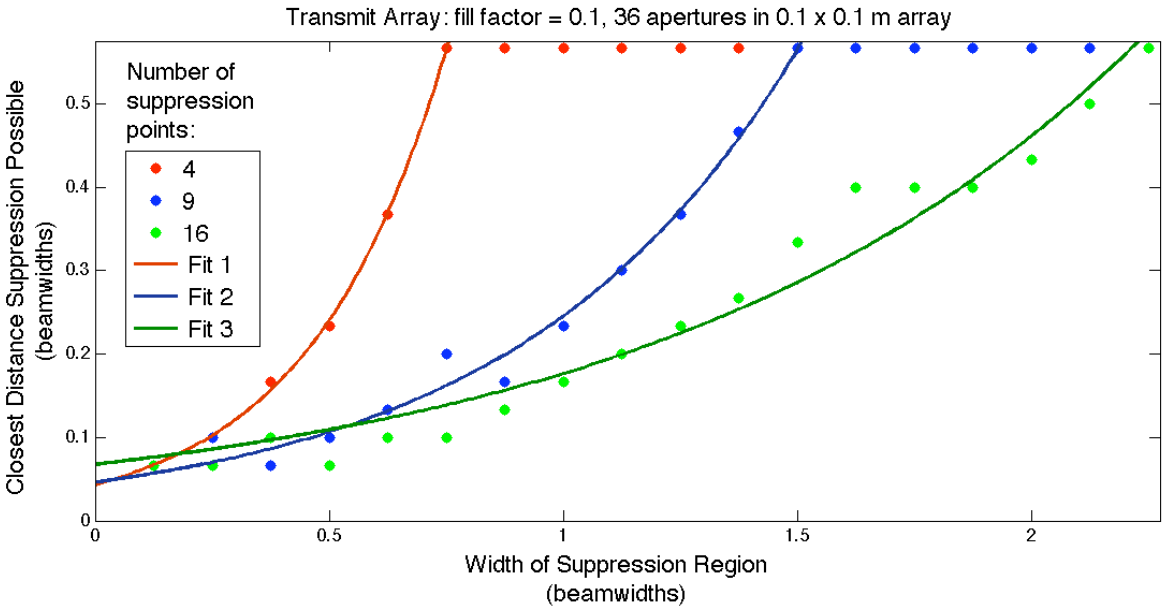

Figure 7.2 Best fit curves (exponential) for the closest distance a signal-to-suppression-region ratio of 10 dB can be achieved in terms of the width of the suppression region, for varying number of suppression points. Table 7.2 shows the coefficients of the exponential curves.

$y = a_1 e^{a_2 x}$	$\boldsymbol{a_1}$	$\boldsymbol{a_2}$
Fit 1 (4 suppression points)	0.04339	3.422
Fit 2 (16 suppression points)	0.04622	1.668
Fit 3 (25 suppression points)	0.06758	0.96

Table 7.2 Best fit exponential equations for the curves in Figure 7.2. The value of y is the closest distance a suppression region of the specified width x can be suppressed such that the achieved signal-to-suppression-region ratio is greater than 90% of the desired ratio.

Figure 7.3 shows that there is also an exponential relationship between the closest distance a 10 dB suppression region can be to the receiver and the number of suppression points. This is a decreasing exponential relationship as opposed to the increasing exponential of Figure 7.2. Here, the coefficients inside the exponential increase almost linearly with increasing width of the suppression region. Since 0 suppression points implies no active suppression, we expect every curve to intersect the y-axis at 0.7 beamwidths.

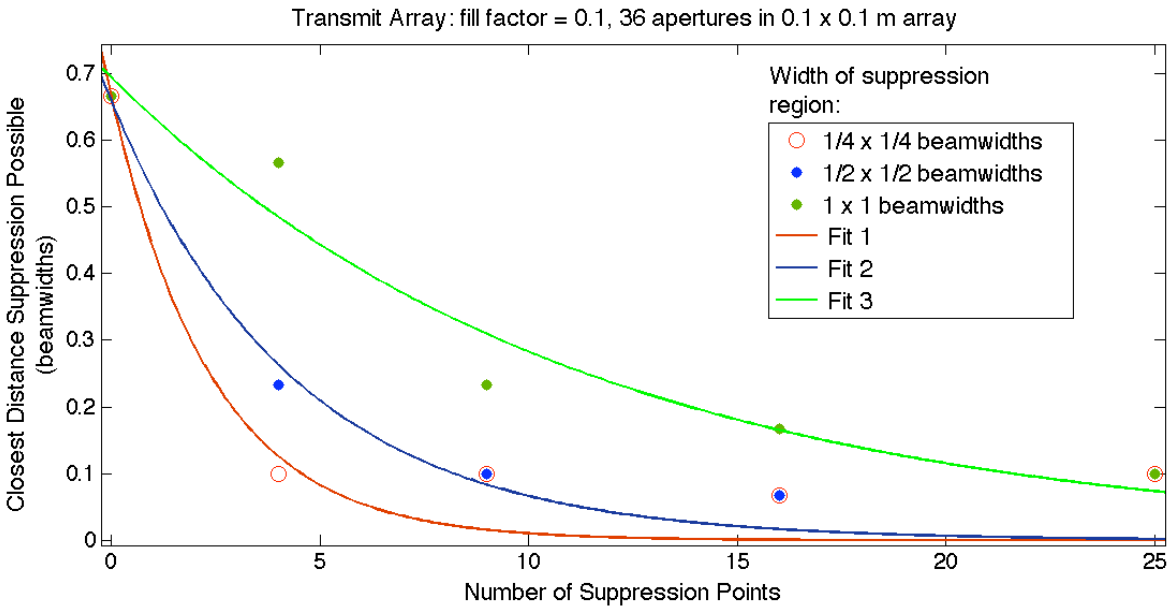

Figure 7.3 Best fit curves (exponential) for the closest distance a signal-to-suppression-region ratio of 10 dB can be achieved in terms of the number of suppression points, for varying width of the suppression region. Table 7.3 shows the coefficients of the exponential curves.

$y = a_1 e^{a_2 x}$	$\boldsymbol{a_1}$	$\boldsymbol{a_2}$
Fit 1 ($\frac{1}{4} \times \frac{1}{4}$ *beamwidth suppression region*)	0.6639	-0.4158
Fit 2 ($\frac{1}{2} \times \frac{1}{2}$ *beamwidth suppression region*)	0.6586	-0.2295
Fit 3 (1×1 *beamwidth suppression region*)	0.6934	-0.08966

Table 7.3 Best fit exponential equations for the curves in Figure 7.3. The value of y is the closest distance a suppression region with x suppression points can be suppressed such that the achieved signal-to-suppression-region ratio is greater than 90% of the desired ratio.

Figure 7.4 reveals a quadratic relationship between the intensity at the receiver and the desired signal-to-suppression-region power ratio. The rate of change of this second order polynomial is less for smaller suppression regions. We considered a cubic approximation for the data, but the best fit curves had very small third order coefficients (~10^{-3}); we therefore fit each data set to a quadratic expression. We know that a quadratic function cannot accurately

represent the asymptotic behavior as the desired signal-to-suppression-region ratio increases, but for desired suppression ratios less than 15, the quadratic approximations fit the data better than the exponential curves that might be more appropriate asymptotically.

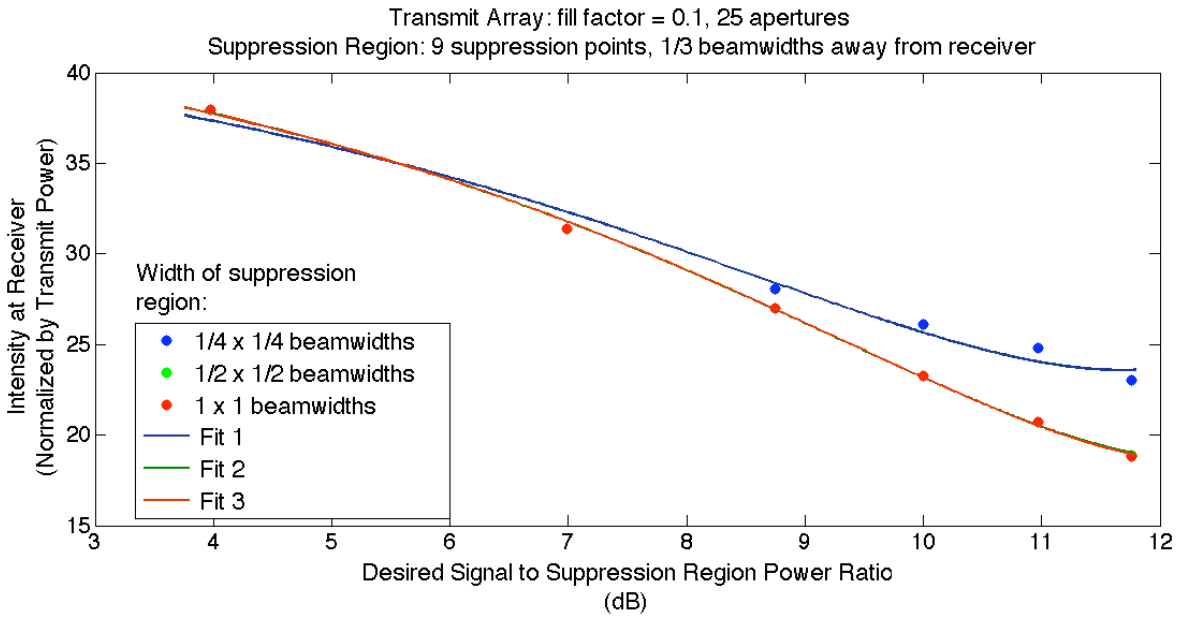

Figure 7.4 Best fit curves (polynomial, order 2) for the intensity at the receiver in terms of the desired signal-to-suppression-region power ratio, for varying size of suppression region. Table 7.4 shows the polynomial coefficients for each curve.

$y = a_1x^2 + a_2x + a_3$	$\boldsymbol{a_1}$	$\boldsymbol{a_2}$	$\boldsymbol{a_3}$
Fit 1 ($\frac{1}{4} \times \frac{1}{4}$ *beamwidth suppression region*)	0.09196	-2.71	43.55
Fit 2 ($\frac{1}{2} \times \frac{1}{2}$ *beamwidth suppression region*)	0.08906	-3.057	44.84
Fit 3 (1×1 *beamwidth suppression region*)	0.08788	-3.041	44.8

Table 7.4 Best fit quadratic equations for the curves in Figure 7.4. The value of y is the intensity at the receiver. In these equations, x is the actual desired signal-to-suppression-region power ratio (i.e. not expressed in dB).

Figure 7.5 approximates the relationship between the closest distance suppression is possible and the desired signal-to-suppression-region ratio with a logarithmic curve. A logarithmic curve is an appropriate approximation for two reasons. First, as the desired signal-to-suppression-region ratio increases, the closest distance suppression to that ratio is possible increases, but the rate of that increase decreases fairly rapidly. Second, if the desired suppression ratio is less than or equal to 1, the closest distance suppression is possible is 0. Therefore we do not need to consider suppression ratios less than 1, and the logarithmic curves cross the distance axis somewhere in or near this region. We note that the outside coefficient increases linearly with the suppression region width. This is because the rate of increase of the closest distance suppression is possible versus the desired suppression ratio is smaller for smaller suppression regions.

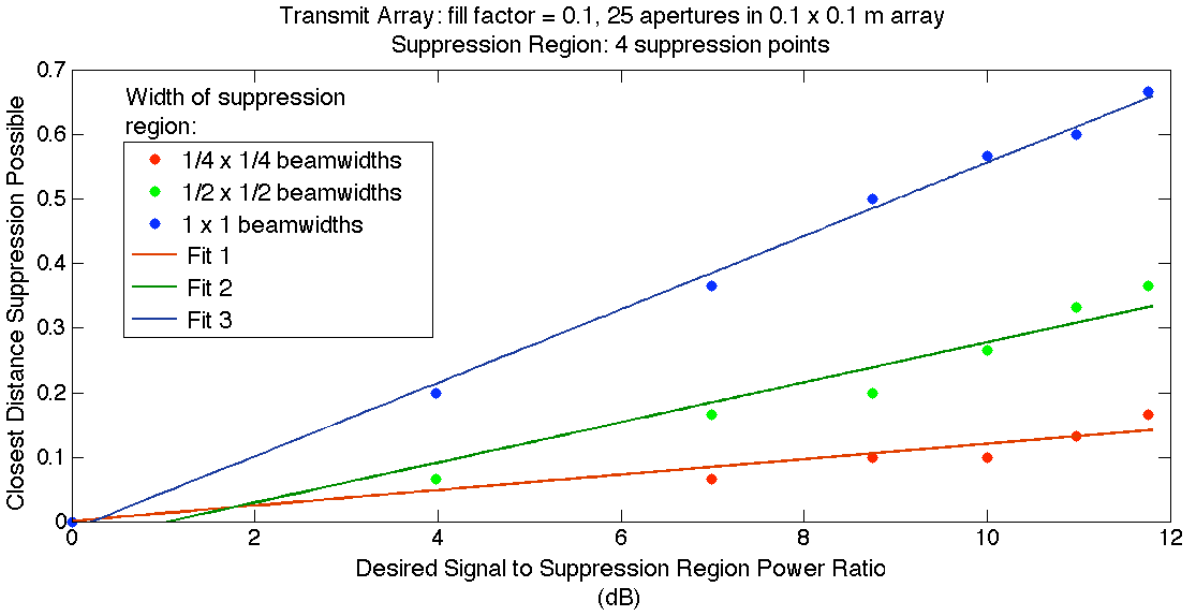

Figure 7.5 Best fit curves (logarithmic) for the closest distance a desired signal-to-suppression-region ratio can be achieved in terms of the desired ratio, for varying size of suppression region. Table 7.5 shows the coefficients of the logarithmic best fit functions.

$y = a_1 \log(a_2 x)$	$\boldsymbol{a_1}$	$\boldsymbol{a_2}$
Fit 1 ($\frac{1}{4} \times \frac{1}{4}$ *beamwidth suppression region*)	0.05214	1.01
Fit 2 ($\frac{1}{2} \times \frac{1}{2}$ *beamwidth suppression region*)	0.1351	0.7828
Fit 3 (1×1 *beamwidth suppression region*)	0.2475	0.9496

Table 7.5 Best fit exponential equations for the curves in Figure 7.5. The value of y is the closest distance a suppression region with 4 suppression points can be suppressed such that the achieved signal-to-suppression-region ratio is greater than 90% of the desired ratio x. In these equations, x is the actual desired signal-to-suppression-region power ratio (i.e. not expressed in dB).

7.2 Accuracy of Toy Example

We now compare the analytical expressions relating various system parameters that we derived in Chapter 3 with the numerical results we obtained in Chapter 6. First, we demonstrate that our toy example in Chapter 3 is comparable to the physical system we analyzed in Chapter 6. Figure 7.6 plots the intensity at the receiver versus the distance of the suppression region from the receiver. The red plot represents the simulated data from Chapter 6; the green shows a scaled version of the equation found in the toy example for the intensity at the receiver versus the angle between the receive and suppression vectors.

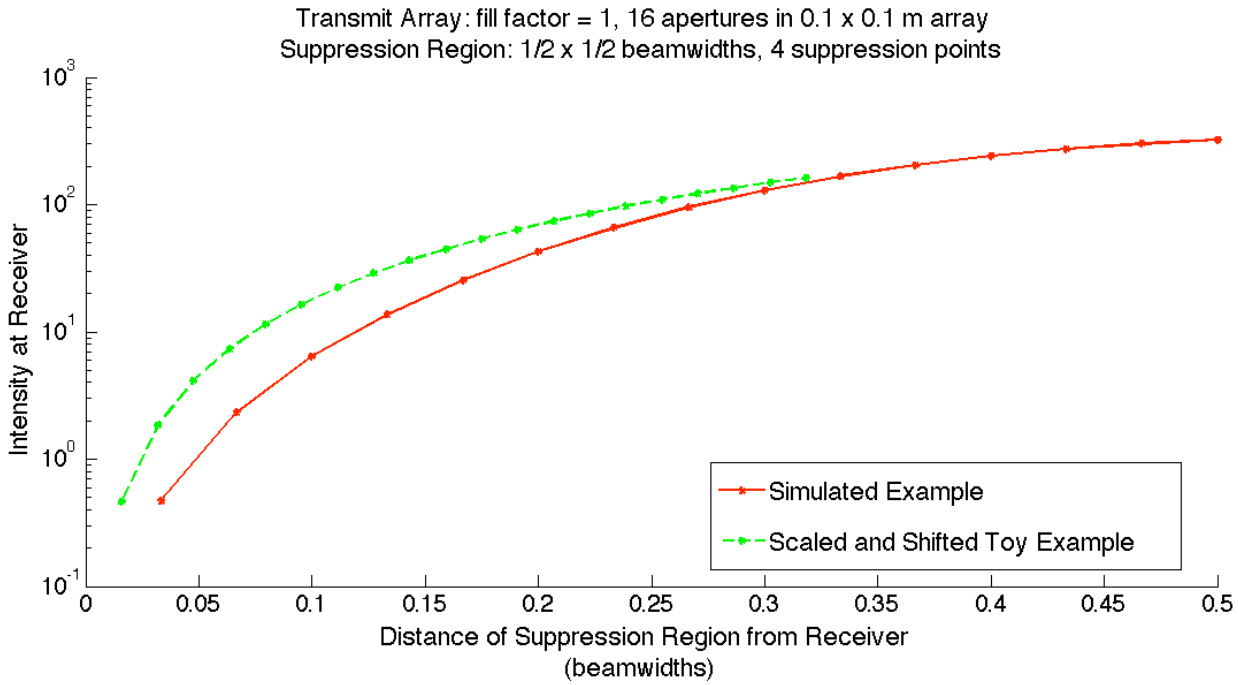

Figure 7.6 Comparison of the relationship between the numerically optimized intensity at the receiver and the distance of suppression region from receiver calculated in Chapter 6 with the same relationship calculated in the toy example in Chapter 3.

Here, we see that the function that describes the post-suppression intensity at the receiver in our toy example is approximately the same shape as the function that describes the intensity at the receiver in our two-dimensional example. The difference between the two curves when the suppression region is close to the receiver – whereby the red curve appears to be a shifted version of the green – is probably due to the greater number of suppression points (four) in the numerical example versus the single suppression point in the toy example. Figure 7.6 then suggests two things: first, that increasing the number of suppression points affects the intensity at the receiver similarly to moving the suppression point in our toy example closer to the receiver; and second, that changing the system parameters changes the coefficients of this function, but not its general shape.

Figure 7.7 shows the relationship between the intensity at the receiver after suppression and the fill factor of the transmit array. This plot shows that this relationship is almost exactly described by a quadratic polynomial. In fact, each of the three curves in the figure match the calculated data points with an adjusted coefficient of determination $R^2 \geq 0.9999$. We predicted this quadratic relationship in Chapter 3 by showing that the intensity at the receiver before suppression was also approximately quadratic with varying fill factor.

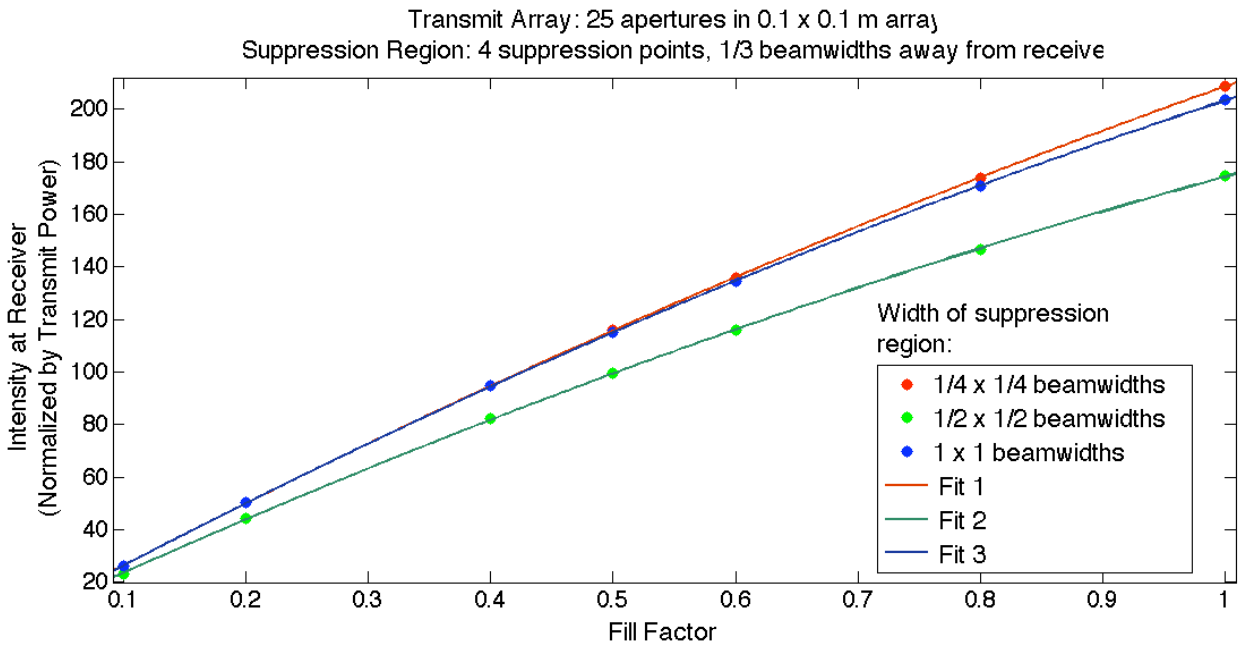

Figure 7.7 Best fit curves (polynomial, order 2) for the intensity at the receiver in terms of the fill factor of a 25-aperture transmit array, for varying suppression region size. Table 7.6 shows the polynomial coefficients for each curve.

$y = a_1x^2 + a_2x + a_3$	$\boldsymbol{a_1}$	$\boldsymbol{a_2}$	$\boldsymbol{a_3}$
Fit 1 ($\frac{1}{4} \times \frac{1}{4}$ *beamwidth suppression region*)	-41.94	248.7	1.934
Fit 2 ($\frac{1}{2} \times \frac{1}{2}$ *beamwidth suppression region*)	-44.43	216.2	2.449
Fit 3 (1×1 *beamwidth suppression region*)	-50.46	252.1	1.652

Table 7.6 Best fit quadratic equations for the curves in Figure 7.7. The value of y is the intensity at the receiver. x is the fill factor of the transmit array.

Recall that $\tilde{m} = \frac{|h_v \cdot w|^2}{|h_{\tilde{u}} \cdot w|^2}$ is the signal-to-suppression-region power ratio at a point $\tilde{u}$ near the desired suppression point u. In Chapter 3 we showed that

$$\tilde{m} = \frac{b^2 \cos^2 \phi}{a^2 \cos^2(\theta + \tilde{\theta} - \phi)}$$

In Chapter 3, we claimed that θ is approximately proportional to the distance between the suppression region and the receiver. We now suggest that $\tilde{\theta}$ in our toy example could represent the distance between suppression points in a physical system. We now compare the curves in Figure 3.9 that showed $\tilde{m}$ versus θ for varying $\tilde{\theta}$ with the curves in Figure 6.5 that show our numerical calculations of the achieved signal-to-suppression-region power ratio versus the distance of the suppression region for varying suppression point spacing. We see in Figure 7.8 that the relationships depicted in these two plots have generally the same shape; thus we posit that our analysis in Chapter 3 of the effect of the distance between suppression points on the achievable suppression ratio, where we found that $\frac{d\tilde{m}}{d\tilde{\theta}} = -\frac{2b^2}{a^2}\frac{\cos^2\phi\,\sin(\phi-\theta-\tilde{\theta})}{\cos^3(\phi-\theta-\tilde{\theta})}$, is valid.

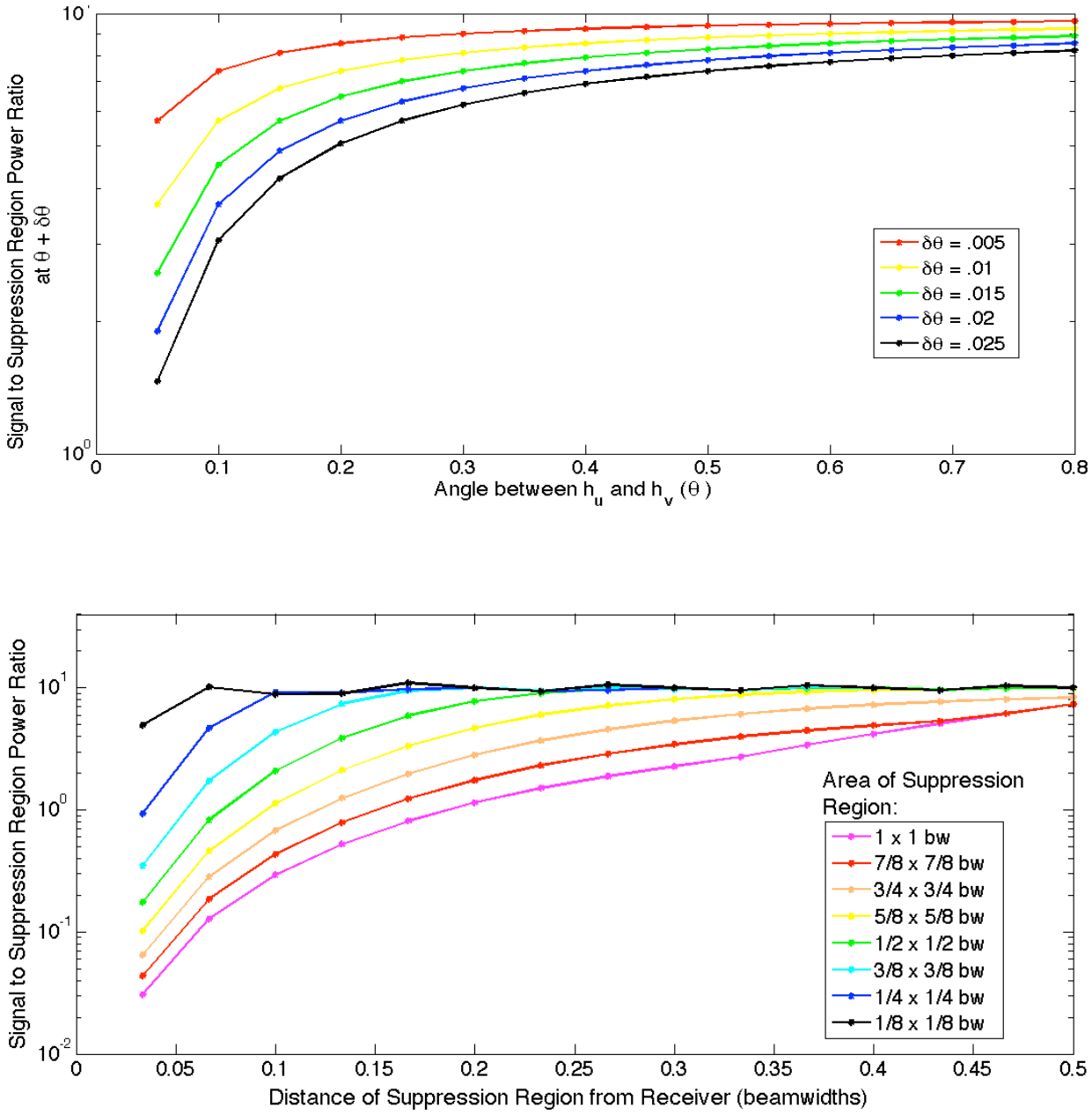

Figure 7.8 The top plot shows how the suppression ratio at a point $\theta + \delta\theta$ as θ increases for $\overrightarrow{\boldsymbol{h_u}} = \begin{bmatrix}\cos\theta \\ \sin\theta\end{bmatrix}$, $\overrightarrow{\boldsymbol{h_v}} = \begin{bmatrix}\sqrt{2} \\ 0\end{bmatrix}$, and a desired suppression ratio of 10. The lower plot shows how the suppression ratio increases as the distance between the suppression region and the intended receiver increases for a 4-point suppression region and a 36-aperture transmit array of fill factor 0.1. Both plots show very similar trends.

7.3 Design Considerations

7.3.1 Transmit Array

Assuming we hold the overall size of the array fixed, the variable parameters in the transmit array are the number of apertures and the fill factor. Increasing the number of apertures gives more control over the output radiation pattern, and thus generally increases the intensity at the receiver. Increasing the fill factor decreases the extent of the energy spreading in the far field, and thus also increases the intensity at the receiver. Ideally, we want a large number of apertures and a large fill factor. This is complicated for two reasons. One, we can increase the fill factor either by increasing the number of apertures or increasing the size of the apertures, both of which increase the cost of the system. Two, increasing the fill factor can cause adjacent apertures to be within one atmospheric coherence length of each other and thus can reduce the achievable spatial diversity of the transmission, and thus the system is more susceptible to the effects of atmospheric turbulence. A sparse array with sub-apertures separated by more than one phase coherence length mitigates the effects of deep fades at the receiver.

For a sparse array, we want fewer apertures to limit the spread of energy in the receive plane. In a sparse array, adding additional apertures decreases both the width of the apertures and the distance between the apertures, causing more significant grating lobes and reducing the power at the receiver. However, with fewer apertures in the transmit plane, we can actively suppress fewer suppression points and therefore can only limit power to a smaller suppression region.

Thus in designing the transmit array, we must consider the following tradeoffs:

- A large fill factor can transmit more power to the receiver, but will have less spatial diversity to mitigate the effects of atmospheric turbulence. A small fill factor can achieve spatial diversity but will also produce grating lobes in the receive plane.
- For a sparse array, increasing the number of apertures decreases the intensity at the receiver and may increase the severity of grating lobes, but it will also allow active suppression of more points in the receive plane. This allows for either a larger suppressed region or a closer suppressed region.

7.3.2 Suppression Region

There are three parameters that define the suppression region: the area of the region, the number of suppression points to which the desired ratio is enforced, and the position of the region with respect to the intended receiver. The first two can generally be considered together; the dominant parameter seems to be the separation between suppression points. Increasing the width of the suppression region in a specified location requires increasing the number of suppression points. However, increasing the number of suppression points limits the power received by the intended user and may also require increasing the number of apertures in the transmit array. Generally, increasing the number of suppression points that approximate a given area allows us to suppress power to a region closer to the receiver. Decreasing the width of the suppression region while keeping the number of suppression points constant has a similar effect.

Thus in specifying the required suppression region, we must consider the following tradeoffs:

- If we are very uncertain about the position of the user to whom we seek to limit power, we must increase the number of suppression points, but increasing the number of suppression points decreases the available power at the receiver.
- We might also consider the benefits of using a non-uniform suppression point spacing. We may be able to decrease the number of required suppression points if we concentrate these points in the part of the suppression region closest to the receiver and use fewer points in the part of the suppression region furthest from the receiver. This would be particularly appropriate for large suppression regions, in which the furthest extent of the suppression region is in a location where the desired signal-to-suppression-region power ratio is achievable even before the aperture phases are adjusted.
- If the user to whom we are limiting power is very close to our intended user's receiver, we must be much more certain about his position than if the user is further away. The same holds true if the undesired user is in or very near a grating lobe of the transmission.

7.3.3 Desired Signal-to-Suppression-Region Power Ratio

Finally, we consider the required signal-to-suppression-region power ratio to meet our goal of preventing eavesdropping and interference in a multi-user network. We posit that in most cases, a signal-to-suppression-region ratio of 10 dB should be sufficient. In a multi-user network, if the users all have similarly capable receivers, such a suppression ratio should be sufficient to prevent one user’s transmission from interfering with another’s. Such a suppression ratio will also significantly increase the difficulty of eavesdropping; an eavesdropper would then

need a larger receive aperture or more sensitive detector than the intended user. If our intended receiver has a very sensitive receiver and we lower the transmit power such that the intended user can just barely receive the transmission, an eavesdropper receiving a 10 dB lower transmission would not be successful.

If a suppression ratio of 10 dB is not sufficient, we showed that it is possible to achieve greater suppression ratios if the eavesdropper is further away from the receiver or if we decrease the separation between suppression points. We showed in Figure 7.5 in Section 7.1 that the closest distance at which suppression is possible does not increase very fast with the desired suppression ratio for small suppression regions. Thus if we are reasonably certain as to the eavesdropper's position, we can achieve suppression ratios greater than 10 dB fairly as close as 0.2 beamwidths away from the receiver.

Chapter 8

Conclusion

8.1 Future Work

As we discussed in Section 7.3, limiting the interference in a multi-user network is easier than preventing eavesdropping. In a multi-user network, we assume that all of the users have similarly sensitive receivers; if we suppress the power in the direction of another user to 10 dB less than the power directed at our intended user, we can significantly reduce the chance that our transmission will be detrimental towards the other user's communication. To prevent eavesdropping, however, we may require a much larger suppression ratio. If the eavesdropper's receiver is much more sensitive than the intended receiver, it is possible that he could still intercept the signal despite the 10 dB suppression. If we increase the sensitivity of our receiver, then the probability of an eavesdropper having a correspondingly better receiver decreases. However, we would still like for the signal-to-noise ratio at the eavesdropper to be suppressed by 30 dB or so. Therefore, we suggest a method of intentionally adding noise to the signal that could be used in concert with our suppression scheme to provide extra security.

There are two potential ways of implementing this suggestion. The first of these is to employ a similar method to the one developed in this thesis and add a random noise signal that is maximized in the direction of the eavesdropper and minimized in the direction of the intended receiver. This would result in another nonlinear optimization problem that would be solved for the optimum weight vector for the noise signal. This optimization problem would be more complicated than the one solved in this thesis; it would either have multiple objective functions

to maximize the noise signal at all of the suppression points, or we would have to choose a point within the suppression region to direct the noise too. If we chose this method, we could combine the two optimization problems, the one to maximize the signal at the receiver and the one to maximize the noise at the eavesdropper, and then optimize the weight vector to find the best ratio

$$\frac{SNR_{rx}}{SNR_{eave}}$$

Where SNR_{rx} is the signal-to-noise ratio at the intended receiver and SNR_{eave} is the signal-to-noise ratio at the approximated eavesdropper location. This method – combined with a transmitter power chosen such that a reasonably sensitive receiver at the intended user can just barely detect the signal after suppression – should allow us to achieve the desired confidentiality of the signal.

Alternatively, a second method would be to add a deterministic encrypted signal on top of the intended transmission. The intended receiver could detect and decrypt this noise signal and subtract it from the intended transmission; the eavesdropper would be unable to distinguish between the "noise" transmission and the signal. Combining this with our method of suppressing the energy transmitted in the direction of the eavesdropper would additionally decrease the possibility of interception.

8.2 Summary

In this thesis, we considered the problem of limiting power to a specified region in the receive plane of a free-space optical communication link. Our goal was twofold: one, to limit the interference of the transmission with other user's transmissions in a multi-user wireless optical network, and two, to prevent the energy of the transmission from propagating in the direction of an eavesdropper who sought to intercept the signal.

We showed that it is possible to use a linear transmit array to suppress by 10 dB the power to a 1-beamwidth suppression region as close as 0.2 beamwidths to the receiver without significantly decreasing the power transmitted to the receiver; we also showed that with a two-dimensional transmit array, we can suppress by 10 dB a ½ x ½ beamwidth suppression region that is even closer to the receiver. We can suppress power to arbitrarily large regions arbitrarily close to the receiver if we have the capabilities to significantly increase the transmit power and the number of transmit apertures. In general, given a required suppression region in the receive plane and a desired signal-to-suppression-region power ratio, we must consider the tradeoffs between increasing the number of apertures and the additional system expense; between increasing the fill factor and reducing spatial diversity; and between increasing the number of suppression points (and therefore the achievable suppression ratio) and the decrease in the intended user's received power. Given fixed system constraints, i.e. the number and size of the transmit apertures, the distance of the region to which we can successfully suppress power grows exponentially with the required size of the suppression region. Generally, the size of the suppression region will be proportional to our uncertainty as to an eavesdropper or other user's position. Thus, to achieve a desired signal-to-suppression-region power ratio, we must be more certain of the eavesdropper or other user's position if he is closer to our intended receiver than if he is further away.

Appendix A

Derivation of Filled Aperture KKT Conditions

Let $\boldsymbol{\gamma = U_i(\xi, \eta)}$.

Finding $\boldsymbol{\delta I}$:

$$I = \iint_{A_T} U_i(\xi,\eta)d\xi d\eta \iint_{A_T} U_i{}^*(\xi,\eta)d\xi d\eta = I_1 I_2$$

$$I_1 = \iint_{A_T} U_i(\xi,\eta)d\xi d\eta = \iint_{A_T} F_1(\xi,\eta,\gamma)d\xi d\eta$$

where $F_1(\xi,\eta,\gamma) = \gamma$

$$I_2 = \iint_{A_T} U_i{}^*(\xi,\eta)d\xi d\eta = \iint_{A_T} F_2(\xi,\eta,\gamma)d\xi d\eta$$

where $F_2(\xi,\eta,\gamma) = \gamma^*$.

$$\delta I = I_2\delta I_1 + I_1\delta I_2$$

$$\delta I_1 = \iint_{A_T} \delta F_1(\xi,\eta,\gamma)d\xi d\eta = \iint_{A_T} \delta\gamma \left.\frac{\partial F_1}{\partial \gamma^*}\right|_{y\ const} d\xi d\eta = 0$$

$$\delta I_2 = \iint_{A_T} \delta F_2(\xi,\eta,\gamma)d\xi d\eta = \iint_{A_T} \delta\gamma \left.\frac{\partial F_2}{\partial \gamma^*}\right|_{y\ const} d\xi d\eta = \iint_{A_T} \delta\gamma\, d\xi d\eta$$

$$\boldsymbol{\delta I = I_2\delta I_1 + I_1\delta I_2 = \iint_{A_T} U_i(\xi,\eta)d\xi d\eta \iint_{A_T} \delta\gamma\, d\xi d\eta}$$

Finding δJ_i:

$$J_i = \iint_{A_T} U_i(\xi,\eta) e^{-j\frac{2\pi}{\lambda L}(x_i\xi + y_i\eta)} d\xi d\eta \iint_{A_T} {U_i}^*(\xi,\eta) e^{j\frac{2\pi}{\lambda L}(x_i\xi + y_i\eta)} d\xi d\eta = J_{i1} J_{i2}$$

$$J_{i1} = \iint_{A_T} U_i(\xi,\eta) e^{-j\frac{2\pi}{\lambda L}(x_i\xi + y_i\eta)} d\xi d\eta = \iint_{A_T} F_3(\xi,\eta,\gamma) d\xi d\eta$$

where $F_3(\xi,\eta,\gamma) = \gamma e^{-j\frac{2\pi}{\lambda L}(x_i\xi + y_i\eta)}$

$$J_{i2} = \iint_{A_T} {U_i}^*(\xi,\eta) e^{j\frac{2\pi}{\lambda L}(x_i\xi + y_i\eta)} d\xi d\eta = \iint_{A_T} F_4(\xi,\eta,\gamma) d\xi d\eta$$

where $F_4(\xi,\eta,\gamma) = \gamma^* e^{j\frac{2\pi}{\lambda L}(x_i\xi + y_i\eta)}$.

$$\delta J_i = J_{i2}\delta J_{i1} + J_{i1}\delta J_{i2}$$

$$\delta J_{i1} = \iint_{A_T} \delta F_3(\xi,\eta,\gamma) d\xi d\eta = \iint_{A_T} \delta\gamma \left.\frac{\partial F_3}{\partial \gamma^*}\right|_{y\ const} d\xi d\eta = 0$$

$$\delta J_{i2} = \iint_{A_T} \delta F_4(\xi,\eta,\gamma) d\xi d\eta = \iint_{A_T} \delta\gamma \left.\frac{\partial F_4}{\partial \gamma^*}\right|_{y\ const} d\xi d\eta = \iint_{A_T} \delta\gamma\, e^{j\frac{2\pi}{\lambda L}(x_i\xi + y_i\eta)} d\xi d\eta$$

$$\boldsymbol{\delta J_i = J_{i2}\delta J_{i1} + J_{i1}\delta J i_2 = \iint_{A_T} U_i(\xi,\eta) e^{-j\frac{2\pi}{\lambda L}(x_i\xi + y_i\eta)} d\xi d\eta \iint_{A_T} \delta\gamma\, e^{j\frac{2\pi}{\lambda L}(x_i\xi + y_i\eta)} d\xi d\eta}$$

Finding $\boldsymbol{\delta H}$:

$$H = \iint_{A_T} U_i(\xi,\eta)U_i^*(\xi,\eta)\, d\xi d\eta$$

$$H = \iint_{A_T} U_i(\xi,\eta)U_i^*(\xi,\eta)\, d\xi d\eta = \iint_{A_T} F_5(\xi,\eta,\gamma) d\xi d\eta$$

where $F_5(\xi,\eta,\gamma) = \gamma\gamma^*$

$$\delta H = \iint_{A_T} \delta F_5(\xi,\eta,\gamma) d\xi d\eta = \iint_{A_T} \delta\gamma \left.\frac{\partial F_5}{\partial \gamma^*}\right|_{y\ const} d\xi d\eta = \iint_{A_T} \gamma\delta\gamma d\xi d\eta$$

$$\boldsymbol{\delta H = \iint_{A_T} U_i(\xi,\eta)\delta\gamma d\xi d\eta}$$

From KKT conditions:

$$\delta I + \sum_{i=1}^{T} \varphi_i \delta J_i + \mu\delta H = 0$$

$$0 = \iint_{A_T} U_i(\xi,\eta) d\xi d\eta \iint_{A_T} \delta\gamma\, d\xi d\eta$$

$$+ \sum_{i=1}^{T} \varphi_i \iint_{A_T} U_i(\,\xi,\eta) e^{-j\frac{2\pi}{\lambda L}(x_i\xi + y_i\eta)} d\xi d\eta \iint_{A_T} \delta\gamma\, e^{j\frac{2\pi}{\lambda L}(x_i\xi + y_i\eta)} d\xi d\eta$$

$$+ \mu \iint_{A_T} U_i(\xi,\eta)\delta\gamma d\xi d\eta$$

$$0 = \iint_{A_T} \delta\gamma \left[\iint_{A_T} U_i(\xi',\eta') d\xi' d\eta' + \sum_{i=1}^{T} \varphi_i e^{j\frac{2\pi}{\lambda L}(x_i\xi + y_i\eta)} \iint_{A_T} U_i(\,\xi',\eta') e^{-j\frac{2\pi}{\lambda L}(x_i\xi' + y_i\eta')} d\xi' d\eta' \right.$$

$$\left. + \mu U_i(\xi,\eta) \right] d\xi d\eta$$

$$\Rightarrow \boxed{0 = \iint_{A_T} U_i(\xi,\eta)d\xi d\eta + \sum_{i=1}^{T} \varphi_i e^{j\frac{2\pi}{\lambda L}(x_i\xi + y_i\eta)} \iint_{A_T} U_i(\xi,\eta) e^{-j\frac{2\pi}{\lambda L}(x_i\xi + y_i\eta)} d\xi d\eta + \mu U_i(\xi,\eta)}$$

KKT Conditions

$$\begin{cases} 0 = \iint_{A_T} U_i(\xi,\eta)d\xi d\eta + \sum_{i=1}^{T} \varphi_i e^{j\frac{2\pi}{\lambda L}(x_i\xi + y_i\eta)} \iint_{A_T} U_i(\xi,\eta) e^{-j\frac{2\pi}{\lambda L}(x_i\xi + y_i\eta)} d\xi d\eta + \mu U_i(\xi,\eta) \\ \varphi_i \left(\iint_{A_T} U_i(\xi,\eta) e^{-j\frac{2\pi}{\lambda L}(x_i\xi + y_i\eta)} d\xi d\eta \iint_{A_T} U_i^*(\xi,\eta) e^{j\frac{2\pi}{\lambda L}(x_i\xi + y_i\eta)} d\xi d\eta - \mathrm{I_T}\lambda^2 L^2 \right) = 0, \qquad \forall\, 1 \le i \le T \\ \varphi_i \ge 0, \qquad \forall\, 1 \le i \le T \\ \iint_{A_T} U_i(\xi,\eta) e^{-j\frac{2\pi}{\lambda L}(x_i\xi + y_i\eta)} d\xi d\eta \iint_{A_T} U_i^*(\xi,\eta) e^{j\frac{2\pi}{\lambda L}(x_i\xi + y_i\eta)} d\xi d\eta \le \mathrm{I_T}\lambda^2 L^2, \qquad \forall\, 1 \le i \le T \\ \iint_{A_T} U_i(\xi,\eta) U_i^*(\xi,\eta)\, d\xi d\eta = 1 \end{cases}$$

Appendix B

Derivation of KKT Conditions for Sparse Aperture With Real Weight Vector Components (for MATLAB computation)

Objective function:

$$f_0(\vec{\boldsymbol{q}}) = (\boldsymbol{a} - j\boldsymbol{b})\boldsymbol{h_v}^{\dagger}\boldsymbol{h_v}(\boldsymbol{a} + j\boldsymbol{b})$$

Gradients:

$$\frac{\partial f_0}{\partial \boldsymbol{a}} = \boldsymbol{h_v a h_v}^{\dagger} + \boldsymbol{h_v}^{\dagger}\boldsymbol{a}\boldsymbol{h_v} - j\boldsymbol{h_v}^{\dagger}\boldsymbol{b}\boldsymbol{h_v} + j\boldsymbol{h_v b h_v}^{\dagger}$$

$$\frac{\partial f_0}{\partial \boldsymbol{b}} = -j\boldsymbol{h_v a h_v}^{\dagger} + j\boldsymbol{h_v}^{\dagger}\boldsymbol{a}\boldsymbol{h_v} + \boldsymbol{h_v}^{\dagger}\boldsymbol{b}\boldsymbol{h_v} + \boldsymbol{h_v b h_v}^{\dagger}$$

Inequality constraints:

$$f_k(\vec{\boldsymbol{q}}) = \frac{(\boldsymbol{a} - j\boldsymbol{b})\boldsymbol{h_{u_k}}^{\dagger}\boldsymbol{h_{u_k}}(\boldsymbol{a} + j\boldsymbol{b})}{(\boldsymbol{a} - j\boldsymbol{b})\boldsymbol{h_v}^{\dagger}\boldsymbol{h_v}(\boldsymbol{a} + j\boldsymbol{b})} - \mathrm{R} \leq 0$$

Gradients:

$$\frac{\partial f_0}{\partial \boldsymbol{a}} = \Big(\big((\boldsymbol{a} - j\boldsymbol{b})\boldsymbol{h_v}^{\dagger}\boldsymbol{h_v}(\boldsymbol{a} + j\boldsymbol{b})\big)\big(\boldsymbol{h_{u_k} a h_{u_k}}^{\dagger} + \boldsymbol{h_{u_k}}^{\dagger}\boldsymbol{a}\boldsymbol{h_{u_k}} - j\boldsymbol{h_{u_k}}^{\dagger}\boldsymbol{b}\boldsymbol{h_{u_k}} + j\boldsymbol{h_{u_k} b h_{u_k}}^{\dagger}\big)$$

$$- \big((\boldsymbol{a} - j\boldsymbol{b})\boldsymbol{h_{u_k}}^{\dagger}\boldsymbol{h_{u_k}}(\boldsymbol{a} + j\boldsymbol{b})\big)\big(\boldsymbol{h_v a h_v}^{\dagger} + \boldsymbol{h_v}^{\dagger}\boldsymbol{a}\boldsymbol{h_v} - j\boldsymbol{h_v}^{\dagger}\boldsymbol{b}\boldsymbol{h_v}$$

$$+ j\boldsymbol{h_v b h_v}^{\dagger}\big)\Big)\frac{\mathbf{1}}{\Big((\boldsymbol{a} - j\boldsymbol{b})\boldsymbol{h_v}^{\dagger}\boldsymbol{h_v}(\boldsymbol{a} + j\boldsymbol{b})\Big)^2}$$

$$\frac{\partial f_0}{\partial \boldsymbol{b}} = \Big(\Big((\boldsymbol{a}-j\boldsymbol{b})\boldsymbol{h_v}^{\dagger}\boldsymbol{h_v}(\boldsymbol{a}+j\boldsymbol{b})\Big)\big(-j\boldsymbol{h_{u_k}}\boldsymbol{a}\boldsymbol{h_{u_k}}^{\dagger} + j\boldsymbol{h_{u_k}}^{\dagger}\boldsymbol{a}\boldsymbol{h_{u_k}} + \boldsymbol{h_{u_k}}^{\dagger}\boldsymbol{b}\boldsymbol{h_{u_k}} + \boldsymbol{h_{u_k}}\boldsymbol{b}\boldsymbol{h_{u_k}}^{\dagger}\big)$$

$$- \Big((\boldsymbol{a}-j\boldsymbol{b})\boldsymbol{h_{u_k}}^{\dagger}\boldsymbol{h_{u_k}}(\boldsymbol{a}+j\boldsymbol{b})\Big)\big(-j\boldsymbol{h_v}\boldsymbol{a}\boldsymbol{h_v}^{\dagger} + j\boldsymbol{h_v}^{\dagger}\boldsymbol{a}\boldsymbol{h_v} + \boldsymbol{h_v}^{\dagger}\boldsymbol{b}\boldsymbol{h_v}$$

$$+ \boldsymbol{h_v}\boldsymbol{b}\boldsymbol{h_v}^{\dagger}\big)\Big)\frac{\mathbf{1}}{\Big((\boldsymbol{a}-j\boldsymbol{b})\boldsymbol{h_v}^{\dagger}\boldsymbol{h_v}(\boldsymbol{a}+j\boldsymbol{b})\Big)^{\mathbf{2}}}$$

Equality constraints:

$$h(\vec{\boldsymbol{q}}) = (\boldsymbol{a}-j\boldsymbol{b})(\boldsymbol{a}+j\boldsymbol{b}) - 1 = 0$$

Gradients:

$$\frac{\partial f_0}{\partial \boldsymbol{a}} = 2\boldsymbol{a}$$

$$\frac{\partial f_0}{\partial \boldsymbol{b}} = 2\boldsymbol{b}$$

KKT Conditions

$$\begin{cases} h(\vec{\boldsymbol{q}}) = 0 \\ f_k(\vec{\boldsymbol{q}}) \le 0, & \forall\ 1 \le k \le T \text{ null points} \\ \lambda_k \ge 0, & \forall\ 1 \le k \le T \text{ null points} \\ \lambda_k f_k(\vec{\boldsymbol{q}}) = 0, & \forall\ 1 \le k \le T \text{ null points} \\ \nabla_{\boldsymbol{q}} f_0(\vec{\boldsymbol{q}}) + \sum_{k=1}^{T} \lambda_k \nabla_{\boldsymbol{q}} f_k(\vec{\boldsymbol{q}}) + \mu \nabla_{\boldsymbol{q}} h(\vec{\boldsymbol{q}}) = 0 \end{cases}$$

$$\text{where } \nabla_{\boldsymbol{q}} = \begin{bmatrix} \nabla_{\boldsymbol{a}} \\ \nabla_{\boldsymbol{b}} \end{bmatrix} = \begin{bmatrix} \dfrac{\partial}{\partial \boldsymbol{a}} \\ \dfrac{\partial}{\partial \boldsymbol{b}} \end{bmatrix}$$

References

[1] A.L. Puryear, "Optical Communication Through the Turbulent Atmosphere With Transmitter and Receiver Diversity, Wavefront Control, and Coherent Detection," *Ph.D. Thesis*, Massachusetts Institute of Technology, Cambridge, Massachusetts, 2011.

[2] J.P. Choi, "Resource Allocation and Scheduling For Communications Satellites With Advanced Transmission Antennas," *Ph. D. Thesis*, Massachusetts Institute of Technology, Cambridge, Massachusetts, 2006.

[3] J.W. Goodman, *Introduction to Fourier Optics,* 3rd Edition, Englewood, CO: Roberts & Company Publishers, 2005.

[4] J.W. Strohbehn, ed., *Laser Beam Propagation in the Atmosphere*, New York: Spring-Verlag, 1978.

[5] H.L.V. Trees, *Optimum Array Processing*, New York: John Wiley & Sons, Inc, 2002.

[6] E.J. Lee, "Free-space Optical Networks: Fade and Interference Mitigation and Network Congestion Control," *Ph. D. Thesis*, Massachusetts Institute of Technology, Cambridge, Massachusetts, 2010.

[7] V.W.S. Chan, "Free-Space Optical Communications," *Journal of Lightwave Technology (Inivited Paper)*, Volume 24, Issue 12, pp. 4750-4762, Dec. 2006.

[8] H. Steyskal, "Synthesis of Antenna Pattern With Prescribed Nulls," *IEEE Transactions on Antennas and Propagation*, Volume 30, Issue 2, pp. 273-279, Mar. 1982.

[9] S. G. Johnson, The NLopt nonlinear-optimization package, <http://ab-initio.mit.edu/nlopt>.

[10] T. P. Runarsson, X. Yao, "Search biases in constrained evolutionary optimization," IEEE Transactions on Systems, Man, and Cybernetics, Part C: Applications and Reviews, Volume 35, Issue 2, pp. 233-243, May 2005.

[11] R. Sarker, M. Mohammadian, and X. Yao, Eds., *Evolutionary Optimization* Norwell, MA: Springer, 2002.

[12] T. P. Runarsson and X. Yao, "Stochastic ranking for constrained evolutionary optimization," *IEEE Trans. Evolutionary Computation*, vol. 4 (no. 3), pp. 284-294 (2000).

[13] D. Kraft, "A Software Package for Sequential Quadratic Programming," Technical Report DFVLR-FB 88-28, Institut für Dynamik der Flugsysteme, Oberpfaffenhofen, July 1988.

[14] W. Sun and Y. Yuan, *Optimization Theory and Methods*, New York: Springer, 2006.

[15] D. G. Luenberger, *Linear and Nonlinear Programming*, 2nd Edition, New York: Springer, 2005.

[16] C. L. Lawson and R. J. Hanson, *Solving Least Squares Problems*, Philadelphia: Society for Industrial and Applied Mathematics, 1995.